Università degli Studi di Trieste

XXIII ciclo del
Dottorato di Ricerca in Scienze e Tecnologie Chimiche e Farmaceutiche

PhD in Chemical and Pharmaceutical Sciences and Technologies

Carbon Nanotechnologies for Drug Delivery

Settore scientifico-disciplinare CHIM/06

PhD student
Chiara Fabbro

PhD School Director
Prof. Enzo Alessio

Advisor
Prof. Maurizio Prato
Università degli Studi di Trieste

Co-Advisor
Dr. Tatiana Da Ros
Università degli Studi di Trieste

academic year 2009/2010

Table of Contents

Abbreviations I

Abstract III

Riassunto V

1 INTRODUCTION 1

1.1 Carbon nanotubes 1

1.2 CNT functionalization 3

1.2.1 Non-covalent functionalization 4

1.2.2 Covalent functionalization 4

1.2.2.1 Oxidation and defect site chemistry 6

1.2.2.2 1,3-dipolar cycloaddition of azomethine ylides 7

1.3 CNT characterization 7

1.3.1 UV-vis-NIR spectroscopy 8

1.3.2 Resonant Raman spectroscopy 9

1.3.3 Thermogravimetric analysis (TGA) 11

1.3.4 TGA-coupled mass spectrometry (TGA-MS) 11

1.3.5 Transmission electron microscopy (TEM) 12

1.3.6 Atomic force microscopy (AFM) 12

1.4 CNT Toxicity 13

1.5 CNT as delivery system for cancer 16

1.5.1 Uptake Mechanism 18

1.5.2 Delivery of antineoplastic chemotherapeutic drugs 24

1.5.3 Delivery of nucleic acids 37

1.6 Alternative CNT-based anticancer strategies 39

1.6.1 Thermal ablation 40

1.6.2 Radiotherapy & BNCT 42

1.7 References 43

2 SHORTENING OF SWCNTs 53

2.1 Oxidative shortening of SWCNTs 53

2.1.1 *Re-pristinization* of the oxidized SWCNTs 57

2.1.2 Sodium Hydroxide washing 60

2.2 Mechanochemical shortening of SWCNTs 63

2.3 Acknowledgments 71

2.4 References 71

3 CONJUGATION OF ANTIBODIES TO CNTs 73

3.1 IgG-DWCNT 74

3.1.1 Preparation 74

3.1.2 Characterization 77

3.2 Fab'-MWCNT and scFv-MWCNT 81

3.2.1 Preparation 82

3.2.2 Characterization 87

3.2.3 Preliminary biological results 91

3.3 Acknowledgments 95

3.4 References 95

4 CONJUGATION OF DOXORUBICIN TO CNSs 97

4.1 Fullerene derivatives 98

4.1.1 Synthesis 98

4.1.2 Spectroscopic characterization 101

4.2 CNT derivatives: preparation and characterization 102

4.3 Preliminary biological results with fullerene derivatives 109

4.4 Acknowledgments 112

4.5 References 113

5 EXPERIMENTAL PART 115

5.1 Materials and Methods 115

5.2 Instrumentation 116

5.3 Experimental Procedures 118

5.3.1 Organic compounds 118

5.3.2 Fullerene derivatives 122

5.3.3 Antibodies 126

5.3.4 CNT derivatives 127

5.4 References 138

Abbreviations

°C	degree Celsius
µm	micrometre
^{111}In	Indium 111
2-IT	2-iminothiolane
Å	Angstrom
a.a.	aminoacid
Ab	antibody
AcOEt	ethyl acetate
AFM	atomic force microscopy
Alloc	allyloxycarbonyl
aq.	aqueous
Ar	Argon
Boc	*tert*-butoxycarbonyl
C	carbon
CH_2Cl_2	dichloromethane
CNS	carbon nanostructure
CNT	carbon nanotube
CO	carbon monoxide
DIEA	N,N-diisopropylethylamine
DiOC6	3,3'-dihexyloxacarbocyanine iodide
DMF	N,N-dimethylformamide
DMSO	dimethylsulfoxide
DOS	density of states
DTNB	5,5'-dithio-*bis*-(2-nitrobenzoic acid)
DTPA	diethylenetriaminepentaacetic acid *or* diethylenetriaminepentaacetic dianhydride
DWCNT	double-walled carbon nanotube
EDC·HCl	*N*-ethyl-*N*'-(3-dimethylaminopropyl)carbodiimide hydrochloride
EDTA	ethylenediaminetetraacetic acid
ESI-MS	electrospray ionization mass spectrometry
Et_2O	diethyl ether
Fab'	antigen-binding fragment
FITC	fluorescein isothiocyanate
GFLG	glycine-phenylalanine-leucine-glycine
h	hour/hours
H_2	hydrogen (molecular)
H_2O	water
H_2SO_4	sulphuric acid
HCl	hydrochloric acid
He	Helium
HEPES	4-(2-hydroxyethyl)-1-piperazineethanesulfonic acid
HNO_3	nitric acid
HOBt	1-hydroxybenzotriazole
IC_{50}	half maximal inhibitory concentration

ID	injected dose
IgG	immunoglobulin G
IgG-SH	thiol-bearing immunoglobulin G
$KMnO_4$	potassium permanganate
MALDI-TOF-MS	matrix-assisted laser desorption/ionization time-of-flight mass spectrometry
MeOH	methanol
MFI	mean fluorescence intensity
min	minute/minutes
mm	millimetre
MW	microwave *or* molecular weight
MWCNT	multi-walled carbon nanotube
N_2	Nitrogen (molecular)
$NaHCO_3$	sodium bicarbonate (or sodium hydrogen carbonate)
NaOH	sodium hydroxide
NHS	*N*-hydroxysuccinimide
nm	nanometre
NMR	Nuclear magnetic resonance
O_2	Oxygen (molecular)
PBS	phosphate buffered saline
$Pd(PPh_3)_4$	palladium tetrakis
p-HCHO	paraformaldehyde
Pht	phthalimide
PI	propidium iodide
PyAOP	(7-azabenzotriazol-1-yloxy)tripyrrolidinophosphonium hexafluorophosphate
r.t.	room temperature
RBM	radial breathing mode
RPM	revolutions per minute
scFv	single-chain variable fragment
SDBS	sodium dodecylbenzenesulfonate
s-DWCNT	shortened double-walled carbon nanotube
s-MWCNT	shortened multi-walled carbon nanotube
SO_3	sulphuric anhydride
SPR	surface plasmon resonance
s-SWCNT	shortened single-walled carbon nanotube
SWCNT	single-walled carbon nanotube
TB	trypan blue
Tc	Technetium
TEA	triethylamine
TEM	transmission electron microscopy
TFA	trifluoroacetic acid
TGA	thermogravimetric analysis
TGA-MS	TGA-coupled mass spectrometry
THF	tetrahydrofuran
TLC	thin layer chromatography
TM-AFM	tapping mode-AFM
UV-vis-NIR	ultraviolet-visible-near infrared

Abstract

Nanotechnology underwent a very rapid development in the last decades, thanks to the invention of different techniques that allow reaching the nanoscale. The great interest in this area arises from the variety of possible applications in different fields, such as electronics, where the miniaturization of components is a key factor, but also medicine. The creation of smart systems able to carry out a specific task in the body in a controlled way, either in diagnosis or in therapy, is the ultimate goal of a newborn area of research, called nanomedicine. In fact, to reach such an outstanding objective, a nanometre-sized vector is needed and carbon nanotubes (CNTs) are among the most promising candidates.

The aim of this thesis was to study this opportunity, and in particular, the possible application of carbon nanostructures for drug delivery.

In the Introduction (Chapter 1), an overview on CNTs is given, explaining their main features and the key issues associated with their manipulation. The different existing possibilities for CNT functionalization are described, focusing the attention on the covalent approaches exploited in this thesis, namely oxidation and subsequent amidation of carboxyl groups, and 1,3-dipolar cycloaddition of azomethine ylides. The main characterization techniques used are then described, illustrating their advantages and their limitations. Subsequently, the very controversial issue of CNT toxicity is analysed, in terms of possible consequences to CNT exposure and risk for the workers in the field. Finally, a detailed account of the existing literature on CNT application for drug delivery is given, underlining the drawback of non-covalent approaches, and then focusing on the different targeted strategies studied so far in CNT-based nanomedicine.

In Chapter 2, a study on shortening of single-walled carbon nanotubes (SWCNTs) is presented, as a strategy to obtain a more soluble material, quite important for any medical application. Two different options are explored. In the first part, an oxidative treatment of SWCNTs, with a mixture of oleum and nitric acid, is described, reporting a detailed characterization, for the production of shortened and disentangled CNTs, bearing carboxyl groups, with a big improvement in dispersibility. Subsequently, an alkaline treatment, for the removal of the amorphous carbonaceous material introduced with the oxidation, is shown. In addition, a laser-mediated *re-pristinization* of the oxidized SWCNTs is reported for the first time.

In the second part of Chapter 2, a mechanochemical shortening of SWCNTs is presented, as an alternative to the wet chemistry approach. Different complementary characterizations of the SWCNTs obtained are shown, to highlight the very interesting possibility to control the quality of the final product, by tuning experimental conditions.

In Chapter 3, the covalent conjugation of CNTs and antibodies (Abs) is presented, with the aim of studying two different opportunities. Abs could mediate the specific targeting of a CNT-based nanovector with possible applications in both therapy and diagnosis. On the other hand, CNTs could mediate the cellular uptake of Abs, thus paving the way to a variety of unexplored intracellular, Ab-based, therapeutic possibilities. The preparation of different kinds of covalent Ab-CNT conjugates is described, with both double-walled carbon nanotubes (DWCNTs) and multi-walled carbon nanotubes (MWCNTs), using either the whole Ab or smaller fragments. Moreover, a double functionalization strategy is reported, for the simultaneous introduction of a probe, required for biological studies. Different complementary characterizations of the conjugates are presented, to prove the effectiveness of the covalent strategy and the preserved capability of the Ab, bound to CNTs, to specifically recognize its antigen. Also, some preliminary biological data are shown.

In Chapter 4, the functionalization of both fullerene C_{60} and CNTs, either pristine or oxidized, is presented, for studying the delivery of the antineoplastic drug doxorubicin. The drug is attached either directly or introducing a cleavable peptidic sequence to trigger its release inside cells. A detailed account on the adopted synthetic procedure is reported, together with the spectroscopic characterization of all the constructs. Furthermore, preliminary biological data on the fullerene derivatives are presented.

In conclusion, the present thesis reports the covalent modification of different kinds of CNTs, described in a critical way, with the aid of many characterization techniques. All the different constructs prepared could find an application in nanomedicine, giving a contribution to the understanding and the development of this fascinating and promising field.

Riassunto

Le nanotecnologie si sono sviluppate molto rapidamente negli ultimi decenni, grazie all'invenzione di un crescente numero di tecniche che permettono di lavorare su scala nanometrica. Il grande interesse in quest'area trae origine dalle sue svariate possibili applicazioni in diversi campi, quali l'elettronica, dove la miniaturizzazione ha un ruolo fondamentale, ma la medicina. Infatti, lo sviluppo di un sistema 'intelligente' capace di eseguire un compito specifico all'interno del nostro organismo in modo controllato, sia in campo diagnostico che terapeutico, è lo scopo di una nuova branca della ricerca, la nanomedicina. Per raggiungere un così notevole obiettivo, è necessario un vettore di dimensioni nanometriche, e i nanotubi di carbonio (CNTs) rappresentano uno dei migliori candidati.

Lo scopo di questo lavoro di tesi era lo studio di questa opportunità e, in particolare, della possibile applicazione di nanostrutture di carbonio per la veicolazione di farmaci.

Nell'Introduzione (Capitolo 1), viene fatta una breve panoramica sui CNTs, spiegando le loro più importanti caratteristiche e le questioni fondamentali associate alla loro manipolazione. Vengono descritte le diverse possibilità esistenti per la funzionalizzazione dei CNTs, concentrandosi soprattutto sugli approcci covalenti sfruttati in questa tesi, ossia l'ossidazione e la conseguente amidazione dei gruppi carbossilici così introdotti, e la cicloaddizione 1,3-dipolare di ilidi azometiniche. Sono poi trattate le principali tecniche di caratterizzazione impiegate, illustrandone i vantaggi e le limitazioni. In seguito viene affrontato il tema molto controverso della tossicità dei CNTs, in termini di possibili conseguenze a una loro esposizione e di rischio per chi lavora in questo campo. Infine viene fatto un dettagliato resoconto della letteratura esistente sull'applicazione dei CNTs per la veicolazione di farmaci, ponendo l'accento in particolare sugli svantaggi connessi agli approcci non-covalenti, e focalizzando poi l'attenzione sulle diverse strategie di indirizzamento specifico studiate a oggi nella nanomedicina con i CNTs.

Nel Capitolo 2, viene presentato uno studio sull'accorciamento di nanotubi di carbonio a parete singola (SWCNTs), come strategia per ottenere un materiale con migliori caratteristiche di solubilità, estremamente importante per qualsiasi applicazione biomedica. Vengono esplorate due diverse possibilità. Nella prima parte, si descrive il trattamento ossidativo di SWCNTs con una miscela di oleum e acido nitrico, e la loro completa caratterizzazione, per la produzione di nanotubi accorciati e disaggregati, recanti funzioni carbossiliche, con un grande miglioramento

nella dispersibilità. In seguito viene descritto un trattamento basico per la rimozione delle impurezze carboniose amorfe introdotte dall'ossidazione. In aggiunta, viene riportato per la prima volta un fenomeno di *ri-pristinizzazione* dei SWCNTs ossidati, mediante trattamento laser.

La seconda parte del Capitolo 2 riguarda l'accorciamento meccano-chimico di SWCNTs, come alternativa all'approccio in soluzione. Vengono mostrate diverse caratterizzazioni complementari dei SWCNTs ottenuti, sottolineando la possibilità, molto interessante, di controllare la qualità del prodotto finale variando le condizioni sperimentali.

Il Capitolo 3 tratta la coniugazione covalente di CNTs e anticorpi (Abs), con lo scopo di valutare due diverse opportunità. Gli anticorpi, infatti, possono mediare l'indirizzamento specifico di un nanovettore a base di CNTs, con possibili applicazioni terapeutiche e diagnostiche. Viceversa, i CNTs possono mediare l'internalizzazione cellulare degli Abs, aprendo così la strada a svariate possibilità terapeutiche a livello intracellulare, a oggi inesplorate. La preparazione di diversi coniugati covalenti Ab-CNT viene descritta, utilizzando nanotubi a parete doppia (DWCNTs) o multipla (MWCNTs), e sia Abs interi, sia frammenti degli stessi. Inoltre viene descritta una doppia funzionalizzazione dei CNTs, volta a introdurre simultaneamente una sonda necessaria per gli studi biologici. Vengono poi presentate diverse caratterizzazioni complementari dei coniugati, per dimostrare l'efficacia della strategia covalente adottata, e la preservata capacità dell'Ab legato ai CNTs di riconoscere il suo specifico antigene. Infine, vengono presentati alcuni risultati biologici preliminari.

Nel Capitolo 4, viene descritta la funzionalizzazione del fullerene C_{60} e dei CNTs, sia pristine che ossidati, per lo studio della veicolazione della doxorubicina, un farmaco antineoplastico. Il farmaco viene legato sia in maniera diretta che indiretta, mediante l'introduzione di una catena peptidica scindibile a livello intracellulare, al fine di mediarne il rilascio. Viene data una dettagliata descrizione delle procedure sintetiche adottate, oltre alla caratterizzazione spettroscopica di tutti i composti preparati. Infine vengono illustrati i primi risultati biologici ottenuti sui derivati fullerenici.

In conclusione, il presente lavoro di tesi descrive la funzionalizzazione di diversi tipi di CNTs mediante un approccio covalente, con un'analisi critica dei risultati, tramite l'utilizzo di svariate tecniche di caratterizzazione. Tutti i derivati preparati trovano potenziale applicazione nel campo della nanomedicina, contribuendo alla comprensione e allo sviluppo di questa scienza così affascinante e promettente.

Introduction

1.1 Carbon nanotubes

The rapid development of carbon nanotubes (CNTs)-based technology in many different fields rendered this material not as much unknown as few years ago for the scientific community. This paragraph gives a brief overview to remind their main features and to focus attention on the key issues related to CNTs, necessary as a background for the comprehension of the present thesis work. CNTs are tubular structures made of only carbon atoms arranged in an aromatic conjugated network as they are in graphite, but rolled up in a cylindrical shape, and therefore subjected to a curvature, with important consequences in the chemical reactivity (see Chapter 1.2.2). The number of cylinders that constitute a CNT can vary from only one to several, giving raise to different kinds of CNTs, namely single-walled CNTs (SWCNTs), double-walled CNTs (DWCNTs) up to generic multi-walled CNTs (MWCNTs), where the distance between two walls is of ca. 0.35 nm.

The coiling up direction of the graphene sheet determine different kinds of CNT. In fact, the angle between C-C bonds and the axis of the tube can vary, and the so-called chirality of a CNT will depend on this angle.

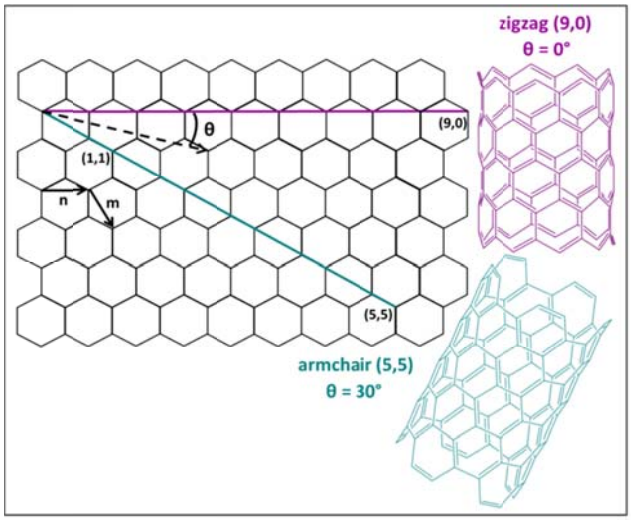

Figure 1. Graphical explanation of the chiral vector θ of a CNT. The vector refers to the direction of rolling up of a CNT. Thus, each CNT can be described by the couple of values (n,m), as in the two examples depicted.

Thus, different kinds of CNTs are described according to a chiral vector, as explained in Figure 1. The two extremes of the huge variety of possibilities are zigzag and armchair CNTs, the former having $\theta = 0°$ and m=0, and the latter with $\theta = 30°$ and $n = m \neq 0$. In-between, all CNTs with $0° < \theta < 30°$ are defined as chiral. Of course, with increasing n and/or m, the diameter of the tube increases. The description of this feature is important not only to define different CNTs with a common vocabulary, but mainly because electronic properties vary a lot depending on the chiral vector. In fact, infinite-length armchair SWCNTs are metallic, whereas infinite-length zigzag or chiral CNTs are semi-conducting, even though these are not strict rules. In the case for example of small diameter tubes, where the curvature plays an important role, some exceptions exist.[1]

Additionally, as a result of the 1-D nature of CNTs, electrons can be conducted without being scattered. The absence of scattering of the electrons during conduction is known as ballistic transport and it allows the nanotube to conduct without dissipating energy as heat.

Besides these unique electronic properties, ideal CNTs exhibit chemical and thermal stability, together with extremely high tensile strength and elasticity.

Nevertheless they still present to date some important drawbacks that need to be addressed by the research in the field. One of the major problems is related to batch-to-batch irreproducibility. In fact, buying the same kind of CNTs by the same supplier does not necessarily mean getting the same product. This lack of reliability is probably due to the big heterogeneity of a CNT sample, that make it subjected to too many unpredictable variables during the synthetic process. This variability is associated with CNT length, diameter, chirality, impurity content (i.e. metal and carbonaceous impurities) and presence of defect. The possible defective structures are vacancies, i.e. incomplete bonding defects, topological changes, such as pentagons/heptagons interrupting the hexagonal network (Figure 2), and doping with elements other than carbon.[2]

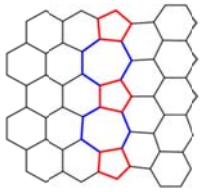

Figure 2. Example of pentagons/heptagons defect in the hexagonal CNT network, inducing local strain. Note the change in tube chirality between left and right side of the defect.

The other big limitation associated with CNT research is their poor dispersibility. In fact pristine CNTs are insoluble in water and in any organic solvent, and a functionalization is

required in order to improve dispersibility for a better manipulation of the material (see Chapter 1.2).

Different synthetic techniques exist for CNTs. The main ones are arc discharge, originally developed for fullerene synthesis, laser ablation and catalytic carbon vapour deposition (CCVD).[3] The first two methodologies involve high-power energy to vaporize solid-state carbon (graphite) and form CNTs at high temperature (thousands of Celsius), while CCVD uses carbon precursors in gas phase and it takes place at relatively low temperatures (500-1000 °C). In general the use of a proper metallic catalyst can switch from the production of MWCNTs to the production of SWCNTs. Usual impurities deriving from the synthetic process are metallic nanoparticles and carbonaceous material other than the desired CNTs, represented mainly by amorphous carbon. Among the three different synthetic methods, CCVD provides a better control in the growth of CNTs and can be scaled up to industry level because of the lower costs. Different CCVD processes have been developed, among which one of the most famous is the high-pressure carbon monoxide disproportionation process (HiPCO), used for producing SWCNTs.[4] This technique exploits carbon monoxide (CO) as the carbon source, and $Fe(CO)_5$ as the catalyst precursor. The process takes place at 800-1000°C through the disproportionation of CO to CO_2 and C for the CNT growth on the iron nanoparticles. Optimized conditions led to the production of SWCNTs with diameters ranging from 0.7 to 1.4 nm, with a good level of purity.

1.2 CNT functionalization

As already mentioned, CNT usefulness is strongly hindered by the difficulty in their handling. In fact, as produced, they are not soluble in water and in all common organic solvents. For this reason, in most cases, a chemical modification is needed prior to application. By means of functionalization, the strong inter-tube interactions are reduced. Moreover, specific groups can be introduced to increase solubility in certain solvents, and to provide an anchor point for further modifications.

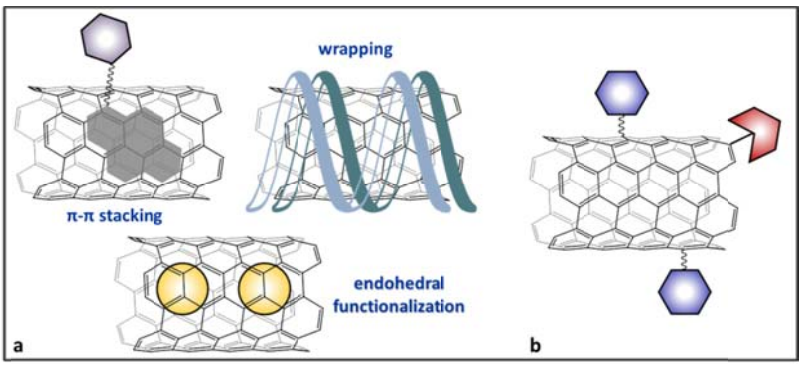

Figure 3. Non-covalent (**a**) and covalent (**b**) approaches for CNT functionalization.

The main distinction to be underlined when speaking of CNT functionalization is between non-covalent and covalent approaches (Figure 3). They both present pros and cons, which should be carefully taken into account when deciding which is the best route to follow, according to the desired application.

1.2.1 Non-covalent functionalization

Among non-covalent CNT functionalization strategies, one possibility is based on small aromatic molecules, bound to the tubes by means of π-π stacking,[5] while another one is based on the wrapping of polymeric molecules around the tubes. The latter method can involve both biological macromolecules, such as nucleic acids,[6] lipids[7] or peptides[8] and synthetic polymers,[9] and it occurs via π-π stacking and/or van der Waals interactions. Another, quite particular, approach for the non-covalent modification of CNTs is the filling of their inner cavity.[10] The main advantage of the non-covalent modification of CNTs is that the electronic and mechanical properties of the tubes are preserved. Therefore this should be the first choice when CNTs are exploited in fields such as molecular electronics. On the other hand, the drawback of a non-covalent approach is the possible reversibility of the bonds involved, which can result in the loss of the functionalization. This risk needs to be considered for example in the case of most biomedical applications, since it is difficult to exactly foresee the fate of a non-covalently bound molecule when the functionalized CNTs are administered *in vivo*. For this reason, a covalent approach should be preferred if CNTs will serve as drug delivery system, as in the work presented in this thesis.

1.2.2 Covalent functionalization

The reactivity of CNTs in terms of covalent chemistry on the C backbone is due to local strain, which is caused by two main reasons: the first one is the curvature-induced pyramidalization of the conjugated carbon atoms, and the second is the π orbital misalignment between adjacent pairs of conjugated carbon atoms.[11] Since pyramidalization angle gives a good measure of the local weakening of π-conjugation and of the strain energy of pyramidalization, it appears clear why this effect is quite important for fullerenes and for CNTs caps, that are like an hemi-fullerene, while it carries less weight in the case of the flatter CNT sidewalls (Figure 4, upper part).

On the other hand, π orbital misalignment accounts for strain in CNT sidewall much more than in fullerenes, where it is very little (in fullerene C_{60} π orbitals alignment is even perfect) (Figure 4, lower part).

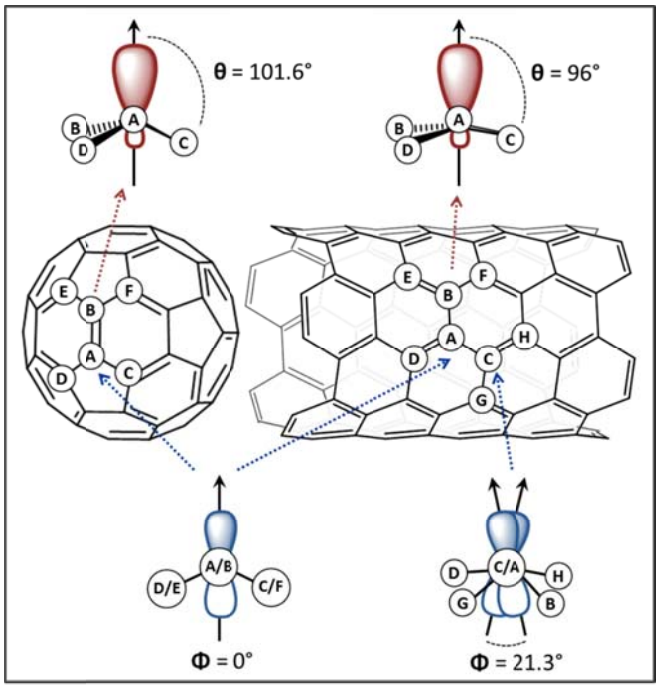

Figure 4. Representation of pyramidalization angle (**θ** – 90°) and of π orbital misalignment (Φ) for fullerene C_{60} and for a (5,5) SWCNT.

Therefore C_{60} and CNT reactivity towards addition reactions are both driven by geometry-dependent strain, but for different reasons. Furthermore, since the pyramidalization angles and the π-orbital misalignment angles of CNTs scale inversely with the diameter of the tubes, a higher reactivity is expected for smaller tubes than for larger ones, if considering just strain-induced reactivity. Nevertheless, there is another parameter that could deeply influence the reactivity of CNT sidewalls: the presence of defects, such as pentagon-heptagon pairs in the hexagons network, that result in a locally enhanced chemical reactivity of the graphitic nanostructures, and can cause an unpredictable chemical behaviour of different diameters CNTs. As already anticipated, covalent sidewall functionalization cause a loss of the high conductivity and of the remarkable mechanical properties of CNTs, since it generates sp^3 carbon sites on CNTs, which disrupt the band-to-band transitions of π electrons. The possibilities for a covalent modification of the unsaturated carbon network of CNTs, though being limited and requiring usually harsh conditions, grew up a lot in the last years, starting from fluorination, one of the first covalent reactions ever performed on SWCNTs in 1998.[12] In this case the degree of functionalization could reach such high levels that in the end the tubes can become insulators. Afterwards CNTs can be further modified using Grignard reagents or with organolithium compounds.[13] Other existing possibilities include addition of both alkyl[14] and aryl[15] radicals, nucleophilic[16] or electrophilic[17] additions and cycloadditions.[18]

Herein the attention will be focused mainly on oxidation of CNTs and the subsequent defect site chemistry, and on 1,3-dipolar cycloaddition of azomethine ylides, widely exploited in this thesis.

1.2.2.1 Oxidation and defect site chemistry

The most common way to oxidize CNTs involves acid treatments, with sonication of CNTs in concentrated acid mixtures, where nitric acid or hydrogen peroxide plays the role of the oxidative agent.[19] Also other oxidative agents have been used, such as phosphomolybdic acid,[20] potassium permanganate,[21] or oxygen O_2, by heat treatment of the CNTs in O_2 atmospheres.[22]

CNTs are oxidized with multiple aims, mainly purification and shortening. In fact, CNTs are typically synthesized with poly-disperse micrometre lengths, bound together into macroscopic entangled ropes, and they contain metallic impurities, deriving from the catalyst used during their synthesis. Many applications, however, require individual short CNTs, void of metallic impurities. Oxidative treatments reduce metal content due to the removal of the amorphous carbon usually covering metallic particles, or the etching of CNTs caps when the particles are still inside them, and the subsequent oxidation of the metal to soluble species, which are then easily removed. Moreover, as a result of chemical oxidation, the ends and the sidewalls of CNTs are covered with oxygen containing groups, mainly carboxylic groups, useful for further derivatization.[23] The process of the oxidation of CNTs can be described as step-wise with (i) an initial attack on the originally existing reactive sites, such the terminal fullerene-like caps, and the heptagon-pentagon defects, which carry the higher strain, (ii) a defect-generation step, when additions to hexagon π bonds take place, generating new defects, and introducing hydroxyl groups, then further oxidized to carboxyl groups, and (iii) a defect-consuming step, when the graphene structure around the defect sites is broken, and the tube is cut. Depending on the strength of the conditions, oxidation can stop at the first step, thus attacking only already existing defects, or proceed with the generation of new defects and finally with the cutting of the nanotubes. A detailed study of diameter-dependent oxidative stability confirmed a direct relationship between diameter and reactivity, as expected on the basis of what has been previously explained in this chapter. Studying the resonant Raman radial breathing mode (RBM), the authors clearly showed that smaller diameter tubes are more easily air-oxidized than larger diameter ones.[24]

As already anticipated, the introduction of carboxylic groups allows a further derivatization of CNTs. Esterification and amidation reactions are in fact widely exploited possibilities for the covalent modification of oxidized CNTs, since they usually permit to easily

obtain highly functionalized material, bearing the desired molecule according to the specific envisaged application.[25]

1.2.2.2 1,3-dipolar cycloaddition of azomethine ylides

The 1,3-dipolar cycloaddition of azomethine ylides, widely exploited in fullerene functionalization since 1993,[26] was translated to carbon nanotubes chemistry as well, starting from 2002.[27] This very versatile reaction consists in the concerted [π4 + π2] pericyclic 1,3-addition of a dipole to a dipolarophile, where the dipole is an azomethine ylide, formed by reaction of an aldehyde (or a ketone) with an α-amino acid, and the dipolarophile is a double bond on the fullerene cage or on the CNT (Scheme 1).

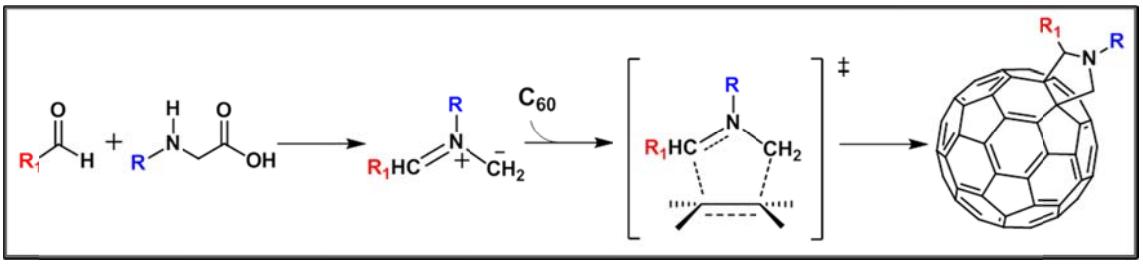

Scheme 1. General mechanism of 1,3-dipolar cycloaddition of azomethine ylides to C_{60}.

In fullerene C_{60}, the first addition takes place in any of the [6,6] double bonds, since they are all equivalent. Instead, CNTs sidewall is made only of [6,6] double bonds, but they are not all equivalent. In fact, it was found by theoretical studies that armchair tubes favour functionalization at C-C bonds tilted with respect to tube axis, (i.e. bond A-C in Figure 4), whereas zigzag CNTs prefer attachment of the ylides at segments parallel to the tube axis.[28] Since real samples of CNTs are normally made of a mixture of different tubes in terms of diameter, length, chiralities and defects, we should ask ourselves which is the behaviour of the different CNTs. Theoretical calculations showed that reactivity depends mainly on tube diameter, and only weakly on the chirality, as expected considering pyramidalization angles and the π-orbital misalignment angles.[29] Moreover, this particular kind of 1,3-dipolar cycloaddition, being the dipole a nucleophile, is in principle accelerated by the presence of electron-donating groups in the dipole, and electron-withdrawing groups in the dipolarophile, such as carboxylic groups introduced on the tubes by an oxidation step.[29,30]

1.3 CNT characterization

A great difficulty associated with CNT functionalization, especially when a covalent approach is chosen, is their characterization. In fact all the normal techniques used in organic synthesis cannot be translated to this material. The main reason is that the amount of functional

groups is usually too low, with respect to the CNT component of the sample, to be detected. Also, for techniques performed in solution, the choice of the solvent is highly limited, even for functionalized CNT, and the required concentrations are usually far too high to be achieved. For what concerns NMR, further problems are given by the presence of ferromagnetic or paramagnetic metallic particles in CNT samples, due to the magnetic field.

Herein some of the main characterizations exploitable for CNT will be presented.

1.3.1 UV-vis-NIR spectroscopy

The electronic density of states of SWCNTs, being one dimensional objects, is not a continuous function of energy, but it possesses spike-like features known as van Hove singularities (Figure 5a). Optically allowed transitions between these features are typically observed in the UV-vis-NIR region as sharp peaks, even though the sharpness is not fully appreciable due to the overlap of similar transitions given by different SWCNTs. Moreover, interactions between nanotubes in a bundle broaden optical lines. In the specific case of commercial HiPCO SWCNTs, the main features represent transitions between the first pair of singularities in metallic tubes (M_{11}) and between the first and the second pairs of singularities for semiconducting tubes (S_{11} and S_{22}), as indicated in Figure 5b. Moreover, the energy of electronic transition is inversely proportional to tube diameter.[31]

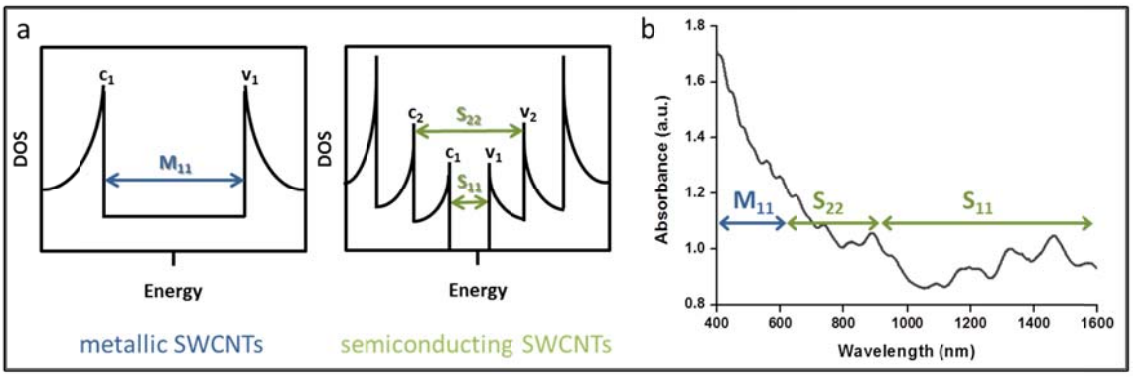

Figure 5. a) Density of states diagrams for metallic and semiconducting SWCNTs; **b**) UV-vis-NIR spectrum of pristine HiPCO SWCNTs (DMF).

UV-vis-NIR spectroscopy could provide information on the functionalization of SWCNTs. In fact, covalent modifications can disrupt the periodicity of SWCNTs conjugated electronic structure, and hence perturb their electronic transitions, resulting in a loss of van Hove features.

1.3.2 Resonant Raman spectroscopy

When a beam of light pass across a transparent sample, a small fraction of it is scattered, and a small fraction of this small fraction is scattered inelastically, i.e. at different frequencies than the incident light. In fact, the interaction between the incident photon and the sample could result in an energy exchange, namely the Raman effect. Usually Raman scattering signal is weak. However, its intensity can be strongly enhanced working in resonance Raman scattering, i.e. using a laser energy that matches the energy of optically allowed electronic transitions in the material studied.

SWCNTs, due to their broad range of optically allowed transitions, always give a resonance Raman response, and consequently only tubes with one of the band-gaps equal to the exciting laser energy are probed. Therefore, using different laser energies, different populations of tubes in a heterogeneous SWCNT sample are analysed (Figure 6a). The main features of a typical SWCNT Raman spectrum are depicted in Figure 6b.

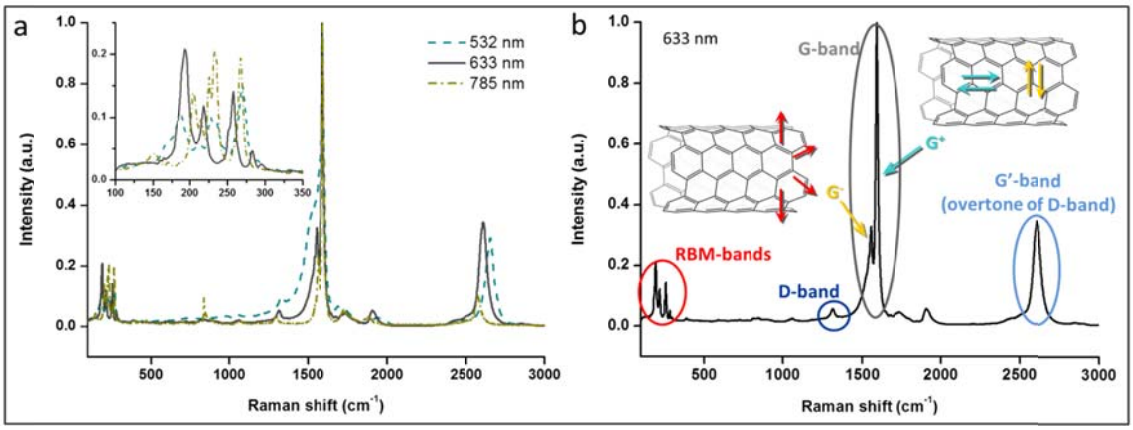

Figure 6. a) Raman spectra of pristine HiPCO SWCNTs obtained with different lasers; **b**) main SWCNT Raman features.

Radial breathing mode (RBM) corresponds to radial expansion-contraction of SWCNTs, exactly as if the tube was breathing. In fact, it depends on nanotube diameter: RBM frequency is inversely proportional to tube diameter. RBM range is typically 100-350 cm^{-1}, and, if its intensity is particularly high, weak overtones can be observed at double frequency.

G-mode corresponds to tangential planar vibrations of carbon atoms and it is present also in graphite, from which the name derives. However, differently from graphite, SWCNT G-band (1580 cm^{-1}) is split into up to six peaks, due to the loss of symmetry. Just the two main ones are normally considered, i.e. the G^+, which is given by vibrations along tube axis, and the G^-, due to vibrations in the circumferential direction (Figure 6b). In this latter band, there is an

evident difference in the line-shape between semiconducting SWCNTs, which give a Lorentzian-like peak (as G^+) and metallic ones, where the peak is broadened, due to the presence of free electrons.[32] This difference can be clearly appreciated comparing the spectra depicted in Figure 6a: when using 532 nm laser, mainly metallic tubes are in resonance, due to their M_{11} transition (see Figure 5 in Chapter 1.3.1), and in fact the G^- line-shape is much broader than in the case of the 785 nm laser, which is instead in the semiconductor S_{22} transition region.

Another important Raman feature is the D band, whose position is at around 1300 cm^{-1}, and it shifts to higher wavenumbers as the laser excitation energy is increased. This mode is associated with disorder, i.e. with the sp^3-hybridized carbon atoms present in the tube or in the carbonaceous impurities. Therefore, it is often used to evaluate the structural quality of SWCNTs, expressed usually as D/G ratio. Moreover, the full-width-at-half-maximum (FWHM) intensity of the D-band of the various carbon impurities is generally much broader than that of CNT D-band, and thus D-band line-width could give an indication of the SWNCT purity level.[33]

Other less significant bands are typically present in a SWCNT Raman spectrum, due to overtone modes of single bands or combinations of different ones. Among them the strongest one is usually the G' band. The name of this band is misleading, since it derives from graphite, where this mode is usually the second strongest after the G mode, but it is actually the overtone of the defect-induced D mode, even though being present even in defect-free nanotubes.

The main changes that could be appreciated in a SWCNT Raman spectrum upon chemical modification are the following:

- loss or decrease of some RBM bands, due to destruction or extensive modification of the corresponding kind of CNTs;
- change in the D/G ratio, due to modification of sp^3/sp^2 carbon atoms ratio (an increased D/G ratio could give a quali-quantitative information on the degree of covalent functionalization, but it could also be due to increased amorphous carbon content);
- change in the FWHM intensity of the D-band, according to the amorphous carbon content of the sample, as already explained;
- change in the baseline height (a great content of amorphous carbon can give a strong fluorescence, perturbing the Raman spectrum).

A big drawback of the two characterizations just described is that their usefulness is usually limited to SWCNTs.

In fact, MWCNT UV-vis-NIR absorption, deriving from the overlap of many different contributions in each tube, does not result in the typical well-defined van Hove features of a SWCNT spectrum, and thus it cannot give information on CNT covalent functionalization.

Concerning Raman, MWCNTs do not present defined RBM, being each tube made of several concentric walls. Moreover, the D band is quite intense, often more than the G-band, because of the high extent of defects usually present in MWCNTs. Consequently, it is difficult to appreciate an increase in the D/G ratio due to functionalization. For DWCNTs the situation is intermediate between single and multi-walled CNTs and it is normally possible to appreciate RBM and D/G ratio variations.

1.3.3 Thermogravimetric analysis (TGA)

TGA is an analytical technique for determination of the thermal stability of a material. The weight of the sample is recorded, while heating it in a furnace under a controlled atmosphere, which can be either inert (using gases as N_2 or He), or oxidative (using air or pure O_2).

In the latter case CNT combustion takes place usually between 400 and 600°C, depending on different factors, and resulting in the formation of CO_2. CNT combustion temperature, easily determined as the maximum in the first derivative (see Figure 4 in Chapter 2.1), depends on different factors. For example, smaller diameter nanotubes are believed to oxidize at lower temperature due to higher curvature strain. The same effect could be given by defects in the CNT structure. Also the presence of metal particles could lower combustion temperature, since they can catalyse carbon oxidation.[34] Furthermore, it is possible to use air TGA to determine the metal content of a sample, since the residual weight after completeness of CNT combustion is ascribable to metals in their oxidized form.

On the other hand, in the case of TGA run under inert atmosphere, CNTs are stable up to ca. 800°C, and therefore it is possible to ascribe the weight loss at lower temperatures to the organic material present in the sample, thus estimating the degree of functionalization after a chemical modification of CNTs. Nevertheless, it is important to underline that also amorphous carbonaceous species possibly present in a CNT sample could burn in the same temperature range, and this fact should be taken into account when using TGA measurements for quantitative characterization.

1.3.4 TGA-coupled mass spectrometry (TGA-MS)

The possibility offered by MS-TGA is quite interesting: a mass spectrometer has been coupled to the vent-hole of the TGA furnace, in order to analyse the gaseous material evolving during the experiment, thus giving precious information on what is going on. In this case, the TGA analysis should be performed in He, thanks to its low molecular weight (4), so that the mass

spectrometer could screen all the masses with molecular weights bigger than 4. Otherwise the signal given by the gas would completely saturate the instrument. It is important to point out that the mass spectra obtained are not like normal ones. In fact a massive fragmentation occurs during TGA, and so very small fragments are produced. In a typical analysis a big CO_2 peak appears in correspondence of every combustion taking place, associated with a decrease in the O_2 signal (inert gas cylinders always contain some), which is being consumed by the combustion itself. However, also higher molecular weight peaks appear, making it possible to determine the presence of certain molecules if very characteristic fragments are produced (see Figure 5b in Chapter 2.1) or by comparison of the pattern obtained with known samples (see Figure 5 in Chapter 4.2).

1.3.5 Transmission electron microscopy (TEM)

TEM is a major tool for the morphological characterization of CNTs. A TEM image derives from the interference of the sample, deposited onto a grid, with an electron beam transmitted through it. Thus, metal particles interfere more, producing spots with higher contrast. On the other hand, individual SWCNTs are usually very difficult to visualize (with a non-high resolution TEM), due to the low contrast with the grid surface, which is usually made of carbon. Bundles of SWCNTs instead, as well as DWCNTs or MWCNTs, can be easily detected providing different useful information, such as CNT length and diameter, together with a rough assessment of their purity, in terms of metals and amorphous material content. Regarding the evaluation of the dispersibility of a sample, it should be underlined that, during the drying procedure that follows the deposition of the CNT dispersion on the grid, CNTs can easily re-aggregate. Therefore the TEM analysis do not provide reliable information on their original aggregation state.

1.3.6 Atomic force microscopy (AFM)

AFM is a particular kind of Scanning Probe Microscopy, which consists in scanning a sharp tip (radius of curvature = 3-50 nm) over a surface and detect one or more probe/surface interactions. In AFM the result is a topographical image of the surface. The tip is mounted on a flexible cantilever, allowing it to follow the surface profile, and its deflection is measured using a laser spot reflected from the top surface of the cantilever into an array of photodiodes. AFM could be performed in Contact Mode, when the tip actually touches the surface, thus possibly moving objects or damaging soft samples, in Non-Contact Mode, when the tip scans the surface at a certain distance, with a consequent lower resolution, and in Tapping Mode (TM), when the tip is oscillated rapidly against the surface during scanning, and the microscope extrapolates the

surface topography by the change in the oscillation amplitude, triggered by tip/surface interactions (Figure 7).

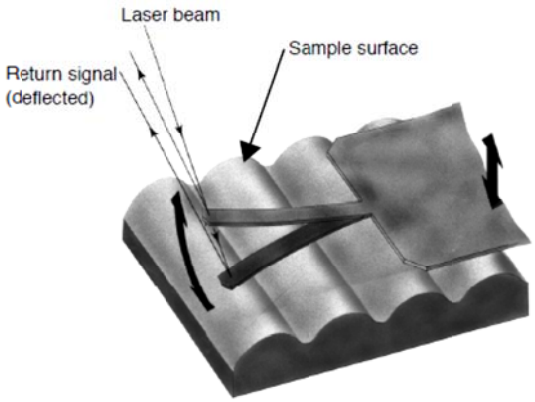

Figure 7. Cantilever tapping on a surface.[35]

Typically, when scanning a surface in TM, two images are obtained: one is the height image, while the other shows the amplitude of the tapping oscillation as the probe scanned across the surface, being a sort of "error" image (see Figure 16a and 16b in Chapter 2.2). In fact, this image shows where and how much the amplitude changed, giving the impression of shadows on sharp feature boundaries, which makes it look like a snapshot of the surface. However, shadows are actually areas where the amplitude had not yet been corrected back to the set value, and the real topographical image is the first one.[36]

TM-AFM analysis could be exploited to gather structural information on a CNT sample deposited on a surface, such as length distribution. However, lateral resolution is usually not precise enough (being in the range 1-5 nm) to evaluate very short distances, such as the diameter of a SWCNT, due to the delay in the response of the cantilever to tip/surface interactions. Nevertheless, it is possible to obtain this information from the height profile of the objects on the surface, since vertical resolution does not suffer from this limitation (see Figure 16c in Chapter 2.2).

1.4 CNT Toxicity

One of the big concerns regarding CNTs is, of course, their toxicity. First of all, the big diversity of this material should be taken into account, both for the as-produced CNTs and for the modified ones. In fact not only commercial pristine samples can differ according to the synthetic methodologies and the supplier, but, more importantly, CNTs always undergo some chemical modification (covalent or non-covalent) when intended to be used for biomedical applications, thus leading to changes in their water dispersibility and in toxicological behaviour.

Therefore results should always be considered as referred to the particular kind of CNTs they have been obtained with, and could not be generalized.

When considering CNT toxicity it is important to distinguish among (i) biocompatibility related to possible biomedical application of CNT-based systems, and (ii) safety related to CNT manipulation by all the workers in the field. In the first case it will be referred to processed CNTs, likely administered in solution via injection (this topic will be reviewed later, see Chapter 1.5), while in the second case the main risk is related to inhalation, and it refers not only to processed CNTs but, primarily, to pristine ones.

Pristine MWCNTs have been compared to asbestos, since they tend to form fibrous aggregates whose dimensions (in the micrometre range) and shape are similar to those reported to be carcinogenic for asbestos. Once the latter non-degradable and bio-persistent particles are inside the body, they deposit. Thus, unsuccessful inflammation and scavenging occur towards them (frustrated phagocytosis), leading to continuous oxidative stress. Furthermore, there is a contribution, given by iron impurities in the samples, that accelerates the generation of reactive oxygen species (ROS). This being true for asbestos, the possibility for CNTs to share the same carcinogenic mechanism was investigated.[37] Experiments on p53 heterozygous mice (reported to be sensitive to asbestos and to fast develop mesothelioma), intraperitoneally administered with MWCNTs, showed the induction of mesothelioma, leading to death of the animals within 25 weeks. Nevertheless, it is necessary to underline that these experiments were carried out with micrometre sized MWCNTs particles (10-20 μm) and there is no evidence, as the authors pointed out, that the same effect would occur using pure nanometre-sized CNTs. In a similar study CNTs, introduced into the abdominal cavity of mice, were proved to cause asbestos-like pathogenicity (inflammation and granulomas formation) in a length-dependent manner, namely only fibers long enough (> 20 micrometre) were able to cause pathogenic response during the 7 days experiment.[38]

Nonetheless, being based on intraperitoneal injection, none of these studies addresses the question if and how much CNTs accumulate in the mesothelium after inhalation. To answer this question other studies on inhaled CNT effects should be considered. Mitchell et al. exposed male mice to MWCNTs (5-15 μm long) aerosol in a whole body inhalation chamber.[39] The aerosol was generated by a jet mill and particles bigger than 3 μm were removed in order to work within a range respirable by a rodent. It is necessary to underline the difference between “inhalable”, which refers to the fraction of airborne material which enters nose and mouth during breathing and is therefore available for deposition in the respiratory tract, and “respirable”, referring to the fraction able to penetrate to the gas exchange region of the lung. The authors observed the

presence of black particles inside alveolar macrophages, but no lung inflammation or tissue damage were evidenced with exposure to up to 5 mg/m^3 for a maximum of 14 days. Nevertheless the treatment caused systemic immunosuppression, response already reported after inhalation of environmental pollutants. Other authors also reported accumulation of MWCNTs in sub-pleural macrophages.[40] In this case CNTs were longer (0.5-50 µm compared to 5-15 µm) and the treatment consisted in a single inhalation exposure at a concentration of 30 mg/m^3 for 6 h with a nose-only inhalation chamber. The authors also observed focal sub-pleural fibrosis, which could be consistent with the induction of mesothelioma, even if normally asbestos causes pleural inflammation and diffuse pleural fibrosis.

It is important to analyze the real risk for people working with CNTs to inhale them. Baron et al. studied, in 2003, the tendency of SWCNTs to form aerosols, in order to evaluate a typical workplace exposure to this material.[41] Vigorously agitating SWCNTs (produced by HiPCO process) led to the generation of particles below 10 µm aerodynamic diameter, and also particles smaller than 100 nm, even if it was unclear whether these smaller particles consisted predominantly of nanotubes, catalyst particles, or compact carbonaceous particles. However, generation rates were approximately two orders of magnitude lower than those from a similar volume of fumed alumina, another low-density material comprised of nanometre-sized primary particles. A field evaluation of the airborne contamination, while manipulating the bulk SWCNTs, was also conducted. The bulk material was removed from the reactors and manipulated (poured from one container into another one) in a closed area with inlet of filtered air, with a continuous monitoring of aerosol number and mass concentration (Figure 8).

Figure 8. Pouring HiPCO SWCNTs for airborne contamination study (adapted from Ref. 41).

There was no clear evidence of increased aerosol mass concentrations during the handling of unrefined nanotube material in the field. The aerosol nanotube concentrations during material handling were estimated to be lower than 53 µg/m^3, a value that is below those

associated with re-suspension of ambient dust due to personal movement, and cleaning operations following handling of material. Importantly, these experiments could therefore lead to the conclusion that a typical aerosol concentration of CNTs during handling of the material is far below the ones used in the *in vivo* inhalation studies conducted so far, thus making those results not relevant. Nevertheless, the CNTs are not the same, so it is necessary to be careful in making comparison.

It is still not possible to reach a clear, unambiguous conclusion on CNTs inhalation toxicity, and therefore, precautions should be taken to prevent any unnecessary release of respirable particles, when handling CNTs, especially the pristine ones, but without getting into a panic. Also, to avoid exposure and guarantee respiratory protection, an adequate personal protective equipment should be used.

1.5 CNT as delivery system for cancer

Anticancer therapy, though being often very effective, still suffers of some severe drawbacks, which render vital and urgent the need for further research. One of the main limitations of almost every cancer treatment so far is the lack of selectivity for tumour tissues. In fact cytotoxic drugs (or other therapies) do not exert their action solely on cancer cells, but also on healthy organs, resulting in severe side effects for patients, therefore limiting their compliance and the maximum administrable dose. Another major problem related to anti-neoplastic chemotherapy is Multi-Drug Resistance (MDR).[42] This phenomenon can be often ascribed to the activity of an efflux pump, namely P-glycoprotein (P-gp), able to recognize the drug and transport it out of the cell once it has been internalized, thus preventing it from exerting its cytotoxic action.[43] Importantly, the P-gp mediated MDR often characterizes residual tumour cells after chemotherapy and tumour stem cells. Once this capability is acquired, it can be directed towards many different drugs to which the tumour had never been exposed before, thus heavily hampering chemotherapy's efficacy.

Nanotechnology can help in overcoming these limitations; in fact a nanovector could be conceived to be targeted towards cancer, either only in a non-specific way, or with a specific targeting agent attached to the carrier itself. The non-specific targeting is based on the Enhanced Permeability and Retention (EPR) effect (Figure 9).[44] Cancer tissue is usually characterized by a rapid and defective angiogenesis, resulting in leaky blood vessels with large fenestrations, due to endothelial cell disorganization. Moreover, the smooth-muscle layer in the vascular wall is frequently absent or abnormal, leading to passive dilatation of vessels. The consequence of these characteristics is an enhanced extravasation of macromolecules in the

tumour tissue, whereas low molecular weight-molecules can rapidly diffuse in the circulation and undergo renal clearance. Moreover, slow venous return and poor lymphatic drainage lead to retention of accumulated macromolecules in the tumour. For these reasons, drug delivery based on Nano-sized systems (macromolecules) would accumulate more in the tumour than the free drug (small molecule). Moreover, this effect can be further enhanced in a specific way, i.e. binding to the nanocarrier targeting agents as antibodies or other molecules able to recognize specific tumour markers. At the same time, the delivery of a carrier driven drug could involve different metabolic and cellular pathways, thus giving the possibility to elude MDR.[45]

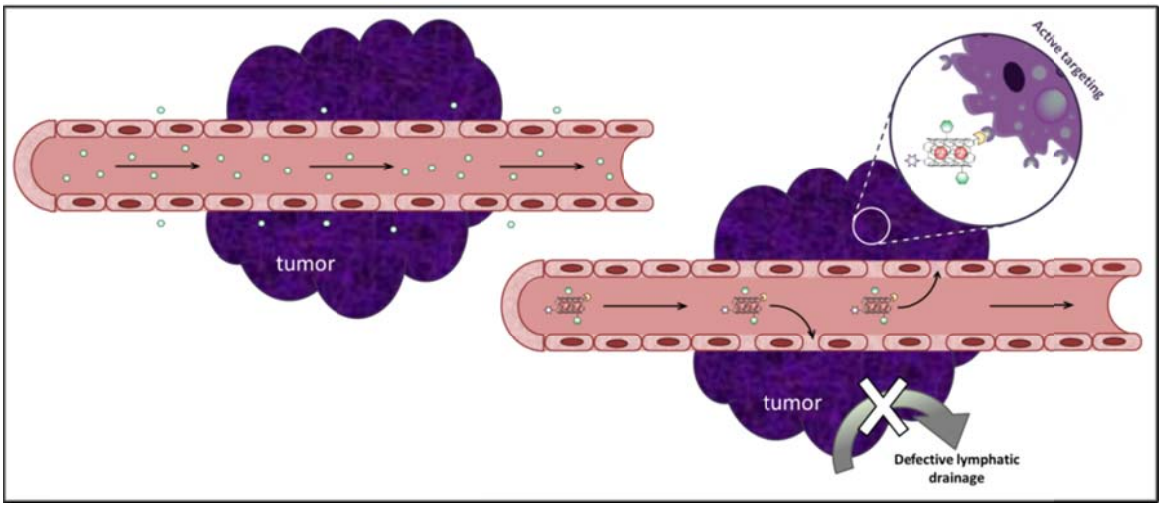

Figure 9. Enhanced Permeability and Retention effect for a model CNT-based drug delivery system.

Carbon nanotubes (CNTs) are among the most promising possible drug nanovectors currently under study. They are made almost entirely of carbon, a part from residual metallic particles coming from the synthetic procedure, which are usually removed by a purification step when a biological application is intended. They combine therefore the biocompatibility of liposomes or polymeric nanoparticles, with the stability of inorganic nanoparticles, such as gold or silica ones.

When a material is proposed for biomedical applications, it is fundamental to establish its toxicity profile and its *in vivo* fate. Even though the question is still under debate, due to the plethora of variables such as the different CNT functionalizations, it appears that adequately functionalized CNTs are non-cytotoxic. In fact, it has been demonstrated that highly water-soluble functionalized CNTs are uptaken by immune system cells without being toxic and preserving their activity,[46] and it has been found that CNTs are more toxic as agglomerates than as good dispersions.[47] Coherently with these observations, other authors reported correlations between a higher degree of functionalization for SWCNTs and a lower toxicity towards human

dermal fibroblast. Interestingly, covalently modified SWCNTs appeared to be less cytotoxic than the ones stabilized trough surfactants.[48] Importantly, numerous studies by different groups have proven so far how surface-modified CNTs are well tolerated *in vivo*.[49] In general they have a blood clearance half-life in the order of hours. Moreover, tissue biodistribution studies showed that they are eliminated into urine, via glomerular filtration, or into faeces with low residual amounts in the body. All these results indicate how the *in vivo* behaviour of these materials could be modulated by the degree and kind of functionalization, two critical aspects that need to be accurately controlled.

Furthermore, some recent works showed *in vitro* enzymatic degradation of SWCNTs, thus presenting another possibility for the elimination of this carrier from the body once the therapeutic function has been exerted.[50] Importantly, it has been shown that MWCNTs take more time to be degraded than SWCNTs, and the process seems to occur gradually from the external walls towards the inner ones. Moreover oxidized MWCNTs were more easily degraded than pristine tubes, indicating that defects introduced through oxidation probably facilitate the attack from the enzyme.[51] Anyway further studies, especially *in vivo*, are necessary to assess if CNT metabolic digestion is actually possible.

1.5.1 Uptake Mechanism

Carbon nanotubes are able to enter cells, as recognized by the scientific community, but the way it happens is still controversial. In fact, although many studies have been carried out so far to understand which is the uptake mechanism, still there is not a unique answer to the question. The type of cell should be taken into account when comparing different results and, more importantly, the type of CNTs could play a crucial role. In fact, the great heterogeneity of this material implies the possibility of heterogeneous behaviour in a biological environment. CNTs can differ a lot in size and functionalization, thus giving a plethora of derivatives, from almost naked to differently coated ones.

Among the existing hypotheses, one is phagocytosis, a process employed by specialized cells, in fact different authors observed engulfment of CNTs by phagocytes. Cherukuri et al. treated mouse peritoneal macrophage-like cells with SWCNTs and visualized the nanotubes inside the cells exploiting their spontaneous NIR fluorescence.[52] They observed the tubes confined in small vesicles, probably phagosomes, derived from an active ingestion process, which is consistent with their observation of a temperature-dependence of the uptake. Porter et al. studied the uptake of SWCNTs by human monocyte derived macrophage cells and found them inside lysosomes and phagosomes,[53] while the treatment of the same cell line with

MWCNTs led to frustrated phagocytosis, an incomplete phagocytosis, probably due to the big size of the nanotubes used (diameter of about 70 nm and length ranging from few to several µm).[54] Four weeks after the subcutaneous implantation of 200 nm long MWCNTs in rats, they were found inside lysosomes of macrophages.[55] On the other hand, frustrated phagocytosis with consequent cellular stress was observed for human monocytes treated with long MWCNTs (also in this case from few to several µm).[56] Other authors also used long MWCNTs (200-400 µm) and observed their internalization by mouse microglia cells and murine glioma cells.[57] Even if they did not specifically investigate the uptake mechanism, their results suggest two main possibilities: phagocytosis, supported by the higher internalization observed for microglia cells, which are phagocytic cells, and a needle-like penetration, supported by TEM images clearly showing single nanotubes piercing the cell membrane.

The needle-like penetration, consisting in a direct insertion of CNTs across cell membranes, and the endocytosis represent the two more important mechanisms for the uptake of CNTs by mammalian cells (Figure 10).

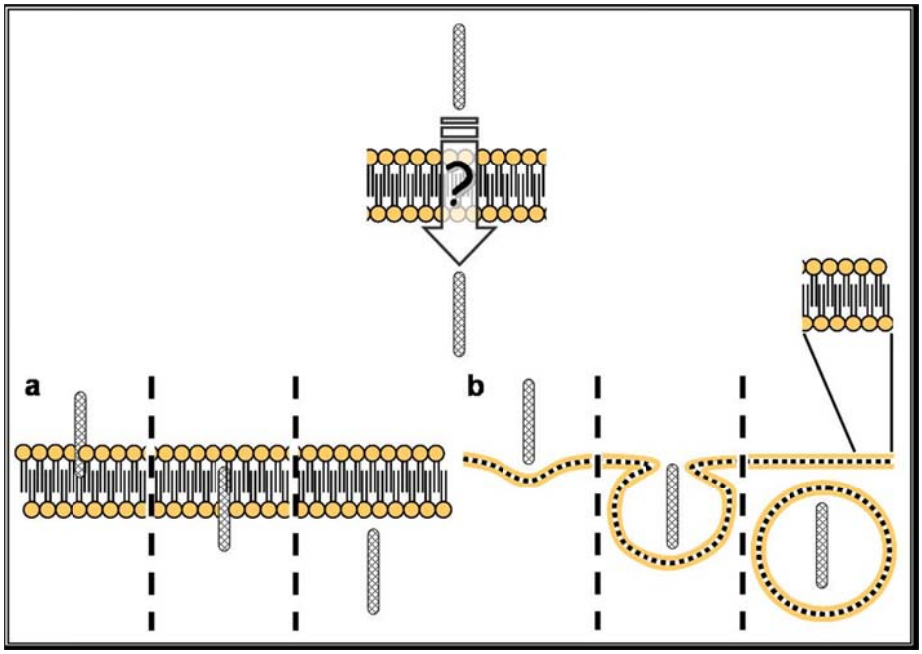

Figure 10. Nano-needle (a) and endocytosis (b) penetration mechanism.

Kam et al. proposed for the first time the endocytosis internalization pathway for CNTs in 2004, treating human leukaemia cells and human T cells with SWCNTs functionalized with biotin and fluoresceinated streptavidin. The intracellular fluorescence distribution was found to overlap the signal of an endosome marker. Moreover, the uptake was blocked at 4°C, consistently with energy-dependent endocytosis.[58] Similarly, in other works by the same authors the lack of intracellular fluorescence at 4°C and the co-staining with endosome markers suggested an endocytotic process for SWCNTs functionalized with fluorescently labelled DNA or

proteins (MW < 80kDa).[59] The authors speculated about a hydrophobic interaction between the naked SWCNTs surface and the cell membrane as the driving force for the internalization. In a later work, they expanded the studies to precisely understand the uptake mechanism.[60] The internalization inhibition was observed with NaN_3 pre-incubation of the cells, confirming endocytosis, since ATP-production and therefore energy-dependent activities are strongly reduced by this chemical agent. Moreover, with a well-designed experimental set endocytosis was found to happen through clathrin-coated pits, rather than through caveolae or lipid-raft pathway. Endocytosis has been suggested as the uptake pathway also by other authors. DNA-wrapped SWCNTs were tracked during *in vitro* trafficking exploiting their intrinsic NIR fluorescence.[61] Each trajectory was then associated with a specific kind of motion, recognizing that SWCNTs were adsorbed onto the membrane and internalized through endocytosis. Once inside the cell they diffused consistently with confinement inside vesicles, and they finally underwent exocytosis. Moreover, co-localization experiments showed an overlap between SWCNTs and lysosomes inside the cells, confirming again the endocytotic uptake. The authors proposed this mechanism as a result of the SWCNTs coverage by the proteins present in the medium. This coating should lead to a subsequent clustering in aggregates, big enough to reach the radius cutoff thermodynamically required for being endocytosed.[62] Wang et al. functionalized MWCNTs with the enzymatic toxic domain of ricin (RTA) in a non-covalent way, and studied its uptake mechanism by HeLa cells, observing clathrin-mediated endocytosis.[63] The internalization of SWCNTs-QD-streptavidin by CD3 positive-leukaemia cells was also studied, monitoring the intracellular QDs fluorescence.[64] In this case the system was rather complex, in fact the uptake was mediated by the recognition of three components. First, a biotinylated anti CD3-antibody bound CD3 receptor on cell membrane and subsequently the streptavidin-bearing SWCNTs attached the biotinylated antibody, showing high internalization. On the contrary, poor internalization was observed when the antibody was absent, with the use of non-biotinylated antibody, when experiments were carried out at 4°C and when the cells did not express CD3-receptor on the membrane (CD3 negative cell line). All these data suggest a receptor-mediated endocytosis for this construct.

To target cancer cells, Bhirde et al. described the use of a drug delivery system based on a cisplatin-SWCNT conjugate, exploiting the interaction of the epidermal growth factor (EGF) with its receptor (EGFR), over-expressed on the surface of many cancer cells.[65] The authors demonstrated the efficient internalization of the SWCNT-EGF conjugate *in vitro*. Moreover they proved that it is actually mediated by the ligand-receptor interaction, since the uptake was drastically reduced knocking down the receptor expression. These findings are consistent with

receptor-mediated endocytosis. Nevertheless, a certain degree of internalization observed even without receptor let consider other possibilities, as stated by the authors themselves. Another paper conceiving two options for the uptake mechanism has been published in 2008.[66] The authors prepared SWCNTs bearing taxoids and biotin molecules, as a drug delivery system targeted towards cancer cells over-expressing the biotin receptor, demonstrating the actual internalization of the whole conjugate, hindered by both incubation at 4°C and presence of NaN_3, and strongly reduced by saturation of accessible receptors *via* biotin pre-treatment, in accordance with receptor-mediated endocytosis. On the other hand, they observed a strong decrease in the uptake of SWCNT derivatives without biotin at low temperatures (4°C), but no changes when NaN_3 was added. This behaviour is consistent with a non-endocytotic process, as the needle-like diffusion through membranes, which is temperature-dependent but energy-independent.

It is necessary to consider that temperature can affect not only endocytosis but also membrane piercing, in fact as simple diffusion of a molecule in a liquid is influenced by temperature, the same could happen to CNTs in biological media. More importantly, the fluidity of cellular membranes, which are made of phospholipidic bilayers, is strongly dependent on temperature. As a consequence, the mobility of an object in the bilayer will increase with temperature. Thus, it is not surprising that a decrease in temperature has been sometimes correlated with a decrease in cellular uptake of CNTs, and this experimental observation alone should not necessarily mean endocytosis, unless it is corroborated by other evidences. Therefore some cases of CNTs internalization ascribed to endocytosis by the authors could be also differently interpreted.[67] The same observation can be applied to the work published by Cheng et al.[68] In this well-conceived study of cellular internalization of fluorescently labelled SWCNTs derivative by several mammalian cell lines, the authors compared the results obtained in normal conditions with the ones obtained at 4°C and in the presence of sodium azide. While for the former the uptake was almost completely blocked, the latter showed an intracellular fluorescent signal weaker but comparable with the normal conditions, differently from what stated by the authors (for a better understanding see Fig. 2B of Ref. 68). Therefore it is possible to conclude that both an energy-dependent and an energy-independent mechanism are contributing to the CNTs uptake by cells in this case. Moreover the author co-incubated cells with labelled Dextran, known to be uptaken by endocytosis, and found it in the endosomes, while the fluorescence from the SWCNTs was in the nucleus, indicating that either the retention time inside the endosomes or the entire uptake pathway was not the same for the two compounds.

The nano-needle penetration mechanism for CNTs was proposed in 2004. Internalization of functionalized CNTs was found even in energy-depleting conditions, and ultrathin transverse sections of HeLa cells incubated with the CNTs were analyzed by TEM, observing MWCNTs inside cells and in the act of crossing the membrane.[69] Therefore the authors hypothesized that the cylindrical shape of CNTs let them directly insert across biological membranes, like a Nano-needle. This description is in accordance with what observed for some peptides and proteins exhibiting non-classical transport activity[70] and also with what has been predicted for nanotube-shaped objects.[71] Another theoretical study, instead, reported that the energy cost for a SWCNT to insert into a model phospholipid bilayer is too high to occur only because of thermal motion energy.[72] Nevertheless further studies on the penetration of a patterned CNT were performed by the same authors. Since probably CNTs in a biological environment will not have a homogeneous surface, but will be covered by biomolecules, they studied a CNT covered by alternating bands of hydrophilic and hydrophobic regions. This model can be also representative of a CNT functionalized with hydrophilic groups, since usually functionalization do not cover the whole CNT surface. In this case the energy required by CNTs to traverse the bilayer was much lower, thus resulting in enhanced penetration.[73] The same internalization pathway was proposed for a huge selection of cell types, since a comprehensive study revealed effective CNTs internalization even by cells unable to carry out endocytosis or under conditions that prevent energy-dependent processes.[74] The cells were treated with differently functionalized SWCNTs and MWCNTs, which were not coated by macromolecules. As speculated by the authors, the discrepancy between these results and the endocytotic hypothesis can lie in the different kind of CNTs derivatives used.

Zeineldin et al. wrapped PL-PEG2000 onto SWCNTs and found that when the PEG integrity was preserved, the coating prevented the non-specific uptake by cells (different ovarian cancer cell lines), while the PEG fragmentation (by sonication for a prolonged period, i.e. 1 hour) allowed CNTs internalization by cells.[75] A further functionalization of the PEGylated, not sonicated, SWCNTs with a specific targeting molecule led to selective uptake by cancer cells over-expressing the receptor for that molecule. Although the authors did not speculate on possible uptake mechanisms, these findings underline the importance of CNTs coatings in determining their biological fate.

CNT size seems to have a role as well. A recent work compares the internalization by human hepatocellular carcinoma cells of different CNTs: namely MWCNTs with a diameter of 10-30 nm (long and short, i.e. 1-2 µm or 0.5-1 µm long) and SWCNTs with a diameter of 1-3 nm (long and short, i.e. 100-200 nm or 50-100 nm long).[76].All the CNTs were non-covalently functionalized

with chitosan. The authors reported internalization only for SWCNTs, and with different mechanism according to size: for long SWCNTs the mechanism observed was mainly clathrin-mediated endocytosis, while for short SWCNTs they describe also endocytosis via caveolae and direct insertion across cell membrane.

Evidences supporting the piercing hypothesis were reported elsewhere. SWCNTs were observed translocating across the lipid bilayer and entering the cytoplasm.[53,77] SWCNTs and MWCNTs were found across the plasma, lysosomal, and nuclear membranes,[78] and, by TEM, MWCNTs were observed both inside cytoplasmic vacuoles of epidermal keratinocytes (consistently with endocytosis) and piercing the nuclear membrane.[79] Similarly, as aforementioned, Kateb et al. presented TEM visual confirmation of membrane insertion of MWCNTs.[57]

A very interesting study, published in 2008, confirmed the ability of CNTs to cross biological membranes, considering the question from a rather different point of view. MWCNTs were visualized while traversing the fenestrated endothelium in the glomerular filtration system of mice and crossing the renal filtration membrane. In order to do so the tubes had to adopt an adequate spatial conformation, facing the filtration barrier perpendicularly, since the fenestration size is compatible only with the traverse dimension of these MWCNTs, to let them pass and pierce the underlying basal membrane.[49c]

Further hint for understanding CNT ability to cross cell membranes could be given by another paper.[80] During an *in vitro* experiment MWCNTs were guided through a magnetic field towards mammalian cells and they cross the membrane spearing it, and thus translocating inside cells their cargo, i.e. a vector containing the sequence for a fluorescent protein, that allowed the recognition of cells internalizing it. SEM pictures of cell surface confirmed the presence of the CNTs that actually look like spearing it. This work aimed to prove that actively guiding CNTs towards cells, it is possible to induce a temporary permeabilization of the membrane, as effect of its Nano-mechanical penetration. The system was thought to be exploited for delivery purposes, since, despite the great efficiency of transfection, it leads to minor perturbation of cells. A recently published work confirmed this property, suggesting the possible use of CNTs as cellular endoscopes.[81] The authors of this paper prepared an endoscope ending with a MWCNT (with a diameter in the range of 50-200 nm or more and a length of 50-60 μm) and found that, thanks to its narrow cylindrical shape, it produced no cell damage, and it resulted in less mechanical stress for the cell compared to common conical glass pipettes, even for prolonged periods.

In conclusion, many different studies aimed at understanding CNT uptake mechanism by cells, considering the question from different points of view. The discrepancy between the results present in literature can lie in the different kind of CNTs derivatives used. Considering all the works published so far, we could conclude that both endocytosis and needle-like piercing of the membrane exist and can contribute to internalization of CNTs, with a predominance of needle penetration when internalization is driven by the CNTs, i.e. when CNTs are functionalized with non-bulky molecules. Whereas, when CNTs are coated with big molecules or with molecules that trigger a specific receptor-mediated endocytosis, this mechanism prevails.

1.5.2 Delivery of antineoplastic chemotherapeutic drugs

The most studied possibility in CNT-based cancer therapy is drug delivery, in which CNTs are used as vehicles for a chemotherapeutic agent, in order to improve its delivery to the target.

Doxorubicin is a drug widely used in clinical cancer treatment and it is very interesting to study its delivery through nanocarriers. So far, a number of works in which carbon nanotubes were used for this purpose has been published. In one of the first papers doxorubicin was bound to copolymer-coated MWCNTs forming a supramolecular complex based on π-π stacking.[82] The cytotoxicity of this derivative was tested *in vitro* on human breast cancer cells showing an increased mortality rate in comparison with doxorubicin alone. This drug was also bound, through supramolecular chemistry, to two different water-soluble SWCNTs: non-covalently functionalized with a phospholipidic-PEG surfactant and oxidized SWCNTs covalently PEGylated through amidation of the carboxylic moieties.[83] The authors suggested π-π stacking and hydrophobic interactions as the binding forces between doxorubicin and nanotubes. Moreover they report a pH-dependent interaction: the loading was made at pH 9, condition at which doxorubicin is deprotonated and so has low water solubility, reaching a doxorubicin/nanotubes weight ratio of ~4:1; a decrease in the pH led to the release of the drug from the SWCNT carrier due to the its consequent higher hydrophilicity. This mechanism could be very useful in cancer therapy due to the acidic environment of extracellular tissues in tumour, potentially leading to selective drug release *in vivo*. The cytotoxicity of the phospholipidic-PEG wrapped SWCNT-doxorubicin construct was tested on human glioblastoma cancer cells. The derivative induced cell death similarly to free doxorubicin at a concentration of 10 μM, although the observed IC_{50} value was higher (~8 μM for the carbon nanotube conjugate compared to ~2 μM for free doxorubicin). Furthermore, a targeted doxorubicin delivery was tested using a cyclic arginine–glycine–aspartic acid (RGD) peptide, which acts as recognition moiety for integrin $\alpha_V\beta_3$ receptors, over-expressed in a wide range of solid tumours. The targeting agent was bound on the PEG

chain of the non-covalent SWCNT derivative, and then doxorubicin was loaded. This conjugate, tested on integrin $\alpha_V\beta_3$-positive cells, showed enhanced drug delivery compared to the derivative without RGD, according to the degree of brightness in confocal fluorescence experiments and to the IC_{50} value, which was smaller (~3 μM) for the RGD-bearing derivative than for the one void of any targeting agent. The behaviour of phospholipidic-PEG wrapped SWCNT-doxorubicin complex was studied also *in vivo* into SCID mice bearing Raji lymphoma xenografts.[84] The authors observed higher tumour uptake, probably due to the prolonged circulation half-life of the construct, and greater inhibition of tumour growth with respect to the free drug but the therapeutic efficacy was not better than DOXIL (liposomal Doxorubicin). On the other hand, differently from DOXIL, SWCNT-doxorubicin caused neither significant toxicity nor mortality, allowing the use of higher doses. Treatments with 10 mg/kg (instead of 5 mg/kg) of SWCNTs-doxorubicin (dose normalized on doxorubicin) led to improved efficacy, still without causing any severe toxicity, whereas 5 mg/kg of free doxorubicin or DOXIL resulted in strong decrease in the weight of the animals and mortality rates of 20% and 40%, respectively. The possible reasons for this behaviour involve different aspects: the bigger size of the SWCNT construct with respect to free doxorubicin probably slowed down glomerular filtration, and, moreover, the PEG coating could have hidden doxorubicin from macrophages. Both these effects could determine prolonged blood circulation, thus enhancing tumour accumulation because of EPR effect. Moreover the slightly acidic microenvironment of tumours should facilitate doxorubicin detachment from the SWCNTs, as previously reported,[83] therefore leading to selective drug release. Nevertheless the same authors observed a slow *in vivo* dissociation of doxorubicin from the SWCNTs after administration, and this fact can suggest that non-covalent constructs cannot guarantee proper *in vivo* stability. An *in vivo* targeting study was also performed with PEGylated SWCNTs functionalized with RGD peptide.[85] After tail vein injection into U87MG tumour-bearing mice, the nanotubes accumulated in tumour (13% ID/g in 24 h), with no obvious toxicity or negative health effects for the animals. Zhang et al. prepared a different kind of SWCNT-based vector for doxorubicin.[86] First CNTs were oxidized, thus introducing carboxylic groups, and then derivatized via wrapping with two different polysaccharides, namely sodium alginate, which is anionic, and chitosan, which is cationic. Doxorubicin was then loaded on the modified SWCNTs and the interaction was mediated probably by electrostatic interactions and π-π stacking. The release of doxorubicin in acidic condition (pH 5.5) was assessed, in order to mimic the typical environment of lysosomes or cancerous tissues, finding a release of almost 40% in 72 h, while the construct was stable at pH 7.4. Finally, an identical conjugate bearing folic acid (linked to chitosan) was prepared, to target

tumours overexpressing the folate-receptor. *In vitro* tests on HeLa cells were performed to evaluate cellular uptake, by fluorescence microscopy, and cell viability. The compound led to stronger reduction in cell viability then the drug itself, proving its efficacy as targeted delivery system. A triple functionalized SWCNT derivative was prepared, bearing doxorubicin, fluorescein and a targeting antibody that recognizes carcinoembryonic antigen (CEA), a tumour marker relevant for a variety of adenocarcinomas.[87] Doxorubicin was non-covalently loaded on oxidized SWCNTs by π-π stacking. Afterwards a fluorescein-labelled BSA was covalently attached through its amines to the carboxylic groups present on the oxidized SWCNTs, via amidation reaction. Finally the antibody was tethered through its amines to the BSA carboxylic groups again with an amidation step. In this way the authors designed a construct that should target CEA-overexpressing cancer cells, be internalized by endocytosis, and release doxorubicin at lysosomal acidic pH. The fluorescein was introduced to localize the SWCNT construct by the fluorescent signal after doxorubicin release. The internalization by WiDr human colon cancer cells was studied by confocal microscopy: after a 4 h treatment, the fluorescently labelled SWCNTs were found in the cytoplasm, while doxorubicin was localized in the nucleus, where the drug exerts its activity. As a control, the fluorescein-labelled BSA did not show internalization to the same high extent, indicating the good ability of CNTs to act as vectors. Nevertheless no information on the cytotoxicity of the complex is reported, nor any stability study to evaluate the release of doxorubicin from CNTs. With a different approach, doxorubicin was linked to pyrene and this system was non-covalently bound to SWCNTs via π-π bonding driven by the polyaromatic unit.[88] The linker between doxorubicin and pyrene was a short chain with a carbamate group, designed to be enzymatically cleaved inside lysosomes. *In vitro* studies on a mouse melanoma cell line were performed to assess the internalization of the construct and its cellular toxicity. The results showed accumulation in the lysosomes and cell growth inhibition (via apoptosis) in a time- and dose-dependent manner, approaching the doxorubicin profile for the 72 h treatment. Furthermore, the therapeutic efficacy was evaluated *in vivo* on melanoma-bearing mice. Free doxorubicin and SWCNT-doxorubicin induced similar reduction of tumour volume, with a significant decrease of systemic toxicity for the CNT construct, according to animal body weight, organs weight and histopathological analyses. Also in this case the release of the drug from the CNTs was studied, comparing the effect of incubation with cell lysate to the use of normal buffer. Though the former system was significantly more efficient, proving that intracellular enzymes play a fundamental role, a release was observed also in the latter case, demonstrating how a non-covalent construct is not completely stable in biological environment. With the double aim of obtaining a targeted drug delivery system and of overcoming MDR, SWCNTs were

functionalized via amidation with an antibody directed towards P-glycoprotein, one of the main actors of MDR.[89] Subsequently the Ab-SWCNTs construct was non-covalently loaded with doxorubicin, via π-π stacking. This construct was tested *in vitro* on human leukaemia cells, overexpressing P-gp on their surface and, therefore, resistant to doxorubicin. Cells were exposed to NIR radiation to trigger doxorubicin release, as a consequence of NIR absorption by SWCNTs. This system was indeed able to triplicate the amount of doxorubicin released in 24 h, but it should be underlined that a partial release was observed without NIR radiation as well. The Ab-CNT construct resulted to be bound to the cell membrane and doxorubicin was localized inside cells, in much higher amount with respect to treatments with free doxorubicin. Doxorubicin alone or together with anti P-gp antibody (at a concentration of 5 μg/mL) could partially inhibit cell growth, but, increasing the incubation time after treatment (from 24 h, to 48 h, to 72 h), cells gradually recovered and started growing again. Instead, very interestingly, the SWCNT construct, used at an equivalent concentration of drug, inhibited cell growth more efficiently than the free drug and in a time-dependent way, probably due to a slow drug release from the vector surface.

Methotrexate is another well-known anticancer drug, which suffers, as many others, from low bioavailability and toxic side effects. Preliminary studies of CNT-based drug delivery with this drug were performed by Pastorin et al.[90] MWCNTs were covalently functionalized with methotrexate and fluorescein at the same time and results obtained on human Jurkat T lymphocytes showed a rapid internalization of the compound, even though the efficacy of the construct was lower than the free drug. In a more recent work the same drug was bound to MWCNTs through cleavable linkers. The use of a peptide recognized by intracellular proteases led to a significant decrease in MCF-7 breast cancer cell viability if compared to free methotrexate.[91] Therefore it is possible to conclude that the lower efficacy in the first approach was probably due to the lack of drug release once the construct was internalized.

Taxanes represent another class of antineoplastic drugs that, to date, have already been conjugated to CNTs for new drug delivery approaches. Paclitaxel (PTX), which belongs to this class, was covalently bound through an ester bond to the PEG of non-covalently PEGylated SWCNTs and i.v. injected into xenograft tumour-mice (PTX resistant 4T1 murine breast cancer mice model) to test the *in vivo* efficacy.[92] Results were very promising, showing a tumour growth inhibition value of almost 60% for the SWCNT-PTX derivative, much higher than the one reported for Taxol and PEG-PTX (28% and 21% respectively). Higher apoptosis level and lower proliferation active cells level were observed after CNT derivative treatment, when compared to the drug alone. It is important to underline the lack of toxicity in mice for these PEGylated

SWCNTs themselves, demonstrated by the authors in another work.[49e] The evaluation of the pharmacokinetics showed a longer plasmatic half-life for SWCNT-PTX, coherently with the enhanced hydrophilicity of the conjugate with respect to the drug itself, and much higher PTX presence in RES organs (liver/spleen) and intestine 2 h after injection. This is a predictable behaviour for nanomaterials in general and could give concern for the toxicity towards these organs. Nevertheless the authors reported differences between the biodistribution of SWCNT and PTX, indicating a rapid release of the drug from the conjugate probably due to ester cleavage by carboxylesterases. As a consequence the drug seemed to be rapidly excreted, lowering its toxicity. Importantly, tumour PTX levels were 10 times higher for SWCNT-PTX derivative than for free taxol 2 h after injection and tumour-to-normal organ/tissue PTX uptake ratio was bigger, thus indicating a better selectivity of the CNTs-delivered drug. Chen et al performed another study with the same class of drugs.[66] They prepared a covalent derivative of SWCNTs bearing a taxoid molecule and biotin as targeting unit towards cancer cells overexpressing its receptor, thus leading to receptor-mediated endocytosis. This construct was intended to be a prodrug, which frees its cargo, once inside the cell, upon reduction of the disulphide bond by endogenous thiols such as glutathione (GSH), whose concentrations are typically more than 10^3 times higher in tumour tissues than in blood plasma. Therefore, the system should act specifically on cancer cells, leading the taxoid to carry out its mitosis inhibition action only in the desired sites. The authors demonstrated the actual internalization of the whole conjugate in leukaemia L1210FR cells, by means of confocal fluorescence microscopy, thanks to the presence of a fluorescent tag covalently bound to the taxoid molecule. Moreover, in the case of a control SWCNT derivative without biotin, they observed a temperature-dependent but energy-independent internalization. This is coherent with a non-endocytotic mechanism, in accordance with the hypothesis of a needle-like diffusion of carbon nanotubes through cell membranes. On the other hand, for the biotin-conjugate, the mechanism observed was endocytosis, and the internalization degree was far higher if compared to the one for cells not expressing the biotin receptor. Furthermore the authors proved the efficient release of the drug by GSH and the binding of the conjugate to the microtubule network, where it exerts its cytotoxic action, with an IC_{50} value smaller than the one for the drug alone, probably due to the increase in the drug uptake.

Also platinum analogues have been investigated in CNT-based drug delivery for cancer treatment. In a first work, Lippard and co-workers reported the preparation of a Pt(IV)-based SWCNTs prodrug able to deliver and release the drug inside cells, leading to intracellular concentrations 6 times higher than the ones reached treating the cells with the free drug.[93]

More recently the same group prepared another Pt-based targeted prodrug using SWCNTs as a longboat.[94] The derivative was prepared binding folic acid, whose receptors are overexpressed in many cancer cells, to a Pt(IV) compound, and tethering this conjugate to CNTs through an amidic coupling with terminal amines of wrapped phospholipid-PEG chains. The Pt(IV), once inside cells, can be reduced thanks to acidic endosomal pH, therefore losing the two axial ligands and leading to the active Pt(II) compound. The authors demonstrated internalization via folate receptor-mediated endocytosis (FRME), and the to kill cancer cells (human choriocarcinoma and human nasopharyngeal carcinoma) with IC_{50} values more than 8 times lower than cisplatin alone. Moreover the formation of the major reaction product of cisplatin with DNA was detected, using a specific monoclonal antibody, proving the actual ability of the system to act as a prodrug, generating the cytotoxic derivative once internalized and thus killing in a selective way folate receptor overexpressing cells. Also cisplatin-delivery systems based on drug-SWCNT covalent bioconjugates were investigated.[65] The interaction of the epidermal growth factor (EGF) with its receptor (EGFR), overexpressed on the cell surface of a big variety of cancers, was exploited to target CNTs both *in vitro* and *in vivo*. The efficient *in vitro* internalization in head and neck squamous carcinoma cells of the SWCNTs-EGF conjugate was proved and resulted to be mediated by the EGF-EGFR ligand-receptor interaction. Furthermore quantum dot (Qdot)-functionalized SWCNTs were administrated to a tumour-bearing athymic mice to study the short-term biodistribution. The results showed a much higher accumulation within the tumour mass of the EGF-conjugate compared to the control without EGF. Small amounts of CNTs were found within spleen, lungs, liver, kidneys and heart, regardless of the presence of EGF. Finally, the animals were treated with SWCNT-cisplatin-EGF showing a decrease in the tumour growth in comparison with the untargeted SWCNTs-cisplatin conjugate, demonstrating that SWCNTs can selectively deliver cisplatin *in vivo* towards EGFR overexpressing cancer.

Another interesting approach for the functionalization of CNTs, exploited also in oncology studies, is the filling of the nanotubes. This method was first investigated by Green's group in 1994 and involves the opening of MWCNTs' caps by a nitric acid treatment and the filling of the inner cavity through a wet chemistry approach.[95] It was applied to fill the tubes with different materials, among which carboplatin, a widely used chemotherapeutic agent for cancer treatment.[96] MWCNTs were opened with nitric acid and subsequently filled sonicating them in a carboplatin solution at different temperatures. Finally, they were cleaned from particles deposited on the outer surface, washing them in water and in ethanol. The derivatives were characterized trough different techniques to confirm the presence of the drug inside the tubes, and it was shown that the best temperature for the filling protocol was 90°C, leading to a drug

loading of 30 % in weight. This derivative was then tested on human bladder cancer cells to evaluate its cytotoxicity and the test showed reduced cell viability compared to the drug alone. More recently also cisplatin was encapsulated into CNTs, in this case single-walled ones, the diameter of which is big enough to host the drug.[97] The SWCNTs were opened by concentrated acid treatment, and subsequently annealed at 850°C under high vacuum in order to remove oxygen functional groups introduced in the first step. The filling with cisplatin was achieved by stirring at 40°C the SWCNTs in a DMF solution of the drug for 48 h. The release of the drug in physiological solution was studied, finding that it started after 24 h and continued up to 72 h, and the inhibition of cell growth on two prostate cell lines (DU145 and PC3) obtained with the construct was comparable to the one caused by the free drug.

Another antineoplastic drug, namely 10-hydroxycamptothecin (HCPT), was covalently attached to MWCNTs to study the influence of CNTs on drug efficacy.[98] MWCNTs were first oxidized with a 36 h acid treatment, and the carboxylic groups thus introduced underwent an amidation step to introduce a spacer bearing a terminal protected amine. After deprotection of the amino group, an ester derivative of HCPT was bound to the construct via an amide bond. The ester linkage, hydrolytically unstable, was introduced to subsequently trigger the release of the drug. The authors observed a small drug release (< 15% after 128 h) under both acidic or basic conditions, and a much higher release (80% after 128 h), when incubating the construct with fetal bovine serum, which contains esterases that could catalyse the hydrolysis. Furthermore a fluorescein molecule was bound to the unreacted amine after HCPT conjugation, for *in vitro* tests on human gastric carcinoma cells. Fluorescence confocal microscopy permitted to localize intracellularly the constructs, with a uniform distribution in the cytoplasm. WST-1 assay revealed a significantly improved cytotoxicity with respect to equal concentrations of HCPT, whereas CNTs alone did not cause any decrease in cell viability. Finally, a different construct bearing DTPA was prepared, in order to chelate technetium (Tc), a radioactive nuclide, for *in vivo* biodistribution studies in tumour-bearing mice. High uptake was found in the liver, spleen, lung, kidney, stomach, femur and tumour. In the latter the maximum uptake level (3.6 % ID/g) was reached within 4 h post injection. The observed blood circulation half-life was of 3.6 h, versus the 30 min reported for HCPT. Since the *in vitro* drug release tests showed that 4 h after incubation with serum only 12% of the HCPT was released, the authors considered that the majority of the conjugate could reach the different organs (and the tumour) without releasing a big amount of drug in the blood stream. The *in vivo* antitumor performance of the HCPT-bearing MWCNTs was also studied, finding a tumour growth inhibition much more efficient than HCPT alone, without causing any severe toxicity to the animals.

Yang et al. delivered gemcitabine-MWCNTs construct to lymphatic vessels, exploiting EPR effect and the specific guidance of an external magnetic field.[99] SWCNTs were functionalized with poly(acrylic acid) and then decorated with magnetite nanoparticles ($FeO{\cdot}Fe_2O_3$) by a co-precipitation step with Fe^{2+} and Fe^{3+}. Three hours after subcutaneous injection in SD rats, the construct was able to reach popliteal lymph nodes without accumulation in the major organs as liver, spleen, kidney, heart and lung, simply by EPR effect. The same CNTs were loaded with the antineoplastic drug gemcitabine by physical adsorption. The system was guided *in vivo* applying a permanent magnet on the projection surface of one popliteal lymph node and very high accumulation of gemcitabine was detected in the lymph node, with a maximum after 24 h. At the same time, the blood plasma concentration was lower if compared to gemcitabine alone, to the treatment without the magnetic field, or to a control represented by nanosized activated carbon decorated with magnetic nanoparticles.

CNTs-based antitumor immunotherapy was explored by Meng et al.[100] This technique employs tumour cell vaccines (TCV), which are made of inactivated cancer cells or dendritic cells presenting tumour antigens, in order to trigger the immune response of the patient against the tumour itself. With the aim of improving the efficacy of TCV, tumour lysate proteins were covalently coupled to oxidized MWCNTs via an amidic bond. The conjugate was injected subcutaneously to H22 hepatoma-bearing mice treated with TCV (controls were performed with TCV + CNTs only and TCV + tumour lysate proteins only). The cure rate was significantly increased with respect to animals treated only with TCV or with TCV + tumour lysate proteins, even if a partial effect was exerted by CNTs alone as well. To assess whether or not the immunity was tumour-specific, the animals survived after treatment with tumour lysate proteins-bearing MWCNTs were challenged again with subcutaneous injection of tumour cells. In the case of H22 cells they rejected the tumour, while they did not reject mouse breast cancer, proving how the therapeutic system made them develop a specific immunity.

Table 1

Compound	CNT type	Drug	Bond drug-CNT		Specific release mechanism (if any)	Specific targeting (if any)	Biological studies		Ref.
			covalent	non-covalent			*In vitro*	*In vivo*	
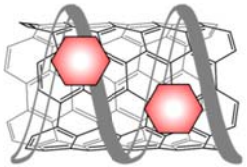	MWCNTs	Doxorubicin		✓	-	-	human breast cancer cells	-	82
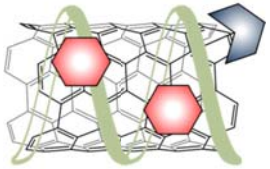	SWCNTs	Doxorubicin		✓	acidic tumour or lysosomal pH	RDG peptide	human glioblastoma cancer cells	-	83
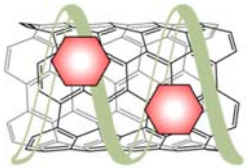	SWCNTs	Doxorubicin		✓	acidic tumour or lysosomal pH	-	-	lymphoma-bearing mice	84
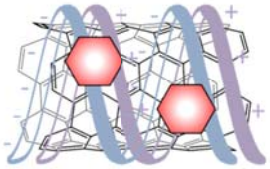	SWCNTs	Doxorubicin		✓	acidic tumour or lysosomal pH	-	human cervical cancer cells	-	86

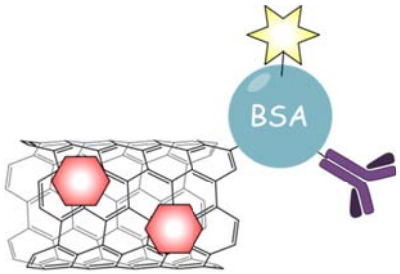	SWCNTs	Doxorubicin		✓	acidic tumour or lysosomal pH	anti-carcinoembryonic antigen antibody	human colon cancer cell line	-	87
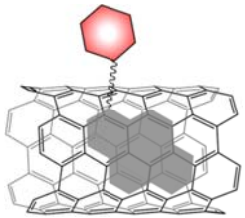	SWCNTs	Doxorubicin		✓	enzymatic cleavage of carbamate	-	murine melanoma cell	melanoma-bearing mice	88
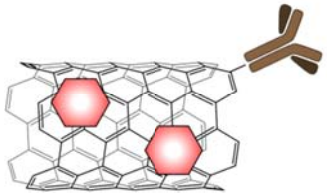	SWCNTs	Doxorubicin		✓	NIR radiation	anti-P-glycoprotein antibody	human leukemia cells	-	89
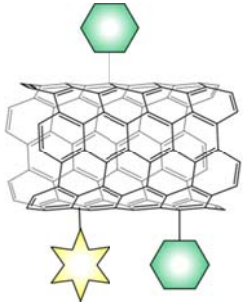	MWCNTs	Methotrexate	✓		-	-	human T lymphocytes	-	90

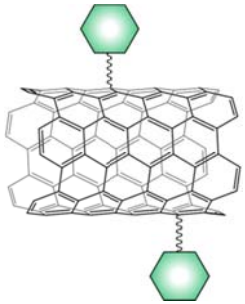	MWCNTs	Methotrexate	✓		enzymatic cleavage of peptidic linker	-	human breast cancer cells	-	91
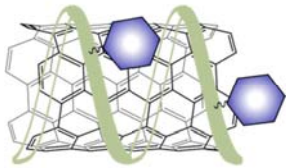	SWCNTs	Paclitaxel		✓	enzymatic cleavage of ester (by carboxylesterases)	-	murine breast cancer cell	murine breast cancer-bearing mice	92
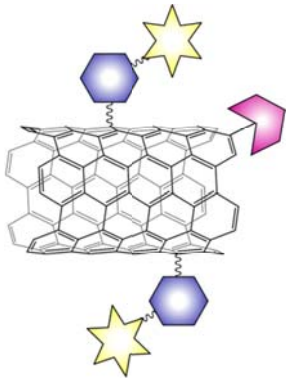	SWCNTs	Taxoid	✓		reduction of the disulphide bond (by endogenous thiols)	biotin	murine leukemia cells	-	66

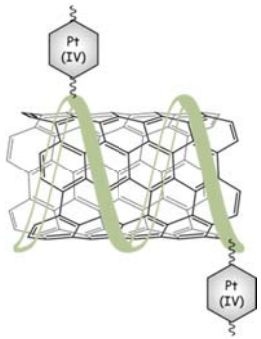	SWCNTs	Cisplatin		✓	reduction from Pt(IV) to Pt(II) due to endosomal acidic pH	-	human testicular carcinoma cells	-	93
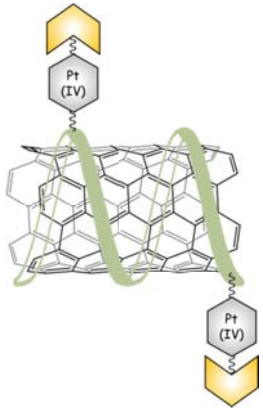	SWCNTs	Cisplatin		✓	reduction from Pt(IV) to Pt(II) due to endosomal acidic pH	folic acid	human choriocarcinoma, nasopharyngeal carcinoma and testicular carcinoma cells	-	94
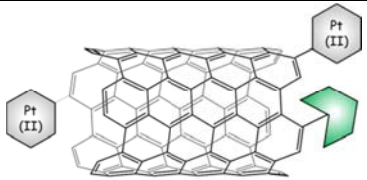	SWCNTs	Cisplatin		✓	ligand exchange (hypothesized)	epidermal growth factor	human head and neck squamous carcinoma cells	human head and neck squamous carcinoma-bearing mice	65
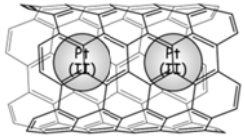	MWCNTs	Carboplatin		✓	-	-	human bladder cancer cells	-	96

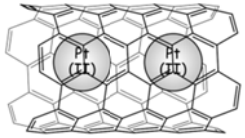	SWCNTs	Cisplatin		✓	-	-	human prostate cell	-	97
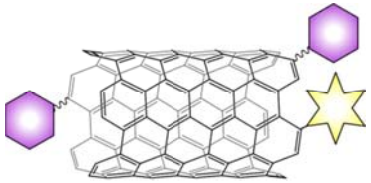	MWCNTs	HCPT	✓		enzymatic cleavage of ester (by esterases)	-	human gastric carcinoma cells	hepatic tumor-bearing mice	98
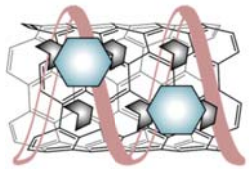	SWCNTs	Gemcitabine		✓	-	magnetite nanoparticles guided with an external magnetic field	-	Sprague–Dawley rats	99
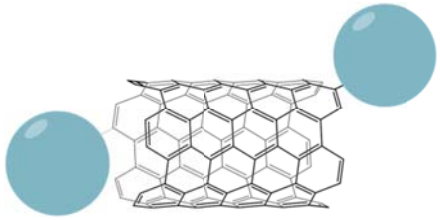	MWCNTs	Tumor lysate proteins (for TCV)	✓		-	-	-	hepatoma-bearing mice	100

1.5.3 Delivery of nucleic acids

The way CNTs can interact with nucleic acids has been extensively studied because it could have very interesting applications. Both antisense oligonucleotides and small interfering RNA (siRNA) are very promising techniques for gene silencing, applicable for the treatment of many diseases. In fact, they can inhibit protein expression, potentially blocking many cellular pathways. Cancer therapy is one of the possible applications, when the targets are oncogenes or genes involved for instance in angiogenesis or chemotherapy resistance.

One of the first studies in this field was performed by Zhang et al.[101] SWCNTs, covalently functionalized via amidation and bearing a terminal ammonium group, were used to complex a siRNA able to silence the expression of telomerase reverse transcriptase and thus to inhibit cell growth. This activity was proved *in vitro,* on different cell lines, both murine and human, and *in vivo*, after intra-tumour injection in xenografted mice. The *in vivo* antitumor activity of a CNT-based siRNA delivery system was also assessed by Podesta et al, using a different kind of construct. MWCNTs, covalently functionalized via 1,3-dipolar cycloaddition and bearing terminal amino groups, were used to load the proprietary siRNA sequence siTOX.[102] The system was injected within the tumour mass on human lung carcinoma (Calu 6) xenografted mice and compared with MWCNTs with a non-coding sequence (siNEG), functionalized MWCNTs alone, and both siTOX and siNEG delivered with cationic liposomes. MWCNTs-siTOX significantly inhibited tumour growth in comparisons to the controls, while cationic liposomes based systems did not affect tumour growth nor increase animal survival. Moreover, tumour tissue analyses revealed extended necrosis in the regions where CNTs accumulated. In the context of targeted delivery, Yang et al. reported the preparation of a folate targeted DNA transporter with CNTs, in principle exploitable to deliver siRNA to cancer cells as well.[103] In fact also in this case the covalently functionalized SWCNTs presented positive charges to form electrostatic interactions with nucleic acids. They bound fluorescently labelled-dsDNA to this derivative, proving by UV a strong enhancement in the loading of ds-DNA for the positively charged SWCNTs in comparison to non-charged SWCNTs. They further functionalized the derivative by wrapping a folic acid modified phospholipid. The complex was tested on mouse ovarian epithelial cells, showing an increased uptake for the derivative with the folic acid, compared to the one without the targeting unit. Furthermore, the fluorescently labelled dsDNA alone was internalized only at a very poor level, thus demonstrating the carrier role of CNTs. In a final experiment, HeLa cells were induced to overexpress folate receptor, culturing them with folic acid free medium, and these cells showed a much higher internalization of the derivative than normal HeLa cells,

confirming the efficacy of the delivery system. In another study, oxidized MWCNTs were complexed to polyethylenimine, to which an antisense sequence was bound by means of electrostatic interactions.[67a] The oligonucleotide was coupled to fluorescent cadmium telluride quantum dots in order to follow the cellular trafficking of the complex. The authors demonstrated for the system an efficient uptake and the expected apoptotic activity. Dendrimer-CNT constructs were also exploited for gene delivery. The anti-survivin oligonucleotide was anchored onto the polyamidoamine (PAMAM) dendrimer covalently attached to the CNTs and transfected into MCF-7 cells.[104] The conjugate distributed mainly in the cytoplasm, endosomes and lysosomes of the cells and was able to release the antisense oligonucleotide, which then exerted its apoptotic activity. The PAMAM dendrimer was also grown directly on MWCNT surface and used as anchoring point for siRNA, after introduction of a trimethylammonium unit on each branch termination. Different dendrimer generations were prepared and their efficacy in delivering a fluorescent oligonucleotide was compared, obtaining the best results for the second generation.[105]

A unique approach conjugated the use of CNTs as nucleic acids delivery system with photodynamic therapy.[106] This therapy represents a very interesting option for cancer treatment, and it is based on the delivery of a photosensitizer, which, upon activation by an appropriate light source, transfers the light energy to tissue oxygen thus generating singlet oxygen, which can react rapidly with cellular molecules and trigger a cellular damage. In this study an aptamer, a synthetic DNA/RNA probe able to recognize and bind a specific target, was covalently bound to chlorine e6 (Ce6), a well-known photosensitizer. Then the aptamer was wrapped on SWCNTs, and they were able to quench 98% of the singlet oxygen generation (SOG) normally occurring upon excitation of Ce6. When the aptamer was involved in the binding to its target, in this case human α-thrombin, it was released from the CNTs, and therefore SOG was not quenched anymore. Phototoxicity on human lymphoma cells treated with the construct was studied, showing a reduction in cell viability comparable to treatment with Ce6 alone, when thrombin was added, indicating the feasibility of a targeted SWCNTs-based system for photodynamic therapy.

All the examples reported demonstrate that CNTs, both single- and multi-walled, are good vectors for nucleic acid delivery and that the transported sequences retain their activity. These results are even more attractive considering that CNTs exert also an important activity against enzymatic digestion.[107] In fact oligonucleotides, when wrapped on SWCNTs, are protected from enzymatic cleavage and interference from nucleic acid binding proteins, increasing their stability in cells.

Furthermore, Li et al. reported that oxidized SWCNTs induced a stabilization of the human telomeric i-motif of DNA. Even though the question still needs to be studied, this very particular possibility could be exploited in anti-neoplastic systems, since the stabilization of telomeric quadruples inhibits telomerase, which is an essential enzyme for the proliferation of cancer cells.[108]

1.6 Alternative CNT-based anticancer strategies

Cancer treatments can be exerted not only by the administration of drugs, and CNT-based systems have been explored also with different approaches.

Some of these works focus mainly on the targeting issue, which is of course of great importance in cancer therapy, without studying a specific therapeutic possibility. A specific recognition of membrane receptor was achieved with Ab-functionalized SWCNTs.[109] They were functionalized with a phospholipid-PEG, in order to increase solubility and to prevent non-specific binding in the biological environment, and subsequently the terminal amines of the PEG were covalently functionalized with two different antibodies (Rituxan and Herceptin). The binding to corresponding membrane receptors (CD20 on B-cells, and HER2/neu on breast cancer cells, respectively) was proved *in vitro* exploiting the intrinsic near-infrared fluorescence of CNTs, thus demonstrating the feasibility of using antibodies as targeting agent in applications such as imaging or drug delivery. Raman spectroscopy was also used as an imaging technique for CNTs.[110] Also in this case a phospholipid-PEG-CNT construct was used. Derivatives bound to different antibodies or to RGD peptide were prepared using SWCNTs with different isotope composition, that display well-shifted Raman G-band peaks. In this way, it was possible to distinguish the different CNT constructs in mixed cellular populations, proving that they were able to selectively recognize their specific target. Raman imaging was used also for both *in vitro* and direct *in vivo* studies by Zavaleta et al., with PEGylated SWCNTs functionalized with RGD peptide (same construct of ref. 85).[111] The *in vitro* data showed that $\alpha_V\beta_3$ integrin-positive tumour cells (U87MG) internalized the construct much better than SWCNTs without RGD and more than $\alpha_V\beta_3$ integrin-negative cells (HT29). Direct i*n vivo* data showed selective prolonged accumulation of the RGD-bearing SWCNTs in the tumour, while the non-targeted SWCNTs gave an initial tumour accumulation, followed by a rapid decrease. With an alternative approach, an antibody was bound to SWCNTs exploiting the high affinity interaction between protein A and the Fc portion of the antibody itself.[112] SWCNTs wrapped with phospholipid-PEG-COOH were bound to protein A by amidation. Then, an anti-integrin antibody, previously marked with fluorescein, was linked to the system. This antibody recognizes a specific integrin overexpressed

on various cancer cells, rendering the construct suitable for cancer targeting. After demonstrating that the construct was not cytotoxic, its internalization was studied via fluorescence confocal microscopy both in integrin-positive (U87MG human glioblastoma cancer cells) and integrin-negative (MCF-7 human breast cancer cells) cell lines, proving the specific targeting. In fact, only U87MG cells internalized the SWCNT construct, while no intracellular fluorescence was detected for MCF-7 cells or for U87MG cells after a pre-treatment with the Ab alone. The authors therefore hypothesized an integrin-mediated endocytosis as uptake mechanism. Bottini et al. studied the internalization of SWCNTs-Quantum Dot (QD)-streptavidin complexes by CD3 positive-leukaemia cells, monitoring the intracellular QD fluorescence.[64] In this case the process was rather complex and the uptake was mediated by a multi-component recognition. First, a biotinylated anti CD3-antibody bound the CD3 receptor on cell membrane, then the streptavidin-bearing SWCNTs attached the biotinylated antibody, showing high internalization. On the contrary, poor uptake was observed when: i) the antibody was absent, ii) a non-biotinylated antibody was used, iii) the experiments were carried out at 4°C and iv) the cells did not express CD3-receptor on the membrane (CD3 negative cell line). All these data suggest a receptor-mediated endocytosis for this construct.

1.6.1 Thermal ablation

A very interesting application of carbon nanotubes in cancer therapy could arise from their intrinsic optical properties, which can be exploited to kill cancer cells by photo-thermal destruction. In fact the optical absorbance of this material is very high in the NIR (near-infrared) region, 700-1100 nm, while biological systems are transparent to these wavelength lights.

It is worth notice that, to our best knowledge, gold nanoshells and gold nanoparticles represent the only other materials which have given good results in photothermal cancer treatment with NIR radiation.[113] In this case the laser intensity and the radiation time used are often higher than the ones needed to kill the cells with CNTs. This observation make CNTs an even more promising candidate in the field, opening the way to further exploration, to reach the laser energy level of 35-45 mJ/cm^2, established as the safety standard for medical lasers.[114]

Among the studies carried out, it is important to distinguish the non-targeted ones, both *in vitro*,[115] and *in vivo*, when CNTs were directly injected in the tumour,[116] and the ones where CNTs were specifically targeted to tumour cells.

The first paper reporting this possibility was published in 2005 by Dai and co-workers.[59a] SWCNTs were non-covalently functionalized with phospholipid-PEG chains bearing a fluorescent tag or a folic acid molecule. The complex was then administered to HeLa cells overexpressing the folate receptor (FR^+ cells) and to normal HeLa cells as a control. The FR^+ cells showed a high

internalization of the folic acid-SWCNTs derivative, imaged by fluorescence microscopy, while the normal cells showed poor uptake. Cells were then radiated by an 808 nm laser (1.4 W/cm^2) for 2 minutes, this treatment resulting in extensive FR$^+$ cell death and in normal proliferation behaviour for cells that did not internalize the carbon nanotubes. A multi-component targeting system was created, binding to SWCNTs two different monoclonal antibodies, specific for breast cancer cells antigens (IGF1R and HER2).[117] The double targeting should ensure high efficacy and selectivity. The derivatives were prepared functionalizing CNTs with 1-pyrenebutanoyl succinimmide, able to stick to the aromatic surface of the nanotubes by π-π interaction, and bearing an anchoring group for linking the antibodies. Cells were incubated with different conjugates and they were then excited by 808 nm photons at 800 mW/cm^2 for 3 minutes. As a consequence, the nanotubes were heated and the increased temperature destroyed the cells that internalized them. After this treatment, all the cells incubated with the IGF1R and HER2 antibody/SWCNTs hybrids were destroyed, while the 80% of the cells incubated with non-specific antibody/SWCNTs hybrids survived, indicating the specific internalization of the nanotubes driven by the presence of specific receptors on cancer cells. In another work, non-covalent SWCNTs-Ab derivatives were prepared exploiting the strong binding between neutravidin attached to the Ab and biotin present on a polymer coating of SWCNTs.[118] They were targeted to human cells presenting the specific antigen for the Ab and subsequent treatment with a NIR laser (808 nm, 5000 mW/cm^2 for 7 min) resulted in a significant decrease in cells viability. Since the disadvantage of non-covalent constructs is, as already mentioned, the possible dissociation in biological fluids, the same authors prepared a covalent SWCNTs-Ab construct by forming amidic bonds between carboxylic groups of oxidized SWCNTs and amines of two different Ab (anti-CD22 or anti-CD25).[119] To assess the specific binding to human Burkitt's lymphoma cells (CD22$^+$CD25$^-$) and phytohemagglutinin-activated normal human peripheral blood mononuclear cells (CD22$^-$CD25$^+$), the cells were treated with the constructs and with fluorescein-conjugated goat anti-mouse immunoglobulin (FITC-GAMIg) and analysed through flow cytometry. The results clearly showed specific recognition of the correspondent cell receptor by the two Ab-SWCNTs conjugates. Finally the thermal ablation of the specifically targeted cells was achieved after exposure to NIR radiation (808 nm laser, 9.5 W/cm^2, for 4 min).

Among cancer thermal ablation studies involving CNTs, an interesting option was recently described by Peng and co-workers.[120] Targeting cancer could be translated more specifically into targeting cancer stem cells. These cells are responsible for formation of metastases, resistance to therapies and restoration of tumours, and therefore they represent a very important target to study and more efforts should be made in this direction. The chosen

targets were $CD133^+$ glioblastoma cells, presenting high tumorigenicity and cancer stem-like properties. SWCNTs were wrapped with chitosan, which was then covalently coupled to CD133 monoclonal antibody. These CNTs were tested *in vitro* with both $CD133^+$ and $CD133^-$ glioblastoma cells, and internalization was observed only by the $CD133^+$ cells, which were subsequently killed upon exposure to NIR laser radiation (808 nm, 2 W/cm^2, for 5 min). Furthermore the treatment with CNTs followed by NIR radiation inhibited spheroid body formation, which represents an index of cells self-renewal. To partially translate the study *in vivo*, CNTs-treated or untreated cells were used to induce tumour formation in nude mice. Two days after the subcutaneous injection the mice were subjected to NIR laser radiation, resulting in significant inhibition of tumour growth when CNTs were used.

All these reports are a further confirmation of the ability of carbon nanotubes to serve as a targeted nanovector for cancer, exploiting in this case a NIR-induced thermal ablation.

1.6.2 Radiotherapy & BNCT

As already mentioned, the main purpose of attaching radioisotopes to CNTs is represented by imaging studies, to determine their biodistribution following the radioisotope traces, but also a therapeutic application can be envisaged. McDevitt et al. reported the preparation of a SWCNT derivative bearing an ^{111}In (Indium 111) chelate and they have studied its biodistribution, finding accumulation mainly in kidney, spleen and liver.[121] The same derivative was then further functionalized with a tumour specific monoclonal antibody, and it was delivered *in vivo* in a murine model of disseminated human lymphoma, showing a selective tumour targeting. Therefore, the replacement of indium with a proper radionuclide would render these constructs ideal for their application in radiotherapy. In fact, the preparation of covalent CNTs-Ab constructs intended to target tumour neo-vasculature for radiotherapy was reported recently by same authors.[122] Angiogenic endothelial cells express on their surface a monomeric cadherin that, forming dimers with cadherins on close cells, constitutes the tight junctions of normal vascular endothelium. In tumours, these cells are poorly connected (that is one of the reasons for EPR effect) and the cadherin are in the monomeric form, which is the only one recognized by antibody E4G10. Doubly functionalized SWCNTs were prepared, binding to the CNTs the specific antibody and the alpha particle-emitting ^{225}Ac (actinium 225) radionuclide generator, able to kill the targeted cell and the tissue in its proximity. The compound was tested *in vivo* via intravenous injection on xenografted tumour-mice: it reduced tumour growth, improving mice survival in comparison to controls bearing different antibody. The success of this approach is very promising because, in principle, the targeting of tumour vasculature renders these kinds of constructs suitable for any kind of solid tumour.

The interesting possibility of employing CNTs in boron neutron capture therapy (BNCT) was explored.[18a] BNCT is based on the reaction between ^{10}B, after it reached the target cells, and a neutron beam, that generates ^{11}B, which subsequently ejects an energetic short-range alpha particle and a lithium ion. These species deposit most of their energy within the cell, seriously damaging DNA. In order to be effective in cancer therapy, the boron needs to reach tumour cells with an adequate concentration and CNTs could be the right candidate, considering their capacity to cross biological membranes. Carborane were derivatized with azides and allowed to react with the double bonds of SWCNTs, leading to the formation of aziridine rings, subsequently opened to give a water-soluble ethoxo-derivative suitable for *in vivo* tests. The derivatives were used in tissue distribution experiments on mice transplanted with EMT6 mammary cancer cells, achieving a maximum boron concentration in tumour tissue (27.9 μg boron/g tissue) 16 hours after administration. The tumour-to-blood boron ratio was favourable, with a much higher concentration in tumour cells than in the bloodstream, probably due to EPR effect. These results permit to seriously consider boron-CNT derivatives suitable for BNCT, even though, to the best of our knowledge, no further toxicity studies on these derivatives have been reported so far.

1.7 References

1. X. Lu and Z. Chen, *Chem. Rev.*, 2005, 105, 3643-3696.
2. J.-C. Charlier, *Acc. Chem. Res.*, 2002, 35, 1063-1069.
3. a) A. Govindaraj and C. N. R. Rao, *Chapter 2* in *Carbon Nanotechnology*, edited by Liming Dai, *Elsevier B.V.*, 2006, 15-51; b) Q. Fu and J. Liu, *Chapter 4* in *Carbon Nanotechnology*, edited by Liming Dai, *Elsevier B.V.*, 2006, 81-107.
4. P. Nikolaev, M. J. Bronikowski, R. K. Bradley, F. Rohmund, D. T. Colbert, K. A. Smith, and R. E. Smalley, *Chem. Phys. Lett.*, 1999, 313, 91-97.
5. a) C. Ehli, G. M. A. Rahman, N. Jux, D. Balbinot, D. M. Guldi, F. Paolucci, M. Marcaccio, D. Paolucci, M. Melle-Franco, F. Zerbetto, S. Campidelli, and M. Prato, *J. Am. Chem. Soc.*, 2006, 128, 11222-11231; b) R. J. Chen, Y. Zhang, D. Wang, and H. Dai, *J. Am. Chem. Soc.*, 2001, 123, 3838-3839.
6. M. Zheng, A. Jagota, E. D. Semke, B. A. Diner, R. S. McLean, S. R. Lustig, R. E. Richardson, and N. G. Tassi, *Nat. Mater.*, 2003, 2, 338-342.
7. a) R. Qiao and P. C. Ke, *J. Am. Chem. Soc.*, 2006, 128, 13656-13657; b) C. Richard, F. Balavoine, P. Schultz, T. W. Ebbesen, and C. Mioskowski, *Science*, 2003, 300, 775-778.

8. a) X. Li, W. Chen, Q. Zhan, L. Dai, L. Sowards, M. Pender, and R. R. Naik, *J. Phys. Chem. B*, 2006, 110, 12621-12625; b) V. Zorbas, A. L. Smith, H. Xie, A. Ortiz-Acevedo, A. B. Dalton, G. R. Dieckmann, R. K. Draper, R. H. Baughman, and I. H. Musselman, *J. Am. Chem. Soc.*, 2005, 127, 12323-12328.

9. A. Star, J. F. Stoddart, D. Steuerman, M. Diehl, A. Boukai, E. W. Wong, X. Yang, S.-W. Chung, H. Choi, and J. R. Heath, *Angew. Chem. Int. Ed.*, 2001, 40, 1721-1725.

10. a) E. Dujardin, T. W. Ebbesen, A. Krishnan, and M. M. J. Treacy, *Adv. Mater.*, 1998, 10, 1472-1475; b) B. W. Smith, M. Monthioux, and D. E. Luzzi, *Chem. Phys. Lett.*, 1999, 315, 31-36; c) M. Wilson and P. A. Madden, *J. Am. Chem. Soc.*, 2001, 123, 2101-2102.

11. S. Niyogi, M. A. Hamon, H. Hu, B. Zhao, P. Bhowmik, R. Sen, M. E. Itkis, and R. C. Haddon, *Acc. Chem. Res.*, 2002, 35, 1105-1113.

12. E. T. Mickelson, C. B. Huffman, A. G. Rinzler, R. E. Smalley, R. H. Hauge, and J. L. Margrave, *Chem. Phys. Lett.*, 1998, 296, 188-194.

13. a) R. K. Saini, I. W. Chiang, H. Peng, R. E. Smalley, W. E. Billups, R. H. Hauge, and J. L. Margrave, *J. Am. Chem. Soc.*, 2003, 125, 3617-3621; b) P. Boul, *Chem. Phys. Lett.*, 1999, 310, 367-372.

14. Y. Ying, R. K. Saini, F. Liang, A. K. Sadana, and W. E. Billups, *Org. Lett.*, 2003, 5, 1471-1473.

15. a) J. L. Bahr, J. Yang, D. V. Kosynkin, M. J. Bronikowski, R. E. Smalley, and J. M. Tour, *J. Am. Chem. Soc.*, 2001, 123, 6536-6542; b) J. L. Hudson, M. J. Casavant, and J. M. Tour, *J. Am. Chem. Soc.*, 2004, 126, 11158-11159.

16. a) M. Holzinger, O. Vostrowsky, A. Hirsch, F. Hennrich, M. Kappes, R. Weiss, and F. Jellen, *Angew. Chem. Int. Ed.*, 2001, 40, 4002-4005; b) R. Graupner, J. Abraham, D. Wunderlich, A. Vencelová, P. Lauffer, J. Röhrl, M. Hundhausen, L. Ley, and A. Hirsch, *J. Am. Chem. Soc.*, 2006, 128, 6683-9; c) Z. Syrgiannis, F. Hauke, J. Röhrl, M. Hundhausen, R. Graupner, Y. Elemes, and A. Hirsch, *Eur. J. Org. Chem.*, 2008, 2008, 2544-2550.

17. J.-P. Tessonnier, A. Villa, O. Majoulet, D. S. Su, and R. Schlögl, *Angew. Chem. Int. Ed.*, 2009, 48, 6543-6546.

18. a) Z. Yinghuai, A. T. Peng, K. Carpenter, J. A. Maguire, N. S. Hosmane, and M. Takagaki, *J. Am. Chem. Soc.*, 2005, 127, 9875-98801; b) C. Ménard-Moyon, F. Dumas, E. Doris, and C. Mioskowski, *J. Am. Chem. Soc.*, 2006, 128, 14764-14765; c) D. Ogrin, J. Chattopadhyay, A. K. Sadana, W. E. Billups, and A. R. Barron, *J. Am. Chem. Soc.*, 2006, 128, 11322-11323.

19. a) J. Liu , A. G. Rinzler , H. J. Dai , J. H. Hafner , R. K. Bradley , P. J. Boul , A. Lu , T. Iverson , K. Shelimov , C. B. Huffman , F. Rodriguez-Macias , Y. S. Shon , T. R. Lee , D. T. Colbert , R.

E. Smalley , *Science* **1998** , *280* , 1253; b) K. J. Ziegler, Z. Gu, H. Peng, E. L. Flor, R. H. Hauge, and R. E. Smalley, *J. Am. Chem. Soc.*, 2005, 127, 1541-1547.

20. C. Warakulwit, J. Majimel, M.-H. Delville, P. Garrigue, J. Limtrakul, and A. Kuhn, *J. Mater. Chem.*, 2008, 18, 4056-4061.
21. T. J. Aitchison, M. Ginic-Markovic, J. G. Matisons, G. P. Simon, and P. M. Fredericks, *J. Phys. Chem. C*, 2007, 111, 2440-2446.
22. a) I. W. Chiang, B. E. Brinson, A. Y. Huang, P. A. Willis, M. J. Bronikowski, J. L. Margrave, R. E. Smalley, and R. H. Hauge, *J. Phys. Chem. B*, 2001, 105, 8297-8301; b) K. L. Strong, D. P. Anderson, K. Lafdi, and J. N. Kuhn, *Carbon*, 2003, 41, 1477-1488.
23. J. Zhang, H. Zou, Q. Qing, Y. Yang, Q. Li, Z. Liu, X. Guo, and Z. Du, *J. Phys. Chem. B*, 2003, 107, 3712-3718.
24. W. Zhou, Y. H. Ooi, R. Russo, P. Papanek, D. E. Luzzi, J. E. Fischer, M. J. Bronikowski, P. a Willis, and R. E. Smalley, *Chem. Phys. Lett.*, 2001, 350, 6-14.
25. a) J. Chen, M. A. Hamon, H. Hu, Y. Chen, A. M. Rao, P. C. Eklund, and R. C. Haddon, *Science*, 1998, 282, 95-98; b) M. A. Hamon, J. Chen, H. Hu, Y. Chen, M. E. Itkis, A. M. Rao, P. C. Eklund, and R. C. Haddon, *Adv. Mater.*, 1999, 11, 834-840; c) E. Del Canto, K. Flavin, D. Movia, C. Navio, C. Bittencourt, and S. Giordani, *Chem. Mater.*, 2011, 23, 67-74.
26. M. Maggini, G. Scorrano, and M. Prato, *J. Am. Chem. Soc.*, 1993, 115, 9798-9799.
27. V. Georgakilas, K. Kordatos, M. Prato, D. M. Guldi, M. Holzinger, and A. Hirsch, *J. Am. Chem. Soc.*, 2002, 124, 760-761.
28. E. Cho, S. Shin, and Y.-G. Yoon, *J. Phys. Chem. C*, 2008, 112, 11667-11672.
29. X. Lu, F. Tian, X. Xu, N. Wang, and Q. Zhang, *J. Am. Chem. Soc.*, 2003, 125, 10459-10464.
30. a) F. A. Carey and R. J. Sundberg, *Chapter 10* in *Advanced Organic Chemistry*, 5th ed. 2007, ISBN: 978-0-387-68346-1; b) D. H. Ess and K. N. Houk, *J. Am. Chem. Soc.*, 2008, 130, 10187-10198.
31. H. Kataura, Y. Kumazawa, Y. Maniwa, I. Umezu, S. Suzuki, Y. Ohtsuka, and Y. Achiba, *Synth. Met.*, 1999, 103, 2555-2558.
32. A. Jorio, A. G. Souza Filho, G. Dresselhaus, M. S. Dresselhaus, A. K. Swan, M. S. Unlu, B. B. Goldberg, M. A. Pimenta, J. H. Hafner, C. M. Lieber, and R. Saito, *Phys. Rev. B*, 2002, 65, 155412(9).
33. A. C. Dillon, M. Yudasaka, and M. S. Dresselhaus, *J. Nanosci. Nanotechnol.*, 2004, 4, 691-703.
34. S. Arepalli, P. Nikolaev, O. Gorelik, V. G. Hadjiev, W. Holmes, B. Files, and L. Yowell, *Carbon*, 2004, 42, 1783-1791.

35. MultiMode SPM Instruction Manual, Copyright © 1996, 1997, 2004 Veeco Instruments Inc.

36. SPM Training Notebook Copyright © 2003 Veeco Instruments Inc.

37. A. Takagi, A. Hirose, T. Nishimura, N. Fukumori, A. Ogata, N. Ohashi, S. Kitajima, and J. Kanno, *J. Toxicol. Sci.*, 2008, 33, 105-116.

38. C. A. Poland, R. Duffin, I. Kinloch, A. Maynard, W. A. H. Wallace, A. Seaton, V. Stone, S. Brown, W. MacNee, and K. Donaldson, *Nat. Nanotechnol.*, 2008, 3, 423-428.

39. L. A. Mitchell, J. Gao, R. V. Wal, A. Gigliotti, S. W. Burchiel, and J. D. McDonald, *Toxicol. Sci.*, 2007, 100, 203-214.

40. J. P. Ryman-Rasmussen, M. F. Cesta, A. R. Brody, J. K. Shipley-Phillips, J. I. Everitt, E. W. Tewksbury, O. R. Moss, B. A. Wong, D. E. Dodd, M. E. Andersen, and J. C. Bonner, *Nat. Nanotechnol.*, 2009, 4, 747-751.

41. Baron, P.A., Maynard, A.D., Foley, M., NIOSH DART-02-191 Rev. 1.1, 2003.

42. D. S.-W. Tan, M. Gerlinger, B.-T. Teh, and C. Swanton, *Eur. J. Cancer*, 2010, 46, 2166-2177.

43. S. V. Ambudkar, S. Dey, C. A. Hrycyna, M. Ramachandra, I. Pastan, and M. M. Gottesman, *Ann. Rev. Pharmacol. Toxicol.*, 1999, 39, 361-398.

44. Y. Matsumura and H. Maeda, *Cancer Res.*, 1986, 46, 6387-6392., A. K. Iyer, G. Khaled, J. Fang, and H. Maeda, *Drug Discov. Today*, 2006, 11, 812-818.

45. a) K. T. Oh, H. J. Baik, a H. Lee, Y. T. Oh, Y. S. Youn, and E. S. Lee, *Int. J. Mo.l Sci.*, 2009, 10, 3776-3792; b) L. S. Jabr-Milane, L. E. van Vlerken, S. Yadav, and M. M. Amiji, *Cancer Treat. Rev.*, 2008, 34, 592-602.

46. H. Dumortier, S. Lacotte, G. Pastorin, R. Marega, W. Wu, D. Bonifazi, J.-P. Briand, M. Prato, S. Muller, and A. Bianco, *Nano Lett.*, 2006, 6, 1522-1528.

47. P. Wick, P. Manser, L. K. Limbach, U. Dettlaff-Weglikowska, F. Krumeich, S. Roth, W. J. Stark, and A. Bruinink, *Toxicol. Lett.*, 2007, 168, 121-131.

48. C. M. Sayes, F. Liang, J. L. Hudson, J. Mendez, W. Guo, J. M. Beach, V. C. Moore, C. D. Doyle, J. L. West, W. E. Billups, K. D. Ausman, and V. L. Colvin, *Toxicol. Lett.*, 2006, 161, 135-142.

49. a) R. Singh, D. Pantarotto, L. Lacerda, G. Pastorin, C. Klumpp, M. Prato, A. Bianco, and K. Kostarelos, *Proc. Natl. Acad. Sci. USA*, 2006, 103, 3357-3362; b) L. Lacerda, H. Ali-Boucetta, M. A. Herrero, G. Pastorin, A. Bianco, M. Prato, and K. Kostarelos, *Nanomedicine*, 2008, 3, 149-161; c) L. Lacerda, M. A. Herrero, K. Venner, A. Bianco, M. Prato, and K. Kostarelos, *Small*, 2008, 4, 1130-1132; d) M. R. McDevitt, D.

Chattopadhyay, J. S. Jaggi, R. D. Finn, P. B. Zanzonico, C. Villa, D. Rey, J. Mendenhall, C. A. Batt, J. T. Njardarson, and D. A. Scheinberg, *PloS ONE*, 2007, 2, e907; e).Z. Liu, C. Davis, W. Cai, L. He, X. Chen, and H. Dai, *Proc. Natl. Acad. Sci. USA*, 2008, 105, 1410-1415; f) B. Kang, D. Yu, Y. Dai, S. Chang, D. Chen, and Y. Ding, *Carbon*, 2009, 47, 1189-1192; g) A. Ruggiero, C. H. Villa, E. Bander, D. A. Rey, M. Bergkvist, C. A. Batt, K. Manova-Todorova, W. M. Deen, D. A. Scheinberg, and M. R. McDevitt, *Proc. Natl. Acad. Sci. USA*, 2010, 107, 12369-12374.

50. a) B. L. Allen, P. D. Kichambare, P. Gou, I. I. Vlasova, A. A. Kapralov, N. Konduru, V. E. Kagan, and A. Star, *Nano Lett.*, 2008, 8, 3899-3903; b) B. L. Allen, G. P. Kotchey, Y. Chen, N. V. K. Yanamala, J. Klein-Seetharaman, V. E. Kagan, and A. Star, *J. Am. Chem. Soc.*, 2009, 131, 17194-205; c) V. E. Kagan, N. V. Konduru, W. Feng, B. L. Allen, J. Conroy, Y. Volkov, I. I. Vlasova, N. A. Belikova, N. Yanamala, A. Kapralov, Y. Y. Tyurina, J. Shi, E. R. Kisin, A. R. Murray, J. Franks, D. Stolz, P. Gou, J. Klein-seetharaman, B. Fadeel, A. Star, and A. A. Shvedova, *Nat. Nanotechnol.*, 2010, 5, 354-359.
51. Y. Zhao, B. L. Allen, and A. Star, *J. Phys. Chem. A*, 2011, doi/10.1021/jp112324d.
52. P. Cherukuri, S. M. Bachilo, S. H. Litovsky, and R. B. Weisman, *J. Am. Chem. Soc.*, 2004, 126, 15638-15639.
53. A. E. Porter, M. Gass, K. Muller, J. N. Skepper, P. A. Midgley, and M. Welland, *Nat. Nanotechnol.*, 2007, 2, 713-717.
54. C. Cheng, K. H. Müller, K. K. K. Koziol, J. N. Skepper, P. A. Midgley, M. E. Welland, and A. E. Porter, *Biomaterials*, 2009, 30, 4152-4160.
55. Y. Sato, A. Yokoyama, K.-I. Shibata, Y. Akimoto, S.-I. Ogino, Y. Nodasaka, T. Kohgo, K. Tamura, T. Akasaka, M. Uo, K. Motomiya, B. Jeyadevan, M. Ishiguro, R. Hatakeyama, F. Watari, and K. Tohji, *Mol. BioSyst.*, 2005, 1, 176-182.
56. D. M. Brown, I. A. Kinloch, U. Bangert, A. H. Windle, D. M. Walter, G. S. Walker, C. A. Scotchford, K. Donaldson, and V. Stone, *Carbon*, 2007, 45, 1743-1756.
57. B. Kateb, M. Van Handel, L. Zhang, M. J. Bronikowski, H. Manohara, and B. Badie, *NeuroImage*, 2007, 37, S9-S17.
58. N. W. S. Kam, T. C. Jessop, P. A. Wender, and H. Dai, *J. Am. Chem. Soc.*, 2004, 126, 6850-6851.
59. a) N. W. S. Kam, M. O. Connell, J. A. Wisdom, and H. Dai, *Proc. Natl. Acad. Sci. USA*, 2005, 102, 11600-11605; b) N. W. S. Kam and H. Dai, *J. Am. Chem. Soc.*, 2005, 127, 6021-6026.
60. N. W. S. Kam, Z. Liu, and H. Dai, *Angew. Chem. Int. Ed.*, 2006, 45, 577-581.
61. H. Jin, D. A. Heller, and M. S. Strano, *Nano Lett.*, 2008, 8, 1577-1585.

62. H. Jin, D. A. Heller, R. Sharma, and M. S. Strano, *ACS Nano*, 2009, 3, 149-158.

63. M. Wang, S. Yu, C. Wang, and J. Kong, *ACS Nano*, 2010, 4, 6483-6490.

64. M. Bottini, F. Cerignoli, M. I. Dawson, A. Magrini, N. Rosato, and T. Mustelin, *Biomacromolecules*, 2006, 7, 2259-2263.

65. A. A. Bhirde, V. Patel, J. Gavard, G. Zhang, A. A. Sousa, A. Masedunskas, R. D. Leapman, R. Weigert, J. S. Gutkind, and J. F. Rusling, *ACS Nano*, 2009, 3, 307-316.

66. J. Chen, S. Chen, X. Zhao, L. V. Kuznetsova, S. S. Wong, and I. Ojima, *J. Am. Chem. Soc.*, 2008, 130, 16778-16785.

67. a) N. Jia, Q. Lian, H. Shen, C. Wang, X. Li, and Z. Yang, *Nano Lett.*, 2007, 7, 2976-2980; b) Y. Liu, W. De-Cheng, W.-D. Zhang, X. Jiang, C.-bin He, T. S. Chung, S. H. Goh, and K. W. Leong, *Angew. Chem. Int. Ed.*, 2005, 44, 4782-4785.

68. J. Cheng, K. A. S. Fernando, L. M. Veca, Y.-P. Sun, A. I. Lamond, Y. W. Lam, and S. H. Cheng, *ACS Nano*, 2008, 2, 2085-2094.

69. a) D. Pantarotto, J.-Paul Briand, M. Prato, and A. Bianco, *Chem. Commun.*, 2004, 16-17; b) D. Pantarotto, R. Singh, D. McCarthy, M. Erhardt, J.-P. Briand, M. Prato, K. Kostarelos, and A. Bianco, *Angew. Chem. Int. Ed.*, 2004, 43, 5242-5246.

70. L. A. Kueltzo and C. R. Middaugh, *J. Pharm. Sci.*, 2003, 92, 1754-1772.

71. C. F. Lopez, S. O. Nielsen, P. B. Moore, and M. L. Klein, *Proc. Natl. Acad. Sci. USA*, 2004, 101, 4431-4434.

72. S. Pogodin and V. A. Baulin, *ACS Nano*, 2010, 4, 5293-300.

73. S. Pogodin, N. K. H. Slater, and V. A. Baulin, *ACS Nano*, 2011, 5, 1141–1146.

74. K. Kostarelos, L. Lacerda, G. Pastorin, W. Wu, S. Wieckowski, J. Luangsivilay, S. Godefroy, D. Pantarotto, J.-Paul Briand, S. Muller, M. Prato, and A. Bianco, *Nat. Nanotechnol.*, 2007, 2, 108-113.

75. R. Zeineldin, M. Al-Haik, and L. G. Hudson, *Nano Lett.*, 2009, 9, 751-757.

76. B. Kang, S. Chang, Y. Dai, D. Yu, and D. Chen, *Small*, 2010, 6, 2362-2366.

77. A. E. Porter, M. Gass, J. S. Bendall, K. Muller, A. Goode, J. N. Skepper, P. A. Midgley, and M. Welland, *ACS Nano*, 2009, 3, 1485-1492.

78. C. Cheng, A. E. Porter, K. Muller, K. Koziol, J. N. Skepper, P. Midgley, and M. Welland, *J. Phys. Conf.*, 2009, 151, 1-15.

79. N. A. Monteiro-Riviere, R. J. Nemanich, A. O. Inman, Y. Y. Wang, and J. E. Riviere, *Toxicol. Lett.*, 2005, 155, 377-384.

80. D. Cai, J. M. Mataraza, Z.-hong Qin, Z. Huang, J. Huang, T. C. Chiles, D. Carnahan, K. Kempa, and Z. Ren, *Nat. Methods*, 2005, 2, 449-454.

81. R. Singhal, Z. Orynbayeva, R. V. K. Sundaram, J. J. Niu, S. Bhattacharyya, E. A. Vitol, M. G. Schrlau, E. S. Papazoglou, G. Friedman, and Y. Gogotsi, *Nat. Nanotechnol.*, 2011, 6, 57-64.

82. H. Ali-Boucetta, K. T. Al-Jamal, D. McCarthy, M. Prato, A. Bianco, and K. Kostarelos, *Chem. Commun.*, 2008, 459-461.

83. Liu, X. Sun, N. Nakayama-Ratchford, and H. Dai, *ACS Nano*, 2007, 1, 50-56.

84. Z. Liu, A. C. Fan, K. Rakhra, S. Sherlock, A. Goodwin, X. Chen, Q. Yang, D. W. Felsher, and H. Dai, *Angew. Chem. Int. Ed.*, 2009, 48, 7668-7672.

85. Z. Liu, W. Cai, L. He, N. Nakayama, K. Chen, X. Sun, X. Chen, and H. Dai, *Nat. Nanotechnol.*, 2007, 2, 47-52.

86. X. Zhang, L. Meng, Q. Lu, Z. Fei, and P. J. Dyson, *Biomaterials*, 2009, 30, 6041-6047.

87. E. Heister, V. Neves, C. Tîlmaciu, K. Lipert, V. S. Beltran, H. M. Coley, S. R. P. Silva, and J. McFadden, *Carbon*, 2009, 47, 2152-2160.

88. P. Chaudhuri, S. Soni, and S. Sengupta, *Nanotechnology*, 2010, 21, 025102 (11pp).

89. R. Li, R. Wu, L. Zhao, M. Wu, L. Yang, and H. Zou, *ACS Nano*, 2010, 4, 1399-1408.

90. G. Pastorin, W. Wu, S. Wieckowski, J.-Paul Briand, K. Kostarelos, M. Prato, and A. Bianco, *Chem. Commun.*, 2006, 1182-1184.

91. C. Samorì, H. Ali-Boucetta, R. Sainz, C. Guo, M. F. Toma, C. Fabbro, T. Da Ros, M. Prato, K. Kostarelos, and A. Bianco, *Chem. Commun.*, 2010, 46, 1494-1496.

92. Z. Liu, K. Chen, C. Davis, S. Sherlock, Q. Cao, X. Chen, and H. Dai, *Cancer Res.*, 2008, 68, 6652-6660.

93. R. P. Feazell, N. Nakayama-Ratchford, H. Dai, and S. J. Lippard, *J. Am. Chem. Soc.*, 2007, 129, 8438-8439.

94. S.Dhar, Z. Liu, J. Thomale, H. Dai, and S. J. Lippard, *J. Am. Chem. Soc.*, 2008, 130, 11467-11476.

95. S. C. Tsang, Y. K. Chen, P. J. F. Harris and M. L. H. Green, *Nature*, 1994, 372, 159-162.

96. S. Hampel, D. Kunze, D. Haase, K. Krämer, M. Rauschenbach, M. Ritschel, A. Leonhardt, J. Thomas, S. Oswald, V. Hoffmann, and B. Büchner, *Nanomedicine*, 2008, 3, 175-182.

97. C. Tripisciano, K. Kraemer, a Taylor, and E. Borowiak-Palen, *Chem. Phys. Lett.*, 2009, 478, 200-205.

98. W. Wu, R. Li, X. Bian, Z. Zhu, D. Ding, X. Li, Z. Jia, X. Jiang, and Y. Hu, *ACS Nano*, 2009, 3, 2740-2750.

99. D. Yang, F. Yang, J. Hu, J. Long, C. Wang, D. Fu, and Q. Ni, *Chem. Commun.*, 2009, 4447-4449.

100. J. Meng, J. Meng, J. Duan, H. Kong, L. Li, C. Wang, S. Xie, S. Chen, N. Gu, H. Xu, and X.-da Yang, *Small*, 2008, 4, 1364-1370.

101. Z. Zhang, Y. Zhang, B. Zeng, S. Wang, T. Zhu, R. B. S. Roden, Y. Chen, and R. Yang, *Clin. Cancer Res.*, 2006, 12, 4933-4939.

102. J. E. Podesta, K. T. Al-Jamal, M. A. Herrero, B. Tian, H. Ali-boucetta, V. Hegde, A. Bianco, M. Prato, and K. Kostarelos, *Small*, 2009, 5, 1176-1185.

103. X. Yang, Z. Zhang, Z. Liu, Y. Ma, R. Yang, and Y. Chen, *J. Nanopart. Res.*, 2008, 10, 815-822.

104. B. Pan, F. Liu, Q. Li, T. Huang, X. You, J. Shao, C. Bao, D. Cui, P. Xu, H. Chen, F. Gao, R. He, M. Shu, and Y. Ma, *Chin. J. Cancer Res.*, 2007, 19, 1-6.

105. M.A. Herrero, F.M. Toma, K.T. Al-Jamal, K. Kostarelos, A. Bianco, T. Da Ros, F. Bano, L. Casalis, G. Scoles, M. Prato, *J. Am. Chem. Soc.*, 2009, 131, 9843–9848.

106. Z. Zhu, Z. Tang, J. A. Phillips, R. Yang, H. Wang, and W. Tan, *J. Am. Chem. Soc.*, 2008, 130, 10856-10857.

107. Y. Wu, J. A. Phillips, H. Liu, R. Yang, and W. Tan, *ACS Nano*, 2008, 2, 2023-2028.

108. X. Li, Y. Peng, J. Ren, and X. Qu, *Proc. Natl. Acad. Sci. USA*, 2006, 103, 19658-19663.

109. K. Welsher, Z. Liu, D. Daranciang, and H. Dai, *Nano Lett.*, 2008, 8, 586-590.

110. Z. Liu, X. Li, S. M. Tabakman, K. Jiang, S. Fan, and H. Dai, *J. Am. Chem. Soc.*, 2008, 130, 13540-13541.

111. C. Zavaleta, A. de La Zerda, Z. Liu, S. Keren, Z. Cheng, M. Schipper, X. Chen, H. Dai, and S. S. Gambhir, *Nano Lett.*, 2008, 8, 2800-2805.

112. Z. Ou, B. Wu, D. Xing, F. Zhou, H. Wang, and Y. Tang, *Nanotechnology*, 2009, 20, 105102 (7pp).

113. a) L. R. Hirsch, R. J. Stafford, J. A. Bankson, S. R. Sershen, B. Rivera, R. E. Price, J. D. Hazle, N. J. Halas, and J. L. West, *Proc. Natl. Acad. Sci. USA*, 2003, 100, 13549-13554; b) X. Huang, I. H. El-Sayed, W. Qian, and M. A. El-Sayed, *J. Am. Chem. Soc.*, 2006, 128, 2115-2120; c) D. P. O'Neal, L. R. Hirsch, N. J. Halas, J. D. Payne, and J. L. West, *Cancer Lett.*, 2004, 209, 171-176.

114. American National Standard for Safe Use of Lasers. ANSI Z136.1, 2000

115. a) S. V. Torti, F. Byrne, O. Whelan, N. Levi, B. Ucer, M. Schmid, F. M. Torti, S. Akman, J. Liu, P. M. Ajayan, O. Nalamasu, and D. L. Carroll, *Int. J. Nanomedicine*, 2007, 2, 707-714; b) L. Gomez-De Arco, M.-T. Chen, W. Wang, T. Vernier, P. Pagnini, T. Chen, M. Gundersen, and C. Zhou, *Mater. Res. Soc. Symp. Proc.*, 2008, 1065, QQ04-07.

116. a) H. K. Moon, S. H. Lee, and H. C. Choi, *ACS Nano*, 2009, 3, 3707-3713; b) S. Ghosh, S. Dutta, E. Gomes, D. Carroll, R. D'Agostino, J. Olson, M. Guthold, and W. H. Gmeiner, *ACS Nano*, 2009, 3, 2667-2673.

117. N. Shao, S. Lu, E. Wickstrom, and B. Panchapakesan, *Nanotechnology*, 2007, 18, 315101 (9pp).

118. P. Chakravarty, R. Marches, N. S. Zimmerman, A. D. E. Swafford, P. Bajaj, I. H. Musselman, P. Pantano, R. K. Draper, and E. S. Vitetta, *Proc. Natl. Acad. Sci. USA*, 2008, 105, 8697-8702.

119. R. Marches, P. Chakravarty, I. H. Musselman, P. Bajaj, R. N. Azad, P. Pantano, R. K. Draper, and E. S. Vitetta, *Int. J. Cancer*, 2009, 125, 2970-2977.

120. C.-H. Wang, S.-H. Chiou, C.-P. Chou, Y.-C. Chen, Y.-J. Huang, and C.-A. Peng, *Nanomedicine: NBM*, 2011, 7, 69-79.

121. M. R. McDevitt, D. Chattopadhyay, B. J. Kappel, J. S. Jaggi, S. R. Schiffman, C. Antczak, J. T. Njardarson, R. Brentjens, and D. A. Scheinberg, *J. Nuclear Medicine*, 2007, 48, 1180-1189.

122. A. Ruggiero, C. H. Villa, J. P. Holland, S. R. Sprinkle, C. May, J. S. Lewis, D. A. Scheinberg, and M. R. McDevitt, *Int. J. Nanomedicine*, 2010, 5, 783-802.

Shortening of SWCNTs

This first part of the work is focused on shortening HiPCO SWCNTs. As already mentioned, the shortening of the CNTs goes with an improvement in their solubility and with the introduction of oxidized functions, mainly carboxylic groups, at their tips and on the sidewall, which not only contribute to solubility improvement, but offer also an anchor point for further covalent derivatization of the material. To reach this objective we explored two distinct options, namely a strong oxidative treatment, with the use of acids, and a mechanochemical approach, with a ball-mill.

2.1 Oxidative shortening of SWCNTs

The acid oxidation of SWCNTs was performed exploiting a procedure described by Tour and co-workers in 2006.[1] Nitric acid was employed as the oxidizing agent, but, ahead of this step, an intercalation step with oleum was performed, in order to obtain a homogeneous distribution of CNTs in solution. Oleum is a solution of sulphuric anhydride in sulphuric acid, whose aim is to help intercalation inside SWCNTs ropes. In fact, it was observed that oleum intercalates inside SWCNTs ropes, making them swell and resulting in individual nanotubes surrounded by few ordered layers of acid (Figure 1).[2] The mechanism for this intercalation is possible only in superacids, where no competing base is present, since it consists in the protonation of the tubes, which disrupts van der Waals inter-tube interactions and triggers surrounding by sulphuric acid anions.[3]

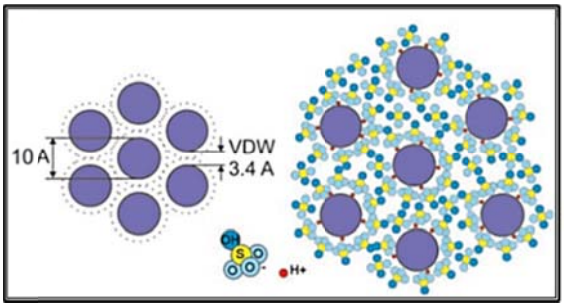

Figure 1. A model illustrating the swelling of a SWCNTs rope in sulphuric acid (adapted from Ref. 2).

We treated HiPCO SWCNTs with oleum for 12 h stirring the mixture under Ar atmosphere, and we subsequently added a mixture of oleum and aqueous nitric acid (65%), to a final ratio oleum/nitric acid of 3/1, exposing the mixture to air at 65°C for 2 h (Scheme 1). Then, the reaction mixture was diluted in water and filtered to remove the acid solvent. Finally, we thoroughly washed the nanotubes with H_2O, MeOH and Et_2O, and we dried them under high vacuum.

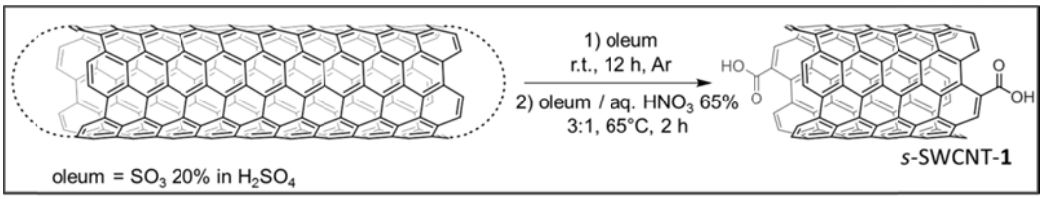

Scheme 1

The shortened SWCNTs thus obtained, *s*-SWCNT-**1**, were fully characterized with different complementary techniques. The dispersibility in both organic solvents and water highly increased with respect to the pristine SWCNTs (Figure 2).

Figure 2. DMF dispersions of pristine SWCNTs (left) and *s*-SWCNT-**1** (right).

TEM images clearly show how the treatment produced shorter and less aggregated CNTs with respect to the pristine ones (Figures 3a and 3b). Nevertheless, they also indicate that a certain amount of amorphous carbonaceous material was present in our sample. The quite aggressive acid treatment oxidized the tubes at a high extent, and part of them finally lost the tubular structure and underwent fragmentation in small pieces, likely characterized by a high content of oxidized groups. Among these highly damaged pieces, the smaller ones were probably removed during the filtration procedure carried out after the oxidation, consistently with the observed overall weight yield of 77%, but a great part of them was still present in the sample. From images, it is also possible to appreciate the decrease in the iron content of the

sample, even though this observation is only qualitative. This phenomenon is triggered by the opening of CNT caps and the oxidation of the metal which was inside the tubes, according to the reaction depicted in Scheme 2: an iron water-soluble salt is formed that could then be washed off during the work-up.

$$Fe^{\circ} + 6\,HNO_3 \longrightarrow 3\,Fe(NO_3)_3 + 3\,NO_2 + 3\,H_2O$$

Scheme 2

Metal particles appear as spots with higher contrast in TEM images, since they can interfere more with the electron-beam of the microscope. The comparison between images c and d (Figure 3) clearly shows how the treatment strongly reduced their presence.

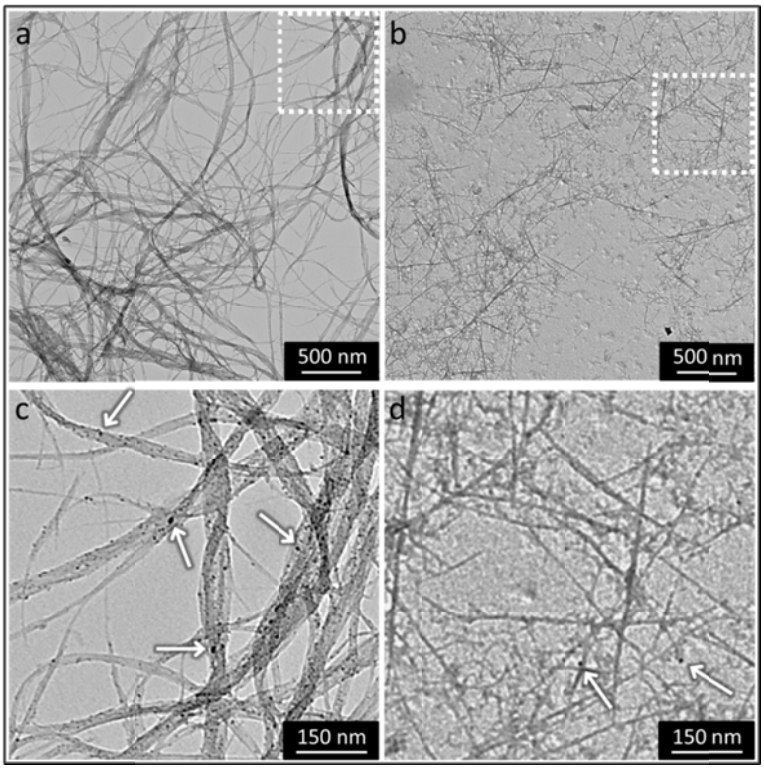

Figure 3. Representative TEM images of pristine SWCNTs (**a** and **c**) and *s*-SWCNT-**1** (**b** and **d**). Lower panels show enlargements of area indicated by the square in the upper ones. Arrows point at metal particles.

More information could be obtained from the thermogravimetric profile of the material in air (Figure 4). In the lower temperature part of the curve, combustion of amorphous material and oxygenated groups takes place. At temperatures above 300-400°C CNTs burn, and the 1st derivative of the curve indicates the precise temperature at which this event takes place. The increase of 35°C in this value is consistent with the decrease of iron content in the sample, as

observed at the TEM. In fact, the presence of metal particles decreases thermal stability of CNTs, since it creates hot spots in the sample during the thermal experiment, and thus it reduces the temperature of CNT oxidation.[4]

Furthermore, the residual weight of air TGA is due to the iron present in the sample, which is oxidized during this analysis, resulting in iron(III) oxide (Fe_2O_3). This value can therefore be used to obtain a quantitative data for the iron content of the CNT sample. For pristine SWCNTs the residue is of 26.1% (in the form of Fe_2O_3). It is therefore possible to calculate an iron content of 19.8%. For *s*-SWCNT-**1** the Fe_2O_3 residue is of 4.7%, which gives a value of 3.3% of iron. However, we need to consider that a big part of this sample is represented by oxygenated groups and amorphous carbon, and therefore the percentage of iron with respect to the only CNTs would be higher.

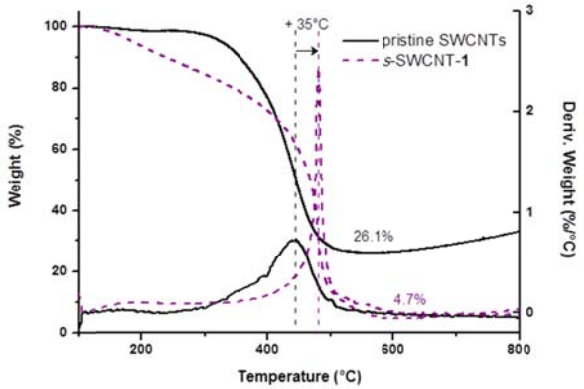

Figure 4. TGA (air) of pristine SWCNTs and *s*-SWCNT-**1**.

Comparing *s*-SWCNT-**1** TGA under N_2 atmosphere with the one of the pristine SWCNTs (Figure 5a), a big increase in the weight loss was observed at temperatures below 800°C (almost 40%), ascribable to different material, namely to the amorphous carbon seen in the TEM pictures, to the carboxylic acids introduced with the cutting, but also to some sulfonic acids. In fact, TGA-MS of *s*-SWCNT-**1** let us analyse the gas evolving from the sample during the thermogravimetric experiment and peaks of mass 48 and 64 were found (Figure 5b). They correspond to SO^+ and SO_2^+ respectively, deriving from decomposition and ionization of SO_2, which is in turn generated by sulfonic acid, in the same way CO_2 is generated by carboxylic acid.

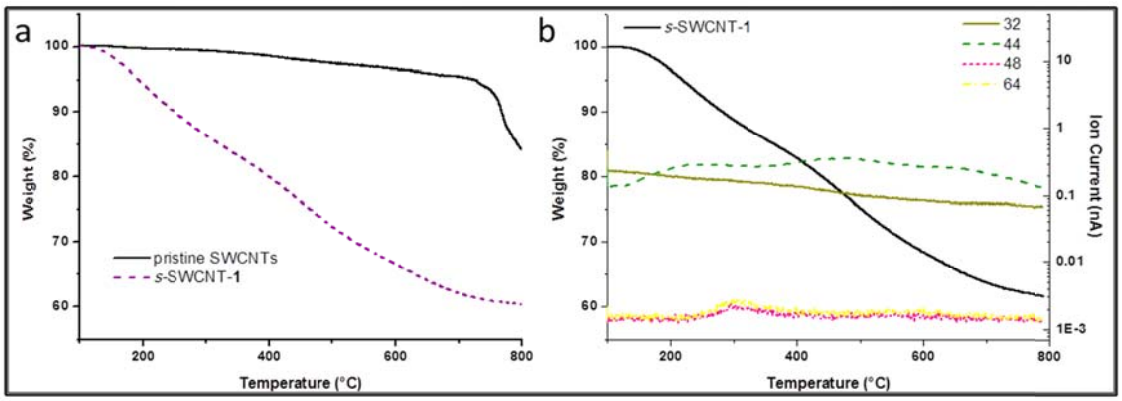

Figure 5. a) TGA (N_2) of pristine SWCNTs and *s*-SWCNT-**1**; **b**) TGA-MS analysis (He) of *s*-SWCNT-**1**.

Other information regarding the modification of CNT structure are given by UV-vis-NIR and Raman spectroscopies, since disruption of the sp^2 network of the CNTs resulted in major changes in both kind of spectra, as can be observed in Figure 6. A partial loss of the van Hove singularities was found, especially in the metallic region of the spectrum, but also in the semiconducting one. Regarding the Raman spectra, the oxidative treatment led, as expected, to a big increase in the D/G ratio, because of the introduction of many defects on the CNTs, together with a background fluorescence, due to the presence of amorphous material. At the same time, a loss of most of the RBM bands was observed, since the smaller and more reactive tubes were destroyed by the harsh conditions of the treatment.

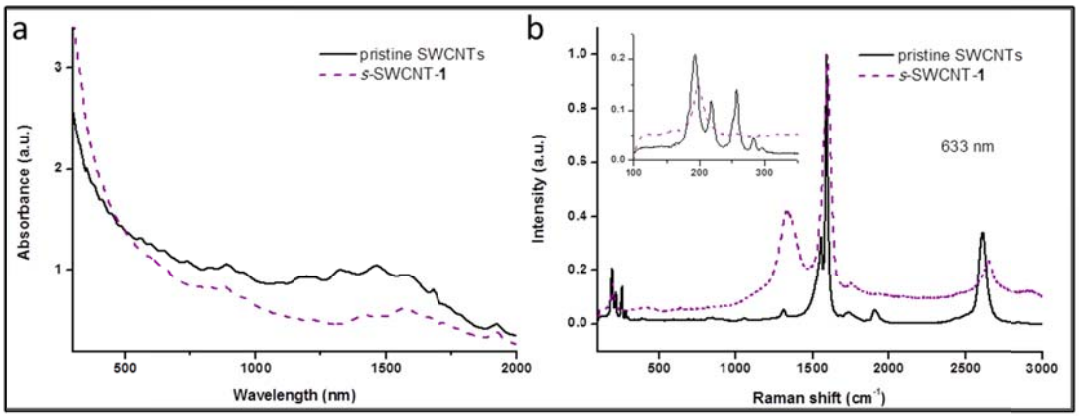

Figure 6. a) UV-vis-NIR spectra of pristine SWCNTs and *s*-SWCNT-**1** (DMF); **b)** Raman spectra (633 nm) of pristine SWCNTs and *s*-SWCNT-**1**. In the inset, the enlargement of the RBM zone is shown.

2.1.1 *Re-pristinization* of the oxidized SWCNTs

During the Raman analyses, we observed a very particular behaviour, which might help in better understanding the nature of the product obtained. Quite surprisingly, increasing laser

power a sort of *re-pristinization* of the sample occurred, as can be clearly observed in Figure 7. We analysed the Raman bands of the sample using not only the 633 nm laser, but also the 785 nm and the 532 nm ones and we obtained spectra similar to the one at 633 nm, in terms of D-band and loss of RBM. The slight differences are, of course, due to the fact that different tubes are in resonance at the energy of the specific laser used.

Considering the 785 nm laser, the starting laser power used was 0.57 mW/μm^2. Laser power density was then gradually increased. At 2.86 mW/μm^2 we started to observe a decrease in the D/G ratio, a lower baseline and a better definition of RBM bands. Afterwards we exposed the sample to a laser power density of 5.73 mW/μm^2, which gave a too high response, corresponding to a saturated spectrum (not reported), but resulted in a complete *re-pristinization* of the sample, appreciable when the analysis was repeated again at lower laser power (Figure 7a). By comparison of this spectrum with the one of the pristine SWCNTs obtained using the same laser wavelength, we can clearly notice that the two profiles are pretty similar, apart from the RBM zone, where an enrichment of certain tubes with respect to others is evident (Figure 7b). Also, an overall increase in the Raman cross section was observed (note that all the spectra are normalized to the G band maximum), in fact we needed to lower the laser power density to collect the spectrum after the *re-pristinization* took place (Figure 7a).

The same phenomenon was observed using the 532 nm and 633 nm lasers, with laser power of 2.07 mW/μm^2 and 2.55 mW/μm^2 respectively. In both cases, the main difference between the pristine SWCNTs and the re-pristinized ones were in the RBM zone and in the shape of the G-band, both correlated with different composition of the SWCNT sample (Figures 7c and 7d).

We hypothesize that this phenomenon is due to thermal effects. In fact, treating CNTs with a high power laser resulted in a local increase of temperature, to which we ascribe an annealing of amorphous carbon and structural defects, and, consequently a re-establishment of the sp^2 network. Of course, the tubes that where completely destroyed during the oxidation were not present anymore, therefore leading to an enrichment of the sample with remaining tubes, as confirmed by the changes in the RBM and G-band patterns. In particular, the loss of the higher wavenumber RBM bands, observed with all the lasers, confirmed the selective destruction of smaller diameter tubes by the aggressive acid treatment.

A confirmation for this thermal effect could arise from the reversible shift in the G-band to lower wavenumbers (from approximately 1593 nm to 1584 nm) upon increasing of laser power density (Figure 7a), since this downshift has been correlated with a lengthening of the C-C distances as the nanotube undergoes thermal expansion.[5]

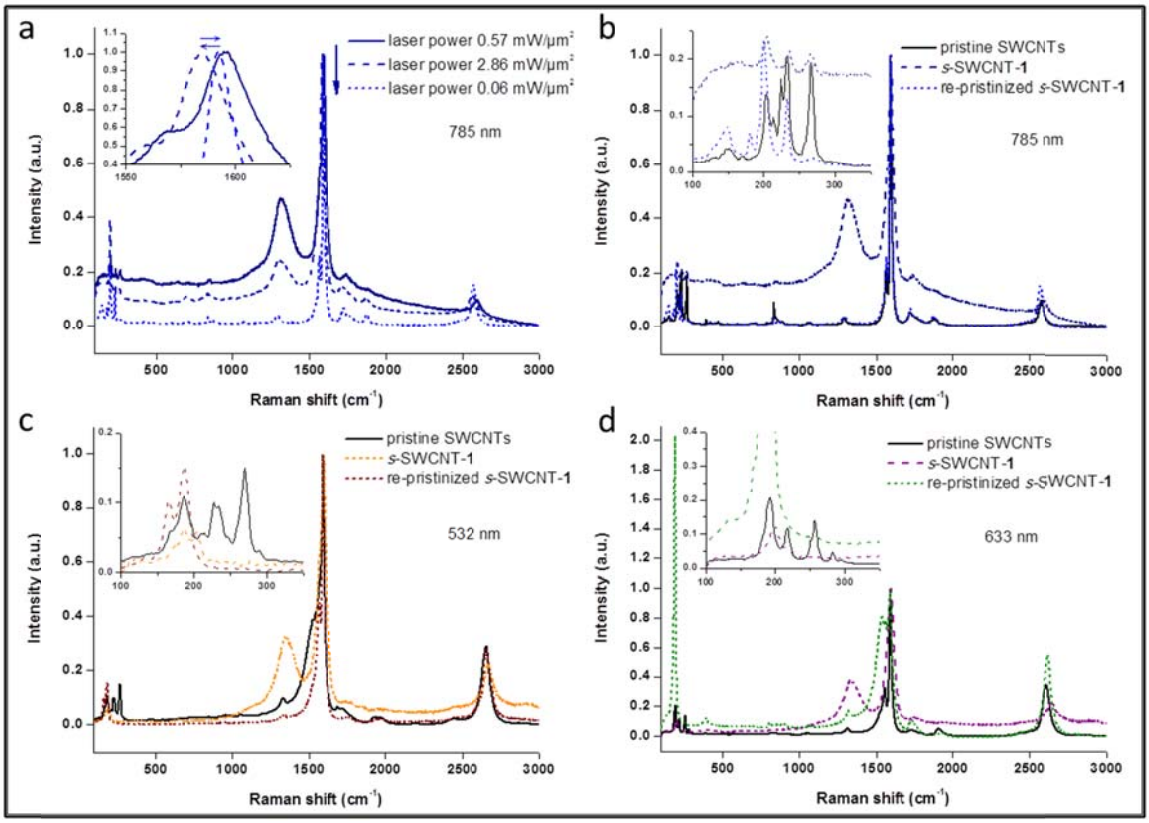

Figure 7. a) Raman re-pristinization process of *s*-SWCNT-**1** with 785 nm laser. In the inset, the enlargement of the G-band zone is shown; **b**, **c**, **d**) Raman spectra of *s*-SWCNT-**1** with different lasers, before and after re-pristinization of the sample, in comparison with the pristine SWCNTs. In the insets, the enlargement of the RBM zone is shown.

Few papers appeared in the literature so far, reporting a similar behaviour, but they refer to pristine CNTs. In two cases, pristine SWCNTs were treated with the 633 nm laser, at laser power densities of 1 or 0.1 mW/μm^2, and the authors observed a decrease in the D/G ratio, a reversible shift of the G peak to lower wavenumbers, and a change in the RBM peaks, together with an increase in their intensities. Also a general increase in the Raman cross section was reported, explained as a result of the higher purity of the sample, since more CNTs produce higher Raman response. Both authors explained the fact as a thermal effect, resulting in annealing of the CNTs. They calculated the temperature reached in their sample, at the higher laser power density used, which was in the range 300-450°C. Nevertheless, it should be pointed out that this value should be considered just as indicative, since it is calculated by the ratio between Stoke and anti-Stoke intensities, which, in resonance Raman spectroscopy, is not a reliable method. In fact different kind of CNTs are resonant in the Stoke and anti-Stoke spectra.[6] Another report appeared, regarding pristine MWCNTs, where a laser treatment resulted in lowering of the D/G ratio, further confirming a sort of annealing and purification effect.[7]

Regarding oxidized SWCNTs, no similar results are present in the literature, to the best of our knowledge. A paper published in 2000 described a similar laser treatment (633 nm, 2.2 $mW/\mu m^2$) of oxidized SWCNTs, resulting in a change of the line shape of the G bands, that the authors ascribed to degassing of the sample due to heating effects, but not to annealing of defects, since they did not observe any decrease in the D/G ratio, nor any change in the RBM zone.[8] Another report on 633 nm laser treatment of pristine SWCNTs at 1 $mW/\mu m^2$ describes, contrary to our findings, the selective destruction of metallic tubes, together with an increase in the D/G ratio, and a decrease in the Raman cross section.[9]

In conclusion, this is the first time that such a laser-induced *re-pristinization* effect is reported for oxidized CNTs. This effect could in principle be exploited to find a purification method for the oxidized SWCNTs, and, quite importantly, it tells us that, even if we cannot appreciate their Raman features, many of the CNTs are still present in the sample even after the harsh treatment.

2.1.2 Sodium Hydroxide washing

In the attempt to purify the oxidized *s*-SWCNT-**1** we decided to perform alkaline washings with sodium hydroxide (NaOH). In fact, as described by several reports, the major amorphous impurities deriving from the strong oxidative treatment are probably represented by highly oxidized carbonaceous material, and could therefore be removed by an alkaline washing that would bring them in solution, allowing their removal through filtration.[10]

We treated *s*-SWCNTs-**1** in aqueous NaOH 8M at 100°C for 48h, under Ar atmosphere. Afterwards, purified CNTs were separated from the dissolved amorphous material by filtration, and thoroughly washed with H_2O, MeOH and Et_2O to afford *s*-SWCNT-**2** (Scheme 3).

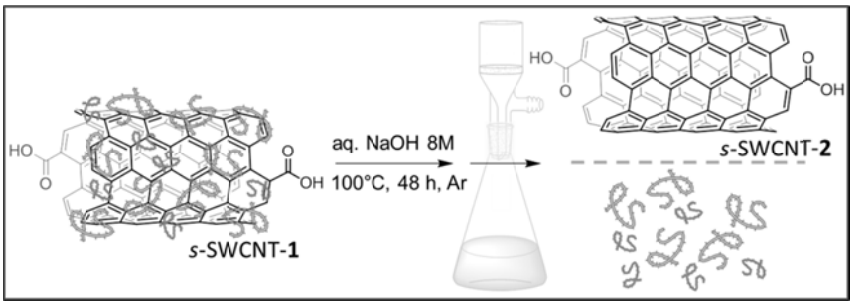

Scheme 3

The purified *s*-SWCNTs-**2** and the filtrate were characterized to evaluate the successfulness of the procedure. TEM images clearly showed much cleaner CNTs, with a reduced content of amorphous material, found instead in the filtrate where no CNTs were detected

(Figure 8). Nevertheless, the dispersibility of *s*-SWCNTs-**2** strongly decreased with respect to *s*-SWCNTs-**1**, and TEM images confirmed it, since many bundles and big aggregates were found for this product, differently from *s*-SWCNT-**1**.

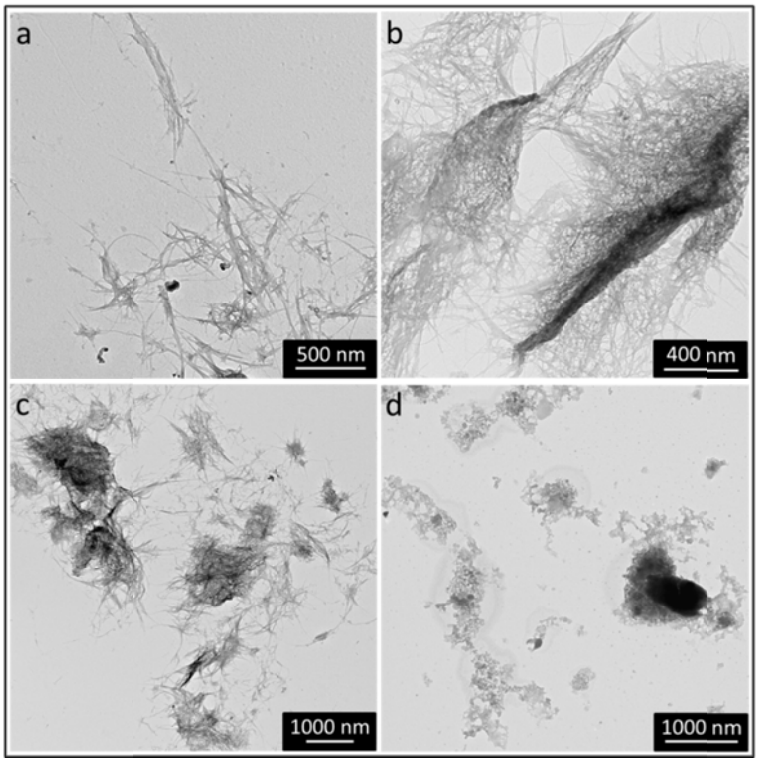

Figure 8. Representative TEM images of *s*-SWCNT-**2** at different magnification (**a**, **b** and **c**) and of the filtrate (**d**).

Coherently with these observations, TGA showed a big decrease in the weight loss, both for N_2 and air measurements, confirming that our treatment effectively removed from the sample the amorphous material, which burns at low temperatures (Figure 9).

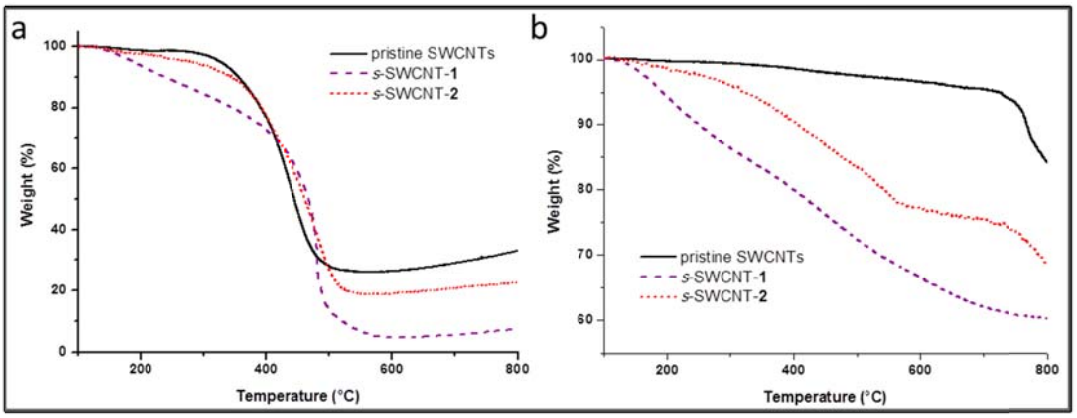

Figure 9. TGA of pristine SWCNTs, *s*-SWCNT-**1** and *s*-SWCNT-**2**, performed in air (**a**) and in N_2 (**b**).

The Raman analyses showed that the NaOH treatment deeply cleaned the nanotubes. In fact, as can be seen in Figure 10, the profile became more similar to the one of pristine SWCNTs, and the Raman spectrum of the filtrate, besides having a very high D-band and a significant fluorescence background, did not present RBM bands.

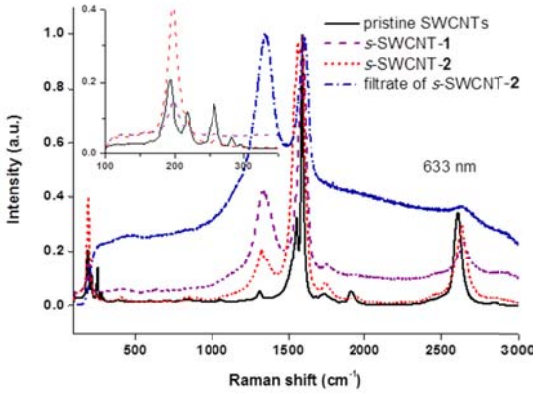

Figure 10. Raman spectra (633 nm) of pristine SWCNTs, *s*-SWCNT-**1**, *s*-SWCNT-**2** and its filtrate. In the inset, the enlargement of the RBM zone is shown.

The Raman spectra obtained at 532 nm and 785 nm resembled even more the ones of pristine SWCNTs, as shown in Figures 11a and 11b, indicating that the alkaline treatment effectively cleaned the sample from carbonaceous impurities. Moreover, since the D/G ratios obtained for *s*-SWCNT-**2** were different according to the laser wavelength, we could conclude that not all the nanotubes in the sample were modified at the same extent, in terms of defects introduced on the structure, by the oxidative treatment.

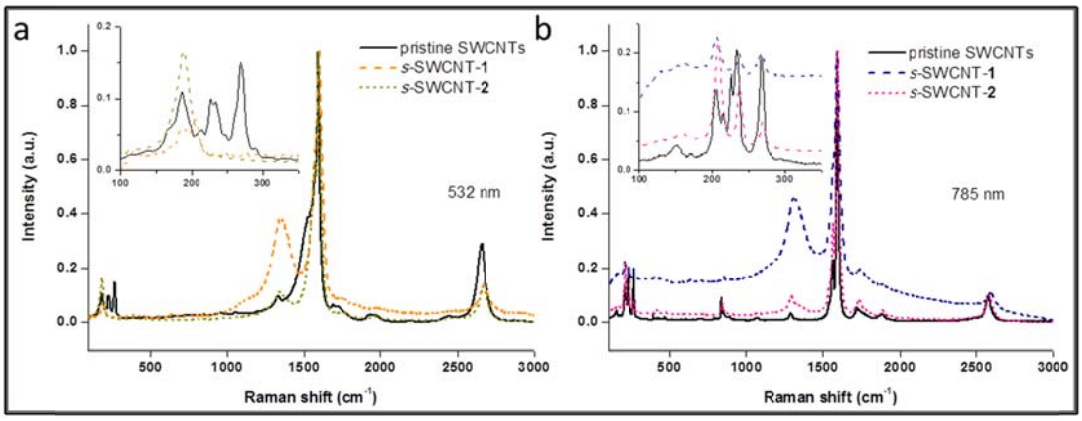

Figure 11. Raman spectra of pristine SWCNTs, *s*-SWCNT-**1** and *s*-SWCNT-**2**, obtained with the 532 nm (**a**) and the 785 nm laser (**b**). In the insets, the enlargement of the RBM zone is shown.

Finally, we performed the re-pristinization experiment also for *s*-SWCNT-**2**, and we obtained exactly the same profile previously reported for re-pristinized *s*-SWCNT-**1** (data not

shown). This is a further confirmation that the phenomenon we observed consisted not only in a purification of the sample from the amorphous carbon content, but also in a structural recovery.

In conclusion, oleum/nitric acid treatment of SWCNTs resulted in the production of shortened and disentangled CNTs, bearing carboxyl and sulfonic groups, with a big improvement in dispersibility. On the other hand, the treatment produced a lot of amorphous carbonaceous material, which was successfully removed by a subsequent NaOH washing treatment. In addition, we observed for the first time a laser-mediated re-pristinization of the SWCNT tubular structure, that effectively mended the defects introduced by the oxidation.

2.2 Mechanochemical shortening of SWCNTs

One of the main limitations of a wet approach for SWCNT shortening is their lack of solubility as pristine material that can determine a non-homogenous cutting, since the material is in form of bundles and therefore the oxidation will not evenly affect all the nanotubes in each bundle. With the oleum-based treatment, as already explained, the intercalation step was intended for a better homogeneity of the dispersion. In the case of the ball milling shortening, the problem of the lack of solubility has been directly bypassed, since we worked in the absence of any solvent. At the same time a dry approach has the advantage of reduced pollution, lower costs, and ease of scale-up. Mechanochemistry involves the transformation of mechanical energy into the driving force for chemical modifications, that can be seen as an alternative way to overcome thermodynamic barriers with respect to more classical systems, such as heating or enzymatic catalysis, and it is generally performed in the absence of any solvent. Few examples have been reported so far in this field: e.g. stress-induced homolytic bond cleavage for polymers has been extensively studied.[11]

In the case of CNTs, the mechanical stress should break them in correspondence of pre-existing defects, where local strain is higher, but could also induce local deformations, such as kinking or twisting, that cause strain energy to concentrate in some points, where breaking will occur. Some studies have already been published where ball milling was used to cut MWCNTs, leading to the formation of carbon nanoparticles similar to carbon onions (spherical form of carbon made of concentric fullerenes),[12] or to shortened MWCNTs.[13] Also a study on the shortening of SWCNTs has been published, but in this case the authors observed an aggregation effect of the ball milling treatment on the CNTs.[14]

We have studied the possibility of using mechanical activation through a planetary ball mill, for obtaining large-scale quantities of shortened SWCNTs (*s*-SWCNT), with a homogeneous distribution of length. The instrument is made of a steel grinding jar containing steel grinding

balls, where the material is placed (Figure 12). Once inside the planetary mill, the jar is rotating in one direction, and the wheel in the opposite one (up to a maximum of 650 rpm in the case of our instrument), thus subjecting the balls to superimposed rotational movements. Their collision with the inner walls of the jar causes frictional and impact forces, thus leading to size reduction of the material.

Figure 12. Planetary ball mill apparatus. Red arrows indicate the direction of rotation.

HiPCO SWCNTs were ball-milled in a set of experiments in which rotational speeds and time of milling were varied (Scheme 4). Following the treatment, the material was washed with HCl in order to remove any Fe_2O_3 possibly deriving from the opening of the tubes during the ball milling, and the air oxidation of the iron present inside, and MeOH, to afford *s*-SWCNT-**3** (**A**, **B**, **C** or **D** according to the different speed and time of treatment). Finally, the weight yield was calculated and the material was fully characterized. Even though characterizations showed that the technique successfully shortened the CNTs without causing severe alteration of their structures, the weight yields were not satisfactory. In fact, high rotational speeds and long milling times led to almost complete destruction of SWCNTs, that could be explained by the formation of volatile by-products and highly oxidized material which could be subsequently eliminated during the washing treatment. For this reason, we decided to compare these results with experiments performed in N_2 atmosphere, giving *s*-SWVNT-**4** (**B**, **C**, **E** or **F**). We found out indeed that the correct choice of the experimental conditions could lead to reasonable yields,

while retaining the structural integrity of SWCNTs. The different conditions used and the final weight yields are summarized in Table 1.

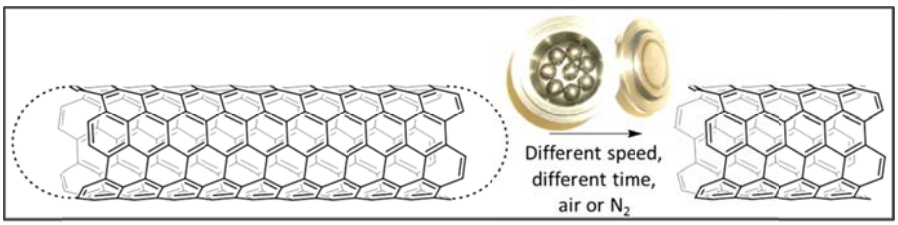

Scheme 4

	Atmosphere	Speed (rpm)	Time (min)	Yield (wt%)
s-SWCNT-3A	air	100	30	39
s-SWCNT-3B	air	250	120	43
s-SWCNT-4B	N_2	250	120	70
s-SWCNT-3C	air	500	30	35
s-SWCNT-4C	N_2	500	30	74
s-SWCNT-3D	air	650	30	9
s-SWCNT-4E	N_2	650	120	71
s-SWCNT-4F	N_2	650	360	48

Table 1. Different experimental conditions for the ball milling treatment.

The dispersibility of *s*-SWCNT depended critically on the milling conditions. According to our results, the milling treatment decreases the amount of bundles and the length of the tubes, producing in general better dispersions. But the atmosphere chosen played an important role: *s*-SWCNT-**3**, obtained in air, presented enhanced dispersibility in polar solvents such as methanol, probably due to the oxidative defects created along the tube during the mechanical process. On the other hand these tubes did not give good dispersions in less polar solvents such as dichloromethane. Differently, the use of a nitrogen atmosphere for the milling treatment, permitted to boost more experimental conditions, thus obtaining smaller tubes, which presented good dispersibility both in methanol and in dichloromethane.

The UV-vis-NIR and the Raman spectra, as already explained, provide reliable structural information on SWCNTs. The UV-vis-NIR spectrum displayed for all the s-SWCNTs the characteristic van Hove singularities, as the example reported in Figure 13a shows. Moreover, the Raman spectra of s-SWCNT obtained with mechanochemical treatment were very similar to the one of the pristine SWCNTs (Figure 13b). These findings indicate that the intrinsic structure of the nanotubes remained largely intact after ball milling.

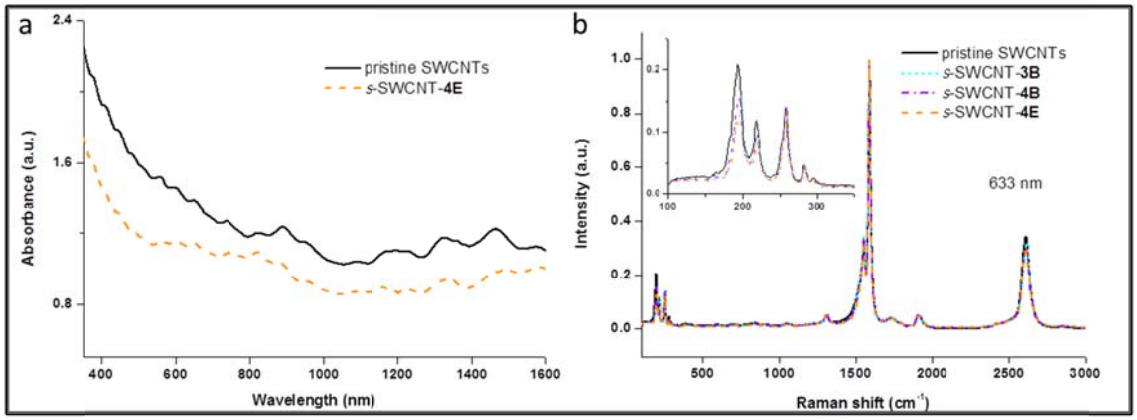

Figure 13. a) UV-vis-NIR spectra of DMF dispersions of pristine SWCNTs and s-SWCNT-**4E** (650 rpm, 120 min, N_2); **b**) Raman spectra (633 nm) of pristine SWCNTs and *s*-SWCNT-**3B** (250 rpm, 120 min, air), **4B** (250 rpm, 120 min, N_2) and **4E** (650 rpm, 120 min, N_2). In the inset, the enlargement of the RBM zone is shown.

By comparison of these spectra with the one obtained with the oxidative shortening of SWCNTs (see Figure 6b in Chapter 2.1), remarkable differences could be appreciated. In fact, the D/G ratio of *s*-SWCNT-**3** and **4** did not present a detectable increase, and, differently from *s*-SWCNT-**1**, all the RBM peaks were preserved. Interestingly, the low decrease in the peak at 193 nm indicates that bigger diameter tubes were the most affected by the mechanical treatment, contrary to the behaviour observed for the oxidative shortening, meaning that different mechanisms were involved in the two cases.

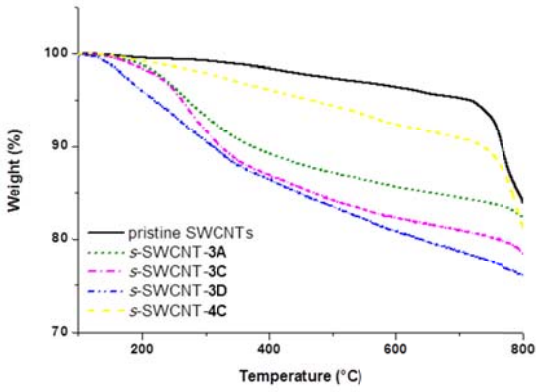

Figure 14. TGA (N_2) of pristine SWCNTs and *s*-SWCNT-**3A** (100 rpm, 30 min, air), **3C** (500 rpm, 30 min, air), **3D** (650 rpm, 30 min, air) and **4C** (500 rpm, 30 min, N_2).

TGA data can be used to estimate CNT purity and the presence and abundance of organic moieties attached to CNT sidewalls. The thermogravimetric profiles of *s*-SWNTs showed a higher weight loss (Figure 14) that may arise from decomposition of defects created along the tubes by the milling treatment, but could also result from adsorbed molecules. In fact it was

reported that CNTs treated with ball mill increase their adsorptive capacity.[15] Moreover, TGA results suggested the presence of much less impurities on *s*-SWCNT-**4**, prepared under N_2, with respect to *s*-SWCNT-**3**, corroborating the hypothesis that less oxidative damage of the CNT structure occurred thanks to the inert atmosphere.

According to the residual mass in the TGA performed in air (data not shown), the amount of iron present in the samples falls from 19.8% for pristine tubes to values in the range 12-14% for the milling treated ones. This decrease could be explained, as anticipated, on the basis of a decomposition of the carbon shells that surround the metal particles, promoted by the milling treatment. Thus, in the presence of O_2, Fe is oxidized to Fe_2O_3, which can be subsequently removed with the acid washings.

Figure 15 shows some typical TEM images of the tubes obtained after milling. Other authors have previously described the undesired formation of large amounts of amorphous carbon, due to the mechanochemical treatment of SWCNTs, and the formation of large aggregates of entangled SWCNTs.[14] Nevertheless, our treatment seems to give clean and dispersed tubes, and to exfoliate the original bundles, as can be appreciated by TEM images. Moreover, as expected, tubes shorten with the increase in the rotational speed and the time of treatment.

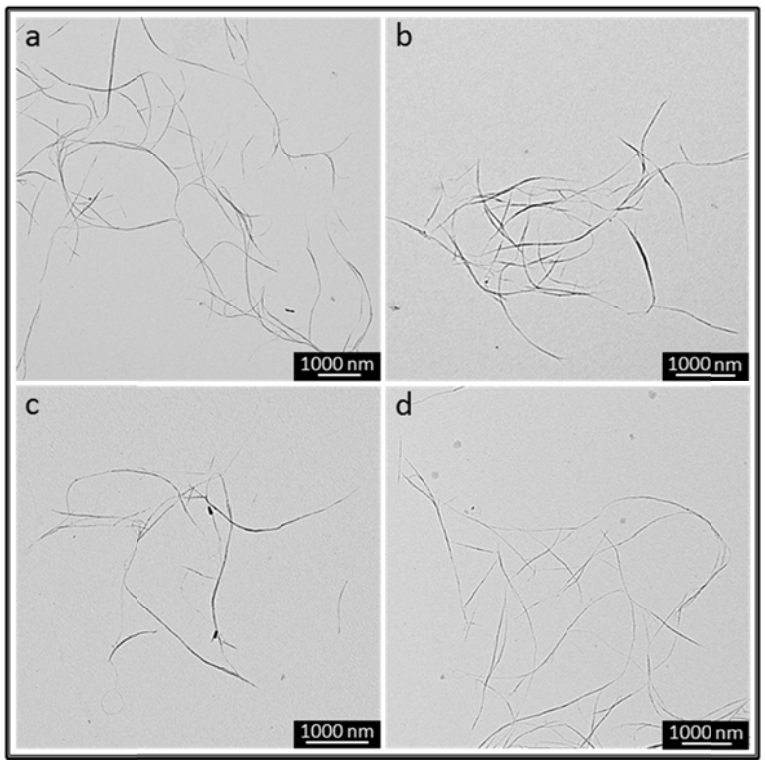

Figure 15. Representative TEM images of *s*-SWCNT-**3A** (100 rpm, 30 min, air) (**a**), **3B** (250 rpm, 120 min, air) (**b**), **4B** (250 rpm, 120 min, N_2) (**c**) and **4E** (650 rpm, 120 min, N_2) (**d**).

In order to evaluate the length distribution of the *s*-SWCNTs obtained with ball milling, we decided to perform statistical analyses using atomic force microscopy (AFM). For a meaningful evaluation, however, we could not settle for the thin bundles observed at TEM, since individually dispersed CNTs were needed. Therefore we used a surfactant known as being quite effective in helping CNTs dispersion, i.e. sodium dodecylbenzenesulfonate (SDBS), to prepare water dispersions of the selected samples. We deposited the dispersions on freshly cleaved mica surfaces by spin-coating, and we thermally removed the surfactant, heating the mica surfaces in an oven.[16] Finally, the surfaces were analyzed through tapping mode-AFM (TM-AFM). Figure 16 reports a representative TM-AFM image of *s*-SWCNT-**4B**, showing individual tubes. The height of the tubular objects observed at the AFM let us distinguish between individual tubes and bundles. The height profile shown in Figure 16b, shows a vertical distance of 0.71 nm, which is in good agreement with the typical HiPCO SWCNT diameters, considering the well-known effect of vertical sample compression of CNTs when they are touched by the AFM tip.[17]

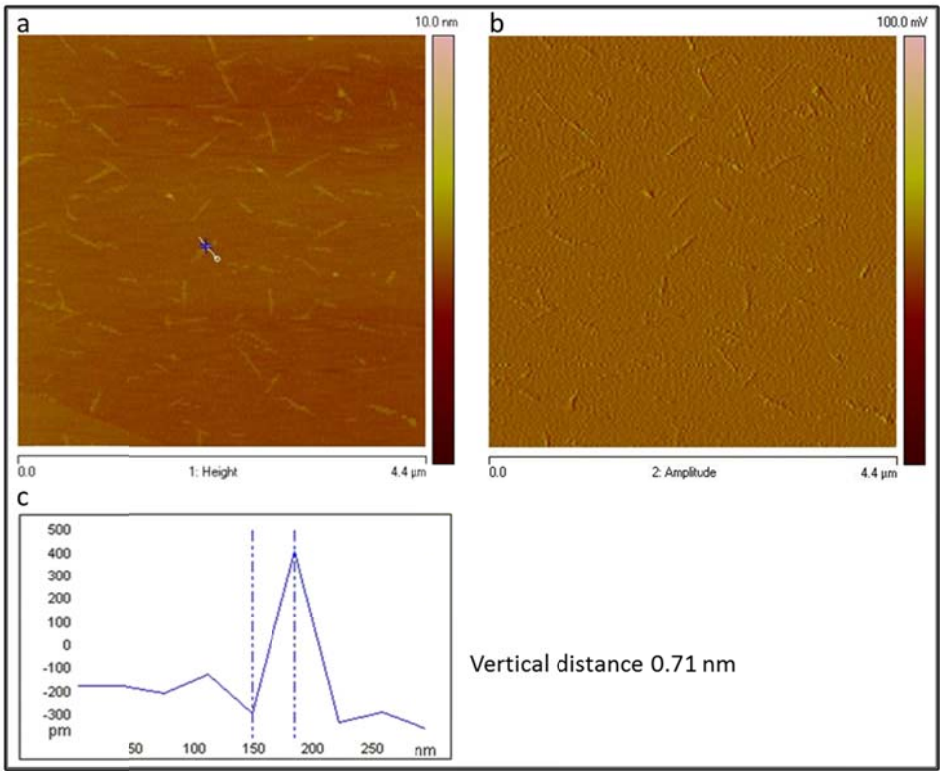

Figure 16. Representative TM-AFM height (**a**) and amplitude (**b**) images of *s*-SWCNT-**4B** (250 rpm, 120 min, N_2); **c**) height profile of the line indicated in the topographic image a.

Samples *s*-SWCNT-**3B** and **4B**, and *s*-SWCNT-**4E** were chosen as representative, to study the length distribution of the tubular objects observed in the TM-AFM images. The comparison between the milling treatment at 250 rpm for 120 min in air or N_2 revealed that the latter conditions led to a narrow distribution of shorter CNTs (Figure 17a). The mean lengths of the

samples were 0.74 ± 0.51 µm and 0.46 ± 0.35 µm for the treatment in air (*s*-SWCNT-**3B**) and in N_2 (*s*-SWCNT-**4B**) respectively. In fact, as previously discussed, air could lead to higher destruction of SWCNTs with respect to N_2, speed and time being equal. Moreover, considering our results we can hypothesize that shorter tubes, once formed, are more easily destroyed in air, therefore leading to the two different length distribution profiles. This fact can also account for the lower yields relative to *s*-SWCNT-**3** with respect to *s*-SWCNT-**4** (43% vs. 70% for samples **3B** and **4B** respectively). Therefore the production of short SWCNTs is prevented when air atmosphere is used. Under N_2 instead, the increase in the rotational speed to 650 rpm further reduced the mean length to 0.36 ± 0.16 µm, with no tubes longer than 1 µm (Figure 17b), confirming our hypothesis that, tuning the conditions, it would have been possible to control the length distribution of the *s*-SWCNT.

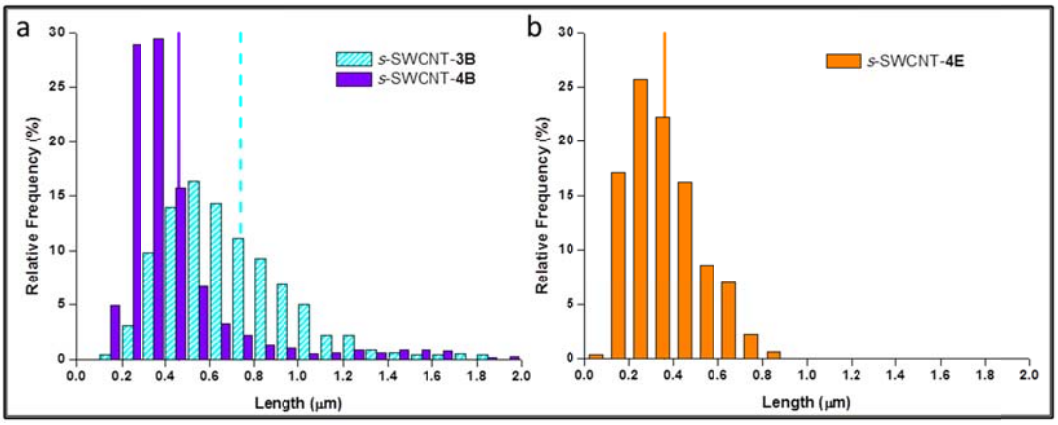

Figure 17. a) Length distribution of *s*-SWCNT-**3B** (250 rpm, 120 min, air, count = 1288) and *s*-SWCNT-**4B** (250 rpm, 120 min, N_2, count = 775); **b**) length distribution of *s*-SWCNT-**4E** (650 rpm, 120 min, N_2, count = 315). Vertical lines indicate the average length of the samples.

In order to determine if there was a limit in boosting experimental conditions, we ball-milled SWCNTs at 650 rpm, for much longer time, namely 6 h. The treatment, though being in N_2, strongly lowered the weight yield (48 %). Moreover, these conditions triggered the damage of the tubes to quite a considerable extent, as can be clearly seen by the Raman spectrum of *s*-SWCNT-**4F** (Figure 18).

We tried to apply the laser re-pristinization observed for *s*-SWCNT-**1** (see Chapter 2.1.1) to this sample, but it was unsuccessful. In fact, tubes not only did not recover after the high power laser treatment, but the opposite effect occurred: Raman cross section strongly decreased, and the focal area appeared emptied when looking at the sample with the microscope after the treatment. Therefore, we could conclude that the sample, either constituted by very short tubes or by amorphous material, was burned by the laser.

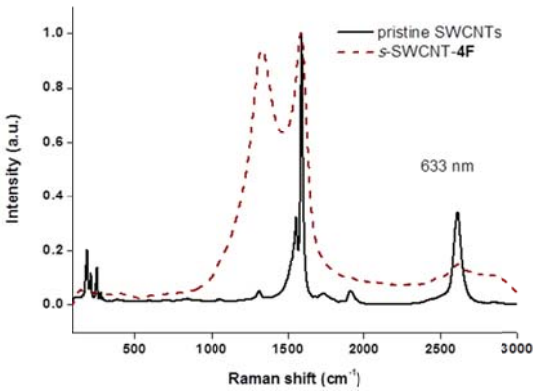

Figure 18. Raman spectra (633 nm) of pristine SWCNTs and *s*-SWCNT-**4F** (650 rpm, 360 min, N_2).

Nevertheless, we could visualize the material obtained at TEM, finding very short linear objects that appeared as 3 D when adjusting the focus of the microscope (Figure 19). Their average length was measured to be 0.15 ± 0.09 µm (count = 84). Even if deeper evaluations (such as HR-TEM) would be needed to assess it doubtless, these objects seemed to be SWCNTs, individually dispersed without the need of any surfactant. However, given these results, the use of shorter treatment time is recommended.

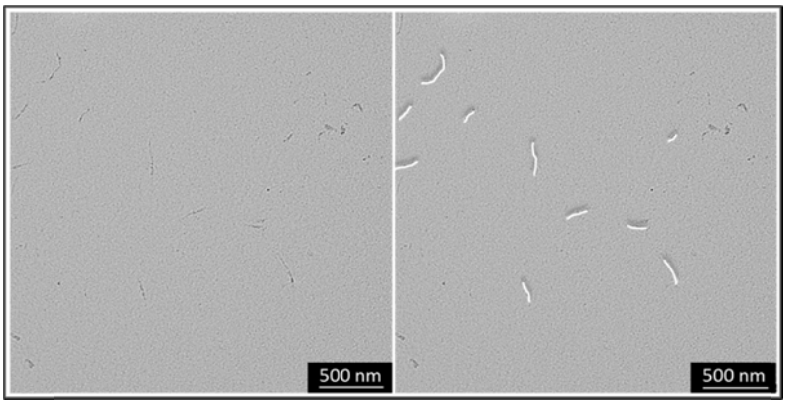

Figure 19. Representative TEM image of *s*-SWCNT-**4F** (650 rpm, 360 min, N_2). The right panel report the same image with white lines drawn to help the eye in recognizing CNTs.

In conclusion, we reported an easy procedure for preparing scalable quantities of shortened SWCNTs with a planetary mill. The different complementary characterizations of these tubes showed that the treatment did not compromise their tubular structure. Moreover, the possibility to control the quality of the final products tuning experimental conditions render it a good alternative to wet chemistry approaches.

2.3 Acknowledgments

The study on mechanochemical shortening of SWCNTs was carried out in collaboration with Noelia Rubio, Prof. M. Antonia Herrero and Prof. Ester Vázquez (Departamento de Química Orgánica, Facultad de Químicas-IRICA, Universidad de Castilla-La Mancha in Ciudad Real, Spain). In particular, I wish to thank Noelia Rubio for some of the milling treatment and TGA.

2.4 References

1. Z. Chen, K. Kobashi, U. Rauwald, R. Booker, H. Fan, W.-F. Hwang, and J. M. Tour, *J. Am. Chem. Soc.*, 2006, 128, 10568-10571.
2. L. M. Ericson, H. Fan, H. Peng, V. A. Davis, W. Zhou, J. Sulpizio, Y. Wang, R. Booker, J. Vavro, C. Guthy, A. N. G. Parra-Vasquez, M. J. Kim, S. Ramesh, R. K. Saini, C. Kittrell, G. Lavin, H. Schmidt, W. W. Adams, W. E. Billups, M. Pasquali, W.-F. Hwang, R. H. Hauge, J. E. Fischer, and R. E. Smalley, *Science*, 2004, 305, 1447-1450.
3. S. Ramesh, L. M. Ericson, V. A. Davis, R. K. Saini, C. Kittrell, M. Pasquali, W. E. Billups, W. W. Adams, R. H. Hauge, and R. E. Smalley, *J. Phys. Chem. B*, 2004, 108, 8794-8798.
4. S. Arepalli, P. Nikolaev, O. Gorelik, V. G. Hadjiev, W. Holmes, B. Files, and L. Yowell, *Carbon*, 2004, 42, 1783-1791.
5. P.V. Huong, R. Carvagnat, P.M. Ajayan, O. Stephan, Phys. Rev. B 51 (1995) 10048.
6. a) P. Corio, P. S. Santos, M. a Pimenta, and M. S. Dresselhaus, *Chem. Phys. Lett.*, 2002, 360, 557-564; b) L. Zhang, H. Li, K.-T. Yue, S.-L. Zhang, X. Wu, J. Zi, Z. Shi, and Z. Gu, *Phys. Rev. B*, 2002, 65, 07340 (4).
7. J. S. Kim, K. S. Ahn, C. O. Kim, and J. P. Hong, *Appl. Phys. Lett.*, 2003, 82, 1607.
8. Z. Yu and L. E. Brus, *J. Phys. Chem. A*, 2000, 104, 10995-10999.
9. H. Huang, R. Maruyama, K. Noda, H. Kajiura, and K. Kadono, *J. Phys. Chem. B*, 2006, 110, 7316-7320.
10. a) E. Heister, C. Lamprecht, V. Neves, C. Tilmaciu, L. Datas, E. Flahaut, B. Soula, P. Hinterdorfer, H. M. Coley, S. R. P. Silva, and J. McFadden, *ACS Nano*, 2010, 4, 2615-2626; b) B. C. G. Salzmann, S. A. Llewellyn, G. Tobias, M. A. H. Ward, Y. Huh, and M. L. H. Green, *Adv. Mater.*, 2007, 19, 883-887.
11. M. K. Beyer and H. Clausen-Schaumann, *Chem. Rev.*, 2005, 105, 2921-2948.
12. Y. B. Li, B. Q. Wei, J. Liang, Q. Yu, and D. H. Wu, *Carbon*, 1999, 37, 493-497.
13. a) N. Pierard, A. Fonseca, Z. Zonya, I. Willems, G. Van Tendeloo, and J. B. Nagy, *Chem. Phys. Lett.*, 2001, 335, 1-8; b) Z. Kónya, J. Zhu, K. Niesz, D. Mehn, and I. Kiricsi, *Carbon*, 2004, 42, 2001-2008.

14. N. Pierard, A. Fonseca, J.-F. Colomer, C. Bossuot, J.-M. Benoit, G. Van Tendeloo, J.-P. Pirard, and J. B. Nagy, *Carbon*, 2004, 42, 1691-1697.

15. Y. F. Sun, A. M. Zhang, Y. Yin, Y. M. Dong, Y. C. Cui, X. Zhang, and J. M. Hong, *Mater. Chem. Phys.*, 2007, 101, 30-34.

16. M. F. Islam, E. Rojas, D. M. Bergey, A. T. Johnson, and A. G. Yodh, *Nano Lett.*, 2003, 3, 269-273.

17. a) T. DeBorde, J. C. Joiner, M. R. Leyden, and E. D. Minot, *Nano Lett.*, 2008, 8, 3568-3571; b) V. Zorbas, A. Ortiz-Acevedo, A. B. Dalton, M. M. Yoshida, G. R. Dieckmann, R. K. Draper, R. H. Baughman, M. Jose-Yacaman, and I. H. Musselman, *J. Am. Chem. Soc.*, 2004, 126, 7222-7227.

Conjugation of antibodies to CNTs

The possibility to combine the technologies of CNTs and antibodies (Abs) was studied. Antibodies, or immunoglobulins, are a family of proteins produced by the immune system, that play a crucial role in the recognition and neutralization of foreign objects in the body. To do so, they have remarkable selectivity and picomolar potency, and this quality could render them an outstanding antineoplastic agent, since they can target key regulators in the development of cancer. Nevertheless, to date, they have not been used for intracellular targets as they do not readily cross cell membranes. The conjugation of antibodies to CNTs should enable their use in an intracellular environment, addressing one of the important limitations of antibody-based cancer therapy, and paving the way to a variety of unexplored therapeutic possibilities. With a different approach, Abs can also serve as targeting agents. If we conjugate them to CNTs, they should specifically direct the system and thus they will enable a targeted drug delivery.

With the aim of studying these different opportunities we prepared different CNTs-Ab constructs. To do so, we decided to use a covalent approach, that should guarantee good stability to the final constructs, avoiding an *in vivo* dissociation of the Ab due to its possible displacement by other biological macromolecules. As a model, hCTM01 Ab was conjugated to CNTs using different covalent approaches.

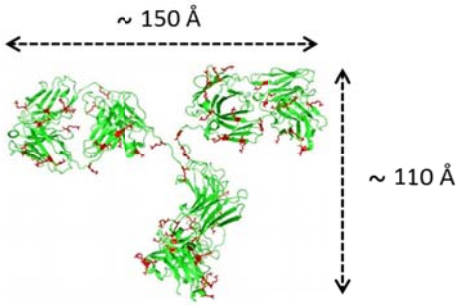

Figure 1. A typical IgG (lysine residues are highlighted in red).

The antibody hCTM01 IgG is a humanized monoclonal antibody that binds to polymorphic epithelial mucins (PEM), the overexpression of which is associated with many tumours.[1] The term “humanized” is used to describe an antibody with an antigen-binding site deriving from a non-human immunoglobulin, and the remaining part deriving from a human one, in order to avoid recognition of the antibody from the body as “foreigner”.

3.1 IgG-DWCNT

3.1.1 Preparation

The first synthetic strategy exploited an amidation process to immobilize the antibody mainly at the tips of oxidized CNTs. An alternative approach was based on a chemoselective reaction to tether the antibody on amino-functionalized CNTs, following the introduction of a solubilizing chain via amidation of the carboxylic groups or via 1,3-dipolar cycloaddition of azomethine ylides on the CNT sidewall. We used DWCNTs, provided by the supplier as already shortened and oxidized and thus bearing carboxylic acids (*s*-DWCNT). They had an average diameter of 3.5 nm, according to the supplier, and confirmed by our TEM analyses. Moreover, TEM let us evaluate the length distribution of the sample (Figure 2), whose average length was of 400 ± 368 nm.

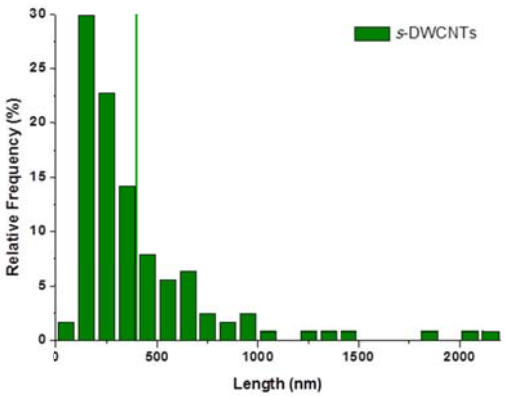

Figure 2. Length distribution of s-DWCNT analysed by TEM (count = 127). The vertical line indicates the average length of the sample.

In the first conjugation strategy, the Ab was introduced at the tips and in correspondence of the sidewall defect sites of CNTs, performing an amidic coupling between the carboxylic functions of *s*-DWCNT and the amine groups of the lysine side chains available on the Ab. As illustrated in Scheme 1, a two-step amidation was performed. First, we activated the carboxylic groups on the *s*-DWCNT to their corresponding NHS-ester, and subsequently, after purification of this construct from any excess reagent, we made it statistically react with the lysine side chains of the Ab, without using additional coupling agents, to obtain *s*-DWCNT-**1**.

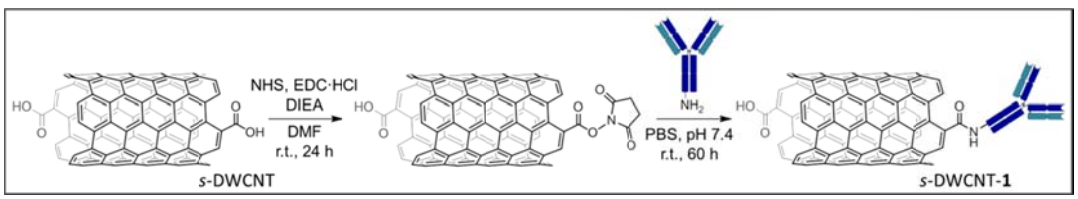

Scheme 1. (Ab and CNT are not in size scale)

This strategy was required to avoid any undesirable side reactions, since intermolecular conjugation of Ab would have been possible in a one-step amidation, because of the high density of both carboxyl and amine groups on the protein.

As an alternative to the direct conjugation to the carboxylic groups we studied also the coupling of the Ab in the same position (i.e. mainly the tips of the CNTs), but introducing in between a solubilizing chain, which served also as a spacer between the nanotube and the Ab. In this case, we first modified the carboxylic groups by an amidation step with amine **1**, yielding, after cleavage of the Boc protecting group with HCl (4 M) in dioxane, ammonium-functionalized *s*-DWCNT-**2**. The amount of amine groups was determined by Kaiser test[2] to be 120 μmol/g. These amines were subsequently modified by reaction with an NHS-activated propionic acid bearing a maleimide group, to give *s*-DWCNT-**3** (Scheme 2), whose degree of functionalization was evaluated by the difference in the Kaiser test to be 60 μmol/g.

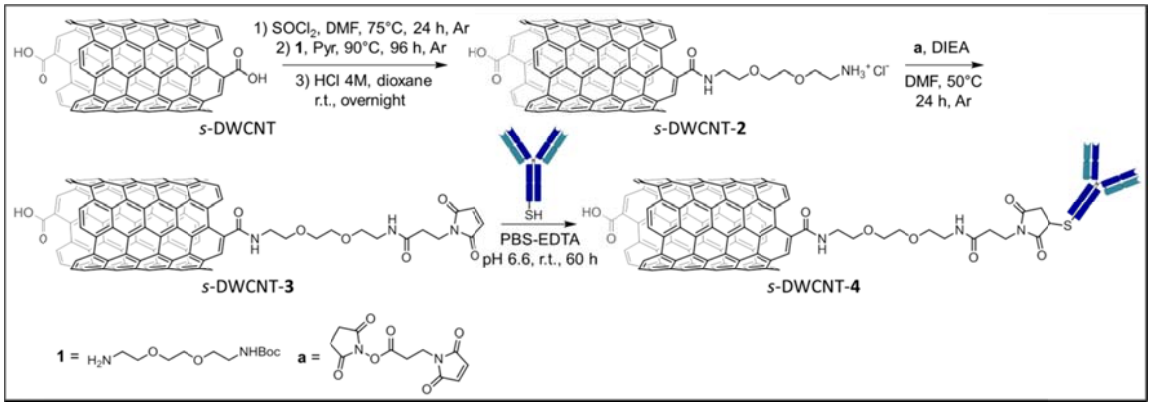

Scheme 2. (Ab and CNT are not in size scale)

The maleimide group allows the covalent conjugation of sulfhydryl-containing molecules to form stable thioether bonds, but all the cysteine residues within the IgG sequence are involved in disulphide bonds to form its quaternary structure. Therefore, it was necessary to treat the Ab with 2-iminothiolane (Traut's reagent),[3] which react with the primary amines of lysine residues introducing sulfhydryl groups (Scheme 3), the amount of which was subsequently determined by Ellman's assay.[4] In a typical experiment we introduced an average of 5 free sulfhydryl groups per Ab, a ratio that is considered reasonable, since reacting all the available lysine amines (more or less 20 in a IgG) could adversely affect Ab function.

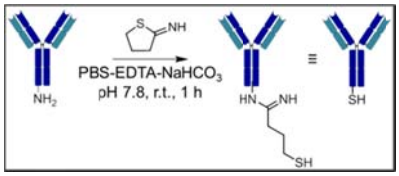

Scheme 3

The SH-bearing antibody was then conjugated to *s*-DWCNT-**3**, giving *s*-DWCNT-**4** (Scheme 2). Maleimide reaction with sulfhydryl groups should be performed at pH 6.5-7.5 since at higher pH the maleimide group could hydrolyse. Moreover, the chain introduced on the Ab through Traut's reagent could undergo cyclization at pH ≥ 7.[5] Therefore coupling reaction was performed at pH 6.6.

With a third synthetic approach, illustrated in Scheme 4, 1,3-dipolar cycloaddition of azomethine ylides was performed on s-DWCNT, using aminoacid **3** and paraformaldehyde. After cleavage of the Boc protecting group (amine content by Kaiser test was 80 µmol/g), the amine group at the end of the triethylene glycol chain was further derivatized to introduce the maleimide group, as we did for *s*-DWCNT-**3,** obtaining a functionalization of 30 µmol/g. The SH-bearing antibody prepared as previously described was then conjugated to *s*-DWCNT-**6**, to afford *s*-DWCNT-**7**.

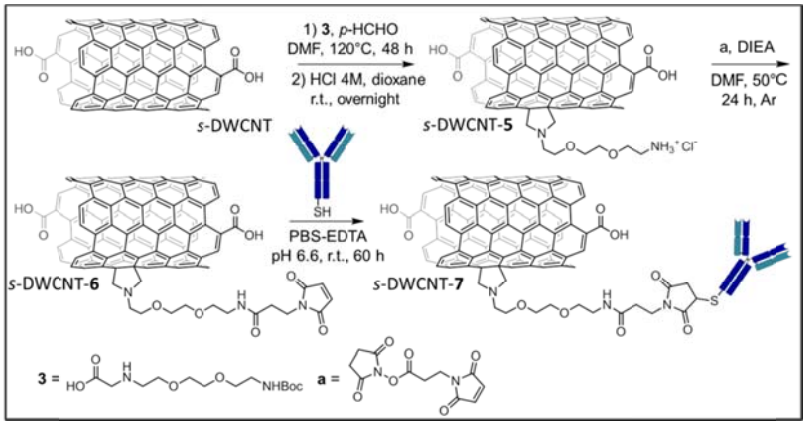

Scheme 4. (Ab and CNT are not in size scale)

The three different coupling reactions between CNTs and Ab were monitored by UV spectroscopy. At certain time intervals, an aliquot of the reaction mixture was centrifuged at high speed (16000 g) to separate the solution containing the unreacted antibody (in the supernatant) from CNTs and Ab-CNT conjugates precipitating to the bottom. The absorbance at 280 nm (due to the side chains of the aromatic amino acids present in the antibody) in the supernatant of the solution decreased as the antibody bound to the nanotube (Figure 3). Following the coupling, the remaining free Ab or the Ab simply adsorbed on the sidewalls of the tubes was eventually eliminated by cycles of centrifugation and removal of the supernatant with fresh PBS.

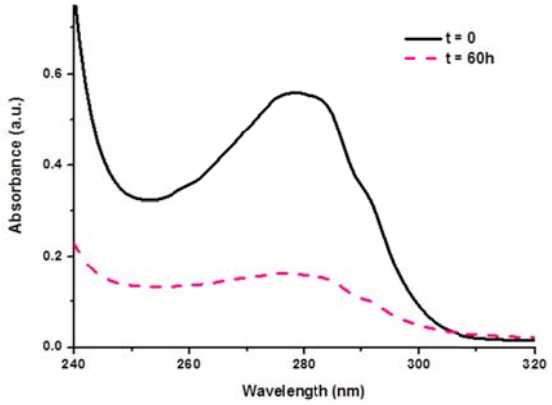

Figure 3. UV-Vis spectra of the supernatant following the coupling reaction between *s*-DWCNT-**3** and the Ab, showing the decrease of the absorption peak at 280 nm.

3.1.2 Characterization

To prove the successful immobilization of the antibody on CNTs, we used different complementary techniques. TEM images of the Ab-CNT conjugates show that the morphological structure of the nanotubes was not affected by the conditions used for the coupling reaction (Figure 4).

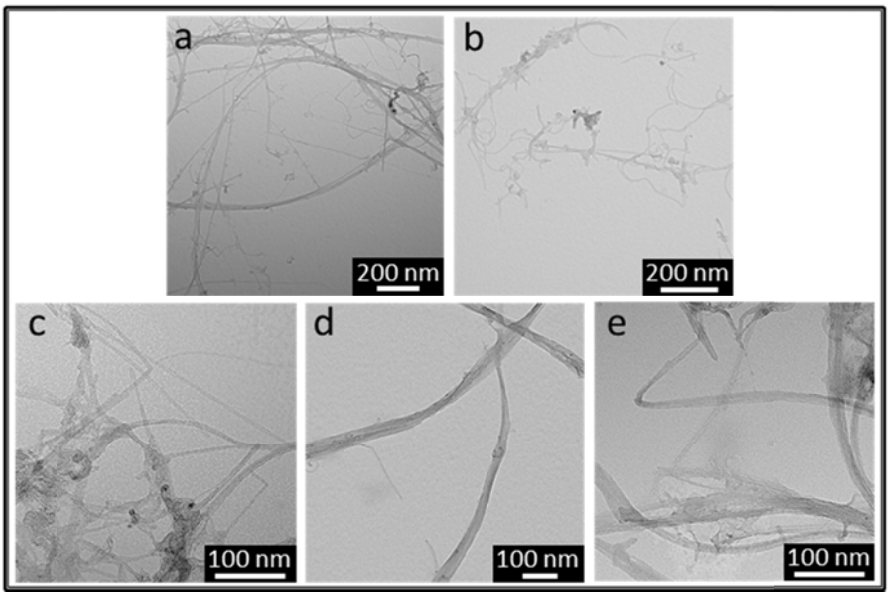

Figure 4. Representative TEM images of pristine DWCNTs (**a**), *s*-DWCNT (**b)**, *s*-DWCNT-**1** (**c**), *s*-DWCNT-**4** (**d**) and *s*-DWCNT-**7** (**e**).

Gel electrophoresis analysis under non-reducing conditions was used to assess to absence of any unbound Ab. In fact, as Figure 5 shows, when loading a CNT sample in the electrophoretic apparatus, the nanotubes are staying in the loading well, since they cannot pass through the gel, and only unbound material is moving.

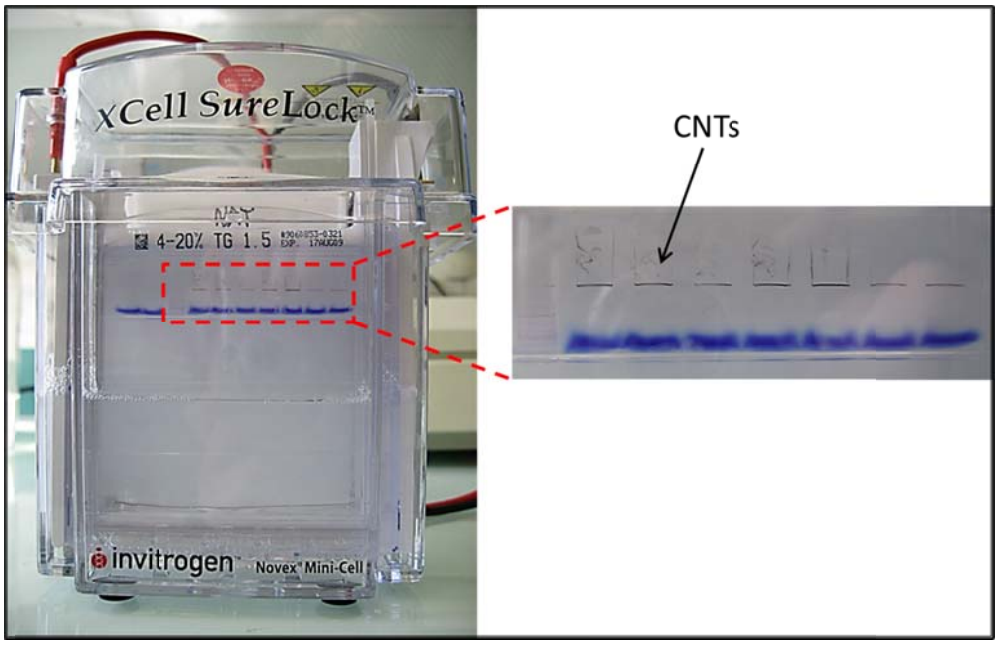

Figure 5. Electrophoretic apparatus used for the analysis with an enlargement of the loading wells.

For derivatives *s*-DWCNT-**4** and **7** we did not observe any unbound proteic material, but the same did not apply to *s*-DWCNT-**1** (Figure 6). Therefore we performed a dialysis of the Ab-CNT using a membrane with a 300 kDa cutoff, in order to remove any residual Ab (whose molecular weight is of 150 kDa) adsorbed on CNT surface, and the electrophoretic gel confirmed the effectiveness of this step (lane 5 vs. lane 4).

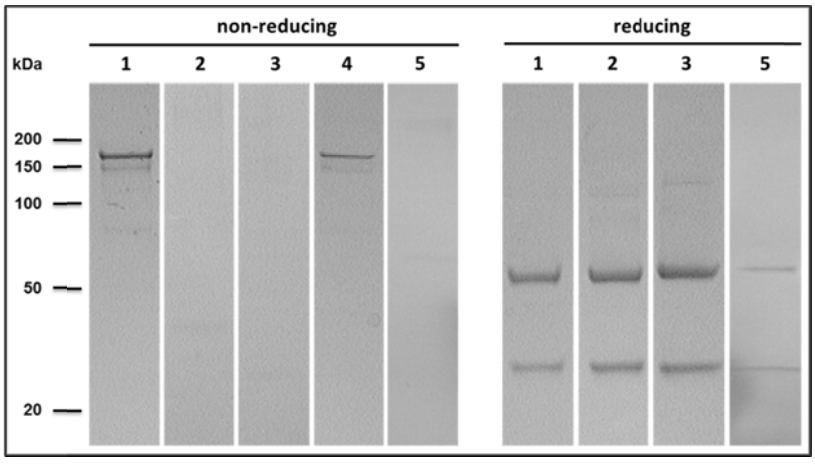

Figure 6. Electrophoretic gels under non-reducing or reducing conditions of Ab (lane 1), *s*-DWCNT-**4** (lane 2), *s*-DWCNT-**7** (lane 3) and *s*-DWCNT-**1** before (lane 4) and after (lane 5) dialysis.

A possible explanation for this event is that *s*-DWCNT-**1** derived from the direct binding of the Ab to naked *s*-DWCNT, while in the case of *s*-DWCNT-**4** and **7** the Ab was bound to s-DWCNT previously functionalized with a chain. As a consequence, it was probably easier for the

Ab to adsorb on CNT surface in the first case, while in the second case the surface was covered by the functionalization, and therefore no longer available to the Ab.

Furthermore, electrophoresis under reducing conditions can be used to visualize portions of the Ab, since in this case the disulphuric bonds between the chains of the Ab are reduced. As expected, a pattern of two bands appeared, due to the heavy chains (50 kDa) and the light chains (25 kDa) of the Ab. These results not only confirm that the Ab was really bound to the CNT, but they also suggest that it was intact after the conjugation.

Thermogravimetric analysis was used to evaluate the degree of functionalization of the Ab-CNT conjugates. Figure 7 shows the weight loss under inert atmosphere. The pristine DWCNTs were stable up to 800°C, while *s*-DWCNT showed an increase in the weight loss, due to the oxidized groups introduced on their structure. This thermal weight loss further increased for functionalized *s*-DWCNT-**2**, **3**, **5** and **6**, in which also the molecules covalently attached to the nanotube could burn. For the final Ab-CNTs conjugates TGA results let us estimate the amount of proteic material bound to CNTs, by comparison with the thermogravimetric profile of their precursors at the temperature at which, according to the first derivative, the weight loss was complete (Figure 7).

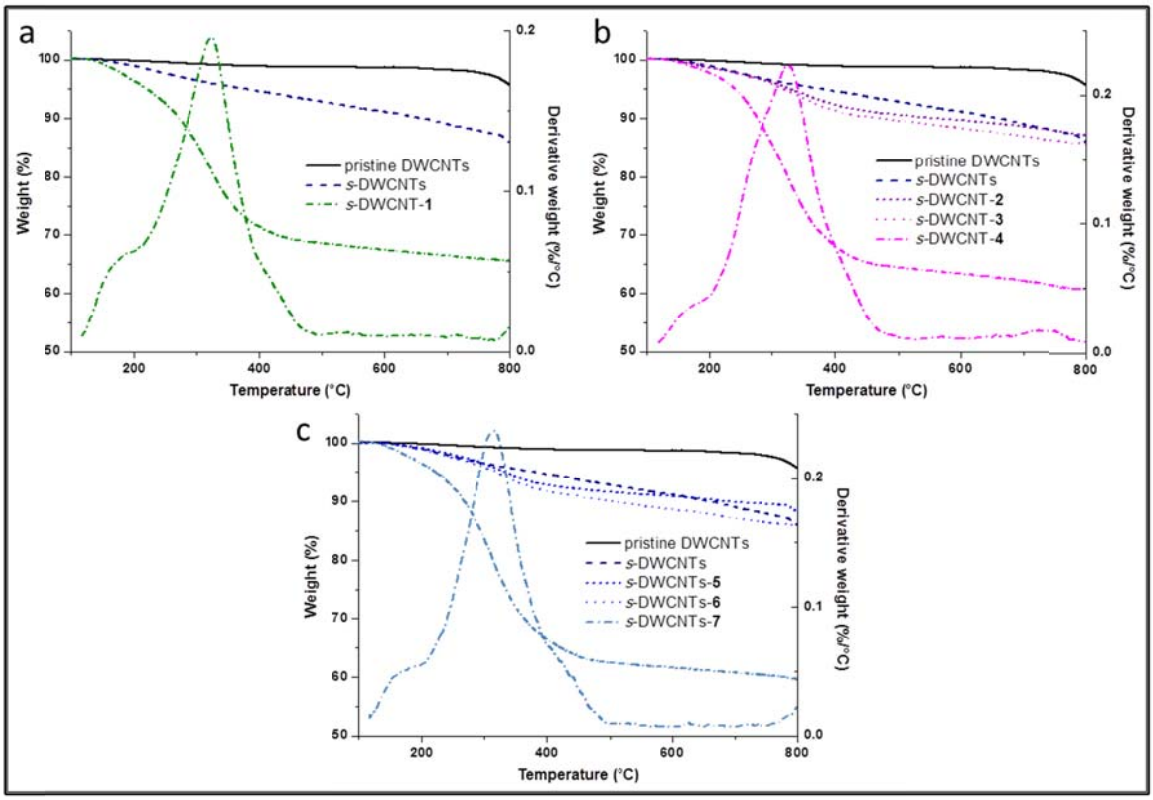

Figure 7. TGA (N_2) of DWCNTs derivatives.

We could calculate a loading of 24% of Ab with respect to the whole conjugate for *s*-DWCNT-**1** (in terms of weight). Similarly, loading values of 25% and 28% were obtained for *s*-DWCNT-**4** and **7**, respectively. These values are in good agreement with the decrease of Ab concentration in the supernatants of the coupling reactions (Figure 3), considering that part of the antibody disappearing from the supernatant was simply adsorbed on CNT and therefore it was washed off after the reaction. The loading calculated by TGA, if expressed in molarity, correspond to concentrations of 2.1, 2.2 and 2.6 μmol of Ab per gram of CNT for the three conjugates respectively, meaning that only a small fraction (less than 10%) of the maleimide groups reacted with the antibody, probably due to steric hindrance.

Finally, the functional activity of the Ab coupled to carbon nanotubes was studied. This is the first fundamental step to prove that the Ab is still able to exert its activity. In this context, we assessed by surface plasmon resonance (SPR) the recognition capability of the CNT-coupled antibody towards its antigen.[6] This technique allows the measurement of the specific interactions between the antibody and its antigen in real time. For this purpose, the antigen is immobilized on a sensor chip surface while the antibody is allowed to continuously flow over it, in order to let it bind to the surface if the recognition takes place. The interaction is then detected as a change in the refractive index at the interface between the chip surface and the aqueous media above it, and it is presented as a sensorgram. The registered sensorgram offers the possibility to calculate the kinetic parameters of the interaction (*i.e.* the association and dissociation rate constants). First of all, the antigen sequence ^{296}HGVTSAPDTRPAPGSTAPPA^{315}, which belongs to the antibody-recognized domain of PEM,[7] was synthesized, together with a control peptide (called “scrambled” antigen, APHADPSTPGAPSVTPRTAG) with the same number and type of amino acids, but placed at different positions in the sequence. This control enabled us to evaluate the non-specific component of the binding between the antibody and the antigen. Each sensorgram was obtained measuring simultaneously (in two different channels) the response to the analyte with the real antigen and with the scrambled one, in order to subtract the non-specific component of the binding. Indeed, the antibody recognized only the antigen but not the “scrambled” antigen, thus confirming its high selectivity. We also performed control experiments using *s*-DWCNT-**2** to evaluate the possibility of non-specific binding between the antigen and the nanotubes and we found a response close to zero (data not shown). Finally, we assessed the interaction of the three Ab-CNT constructs obtained. All conjugates were able to recognize the antigen on the sensor chip, giving a positive response (Figure 8).

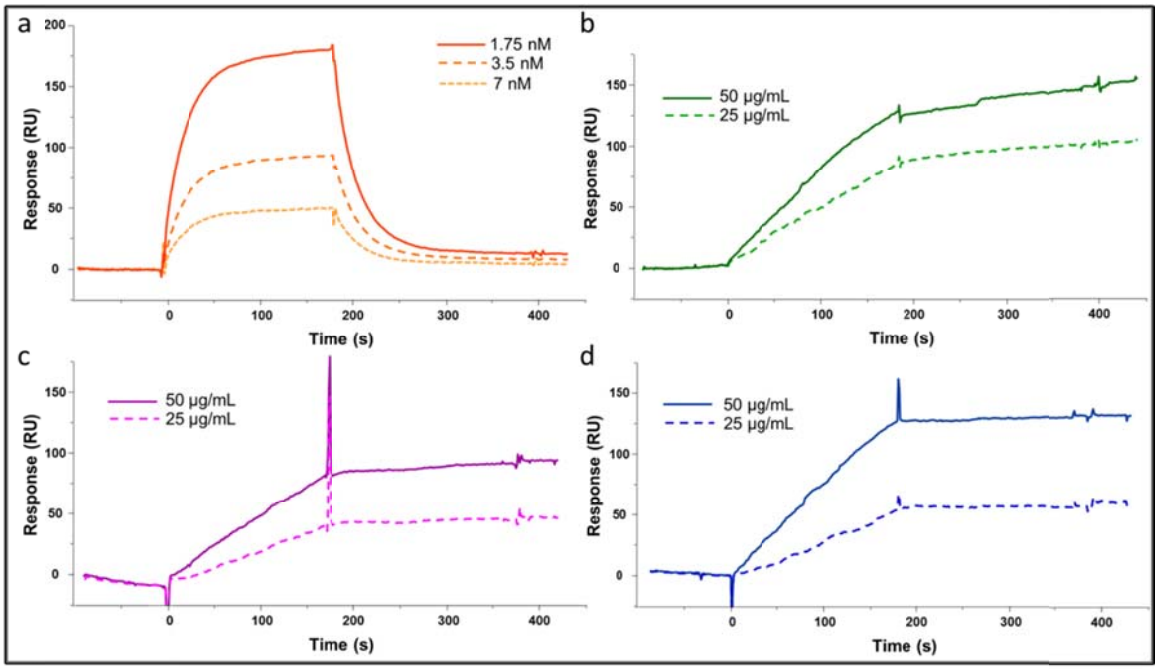

Figure 8. SPR analyses of hCTM01 IgG (**a**) and *s*-DWCNT-**1** (**b**), **4** (**c**) and **7** (**d**).

However, it is worth pointing out that it is not possible, with an Ab-CNT construct, to get quantitative binding information from the SPR, for two main reasons: 1) a precise molecular weight for CNTs, being an heterogeneous material, cannot be determined and hence association and dissociation rate constants could not be obtained from the sensorgrams; 2) Ab in the conjugates are likely distributed with different orientations, and this fact may affect their overall binding capability. Nevertheless, these results highlight very importantly how the covalent attachment of Ab on CNTs does not affect their recognition capability, thus proving the feasibility of the system.

3.2 Fab'-MWCNT and scFv-MWCNT

Exploiting the experience gained in the conjugation of IgG to DWCNTs, we went on in the effort to prepare covalent CNTs-Ab conjugate. Considering our previous results we decided to move to a different kind of CNTs, i.e. MWCNTs, with a completely different aspect ratio, in order to assess the reproducibility of our functionalization strategy with different materials and to get an improvement in the solubility of the derivatives. MWCNTs are in fact able to give better dispersions in both organic solvents and water, with respect to DWCNTs. Also, we decided to prepare a doubly functionalized derivative, using both amidation and cycloaddition, and introducing two chains bearing terminal amines orthogonally protected. Since the different functionalization strategies studied so far for the coupling of the Ab proved all to be effective, we choose to place it on the chain introduced through the cycloaddition, whose

functionalization in terms of maleimide groups was by far high enough for the purpose, in order to leave the chain introduced with amidation for the attachment of a probe, necessary for the biological studies. Furthermore, we moved from the whole Ab to smaller fragments of it, namely the antigen-binding fragment (Fab') and the single-chain variable fragment (scFv), still able to specifically recognize the antigen (Figure 9), which in principle should offer a better control of the conjugation with the CNTs, for reasons that will be discussed in details later.

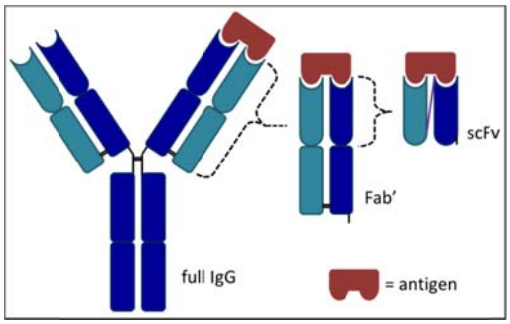

Figure 9. Schematic representation of a full IgG, a Fab' and a scFv.

3.2.1 Preparation

First of all, MWCNTs underwent an oxidative cutting step, using a mixture of aqueous sulphuric and nitric acid and sonicating them for 24 h in a sonic bath. An oxidative treatment for CNTs, as we already explained in Chapter 2.1 in regard to SWCNTs, has the double aim of shortening the nanotubes, improving their solubility, and of introducing carboxylic groups on their structure. These carboxylic groups are necessary for the following amidation step. The shortened MWCNTs (*s*-MWCNT) were analysed by TEM, to check that the harsh conditions of the cutting did not affect their structure (Figure 10a).

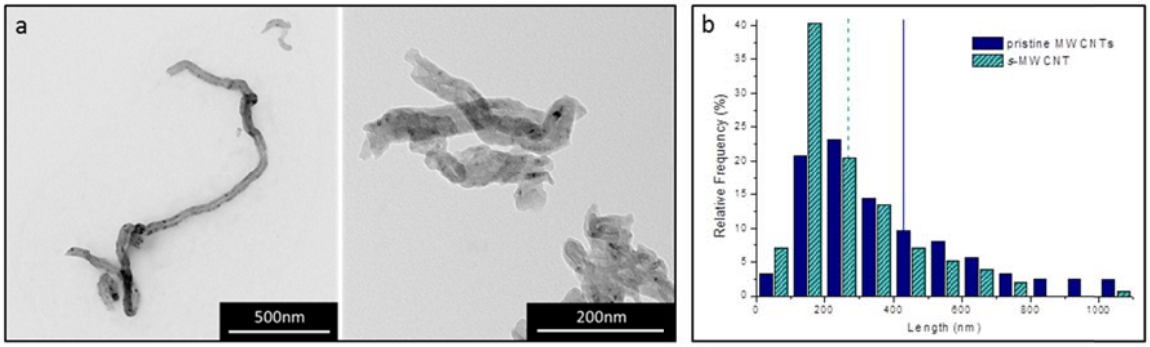

Figure 10. a) Representative TEM images of pristine MWCNTs (left) and *s*-MWCNTs (right); **b**) length distributions of pristine MWCNTs (count = 125) and *s*-MWCNT (count = 156). Vertical lines indicate the average length values.

The average diameter of pristine MWCNTs being 34 ± 10 nm, we compared diameter distribution of pristine and shortened MWCNTs to further confirm that no extensive damage occurred upon the oxidation, and indeed it remained unchanged (data not shown).

Moreover TEM let us study the length distribution of *s*-MWCNT, and compare it with the one of pristine MWCNTs, in order to verify the actual shortening of the tubes (Figure 10b). Indeed, the MWCNTs that we used had an average length of 428 nm ± 354 nm as pristine, and of 268 nm ± 174 nm after oxidation.

s-MWCNT were functionalized in two consecutive steps, exploiting two different approaches, namely amidation and 1,3-dipolar cycloaddition of azomethine ylides, introducing two chains with orthogonally protected amino groups (Scheme 5).

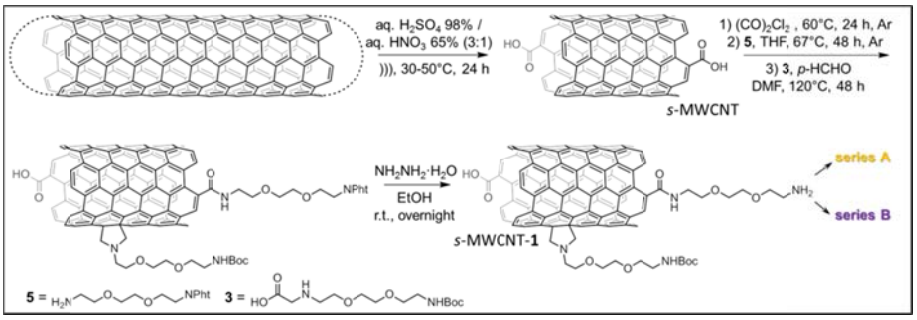

Scheme 5

After these steps, the phthalimide-protected amine introduced through amidation was selectively deprotected with hydrazine, in order to make it react either with fluorescein isothiocyanate (FITC) or with diethylenetriaminepentaacetic dianhydride (DTPA) as shown in Schemes 6 and 7.

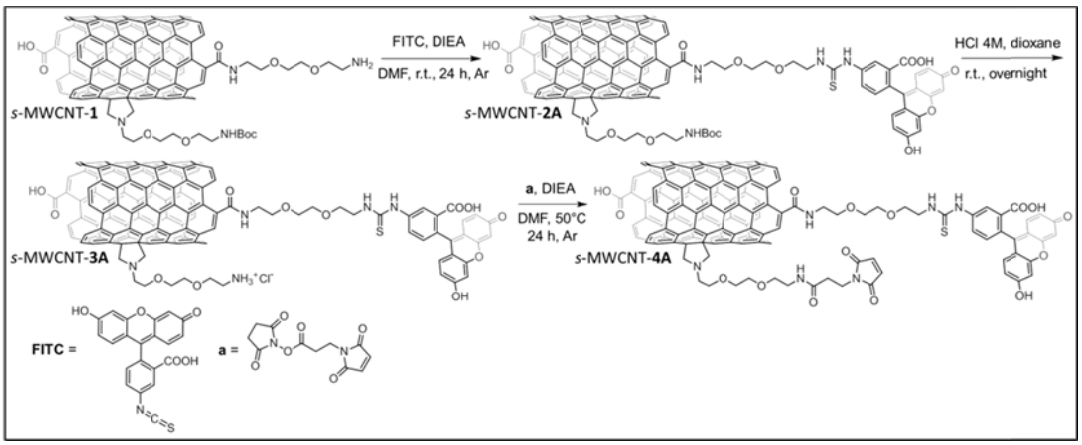

Scheme 6

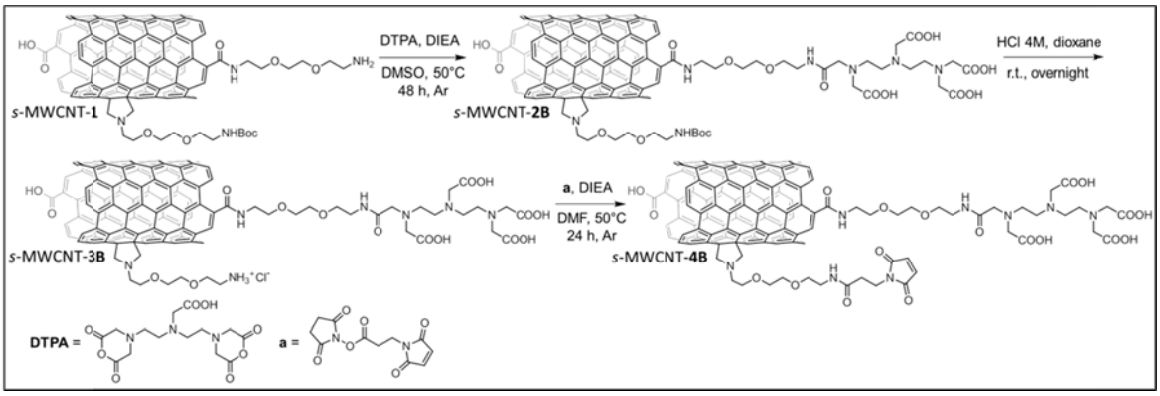

Scheme 7

Fluorescein and DTPA are both needed for biological assays: the first molecule, being a fluorophore, will allow to identify CNTs in *in vitro* tests, while the second is a chelating agent which will be used to trap a radionuclide for *in vivo* localization of the constructs. Afterwards, the second amine was deprotected from the Boc group and both MWCNTs were derivatized with a maleimide group (Schemes 6 and 7), as we did for preparing Ab-DWCNTs conjugates, to allow the coupling with free thiols in the Ab fragments.

In this way, two distinct series of compounds were basically prepared: the FITC series, made of *s*-MWCNT-**2A**, **3A** and **4A**, and the DTPA series, made of *s*-MWCNT-**2B**, **3B** and **4B**. The Kaiser test values for the two series of compounds, as depicted in Figure 11, let us calculate the degree of functionalization obtained in the different steps. The one relative to amidation was 170 µmol/g, whereas cycloaddition gave 35 µmol/g. The fluorescein loading was 60 µmol/g, while the DTPA loading was 50 µmol/g. The maleimide functionalization was 35 µmol/g.

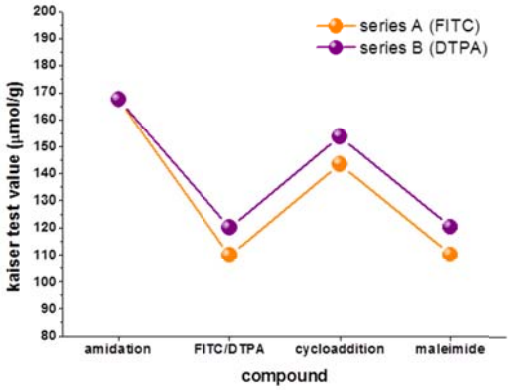

Figure 11. Kaiser test trend for the two series of compounds.

The effectiveness of FITC coupling was also confirmed by absorption and emission spectra of *s*-MWCNT-**2A** (Figure 12), though quenching by CNTs strongly decreased fluorescence intensity.

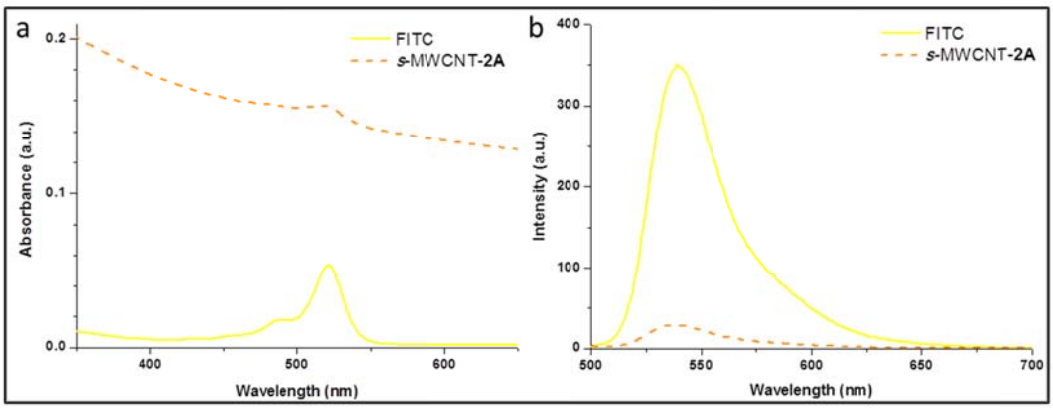

Figure 12. a) Absorption spectra of FITC and s-MWCNT-**2A** (10^{-6} M in DMSO/TEA 0.1 M); **b**) fluorescence spectra of FITC and s-MWCNT-**2A** (10^{-6} M in DMSO/TEA 0.1 M). Spectra were recorded upon excitation at 488 nm.

Once obtained the maleimide-functionalized CNTs **4A** and **4B**, we were ready for the conjugation with thiol groups. Fab' and scFv offered us the opportunity to use this chemistry without further modification of the proteins, since they both present already one thiol per molecule. In the Fab' the thiol derives from a disulphide bond already present in the full IgG, whereas on the scFv it was introduced on purpose. As a consequence, Fab' and scFv exist in part as dimers, due to the spontaneous formation, upon storage, of a disulphide bond between two free thiols in two different monomers. Moreover, Fab' and scFv preparations contain also some glutathione, deriving from their production, and so they could form a disulphide bond with its cysteine thiol. Therefore, prior to conjugation with CNTs, the disulphide bonds had to be reduced in order to restore the free thiols.

As already anticipated, the use of these two fragments should offer an advantage for the conjugation with the CNTs. With the full IgG we had to introduce thiols that where not present before, and to do so some of the amines were modified using a statistic approach. In this way the exact position of the thiols was unknown. Instead, with the use of Fab' and scFv, an already existing thiol was exploited, thus knowing precisely its position. Furthermore, in the case of the Ab fragments, there was only one thiol per molecule, while for the thiolated IgG the ratio was higher and a possible undesired consequence were cross-coupling reactions during conjugation with CNTs. With Fab' and scFv we did not have this risk.

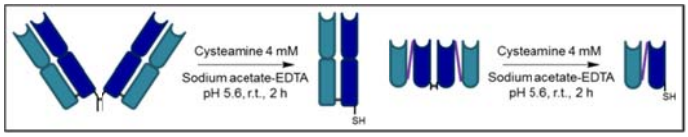

Scheme 8

The reduction step was performed, for both Fab' and scFv, through a treatment with cysteamine (Scheme 8), followed by a purification with size exclusion chromatography. We monitored the reaction via electrophoresis (Figure 13). With this technique we could distinguish the dimer from the monomer, according to their different size, and thus we could control the efficacy of the reduction. In the gel we can see the Fab' band (MW = 48 KDa) and the scFv band (MW = 30 KDa), and, more importantly, we can appreciate the disappearance of the dimer band, both for Fab', where it was at more or less 100 KDa, and for scFv, where it was at more or less 60 KDa (the presence of some minor bands at smaller MW is due to some slight proteolytic cleavage of heavy and light chains during the heating step in the preparation of the gel).

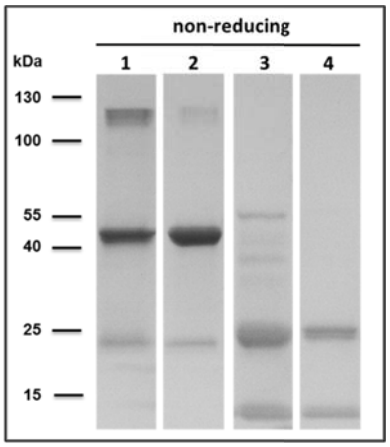

Figure 13. Electrophoretic gels under non-reducing conditions of Fab' before (lane 1) and after (lane 2) reduction and of scFv before (lane 3) and after (lane 4) reduction.

As we already did for the DWCNTs and the IgG, we performed the coupling reaction by simply mixing the two components in PBS-EDTA (pH 6.6), and gently shaking the mixture at room temperature (Scheme 9). At certain time points, a small aliquot of the reaction mixture was centrifuged, to precipitate CNTs, and the concentration of Fab' or scFv in the supernatant (absorption peak at 280 nm), corresponding to the unreacted Ab fragments, was measured. In this way we could follow the coupling reactions. When the coupling was complete we stopped the reaction, and we thoroughly washed the crude with fresh PBS (pH 7.4) by several cycles of centrifugation and removal of supernatant. Afterwards we performed a dialysis against PBS (pH 7.4) using a membrane with a cut-off of 300 KDa, to make sure of the complete removal of any unbound proteic material from the MWCNTs. In this way we prepared the four different constructs depicted in Scheme 9, each one bearing, alternatively, fluorescein or DTPA and Fab' or scFv.

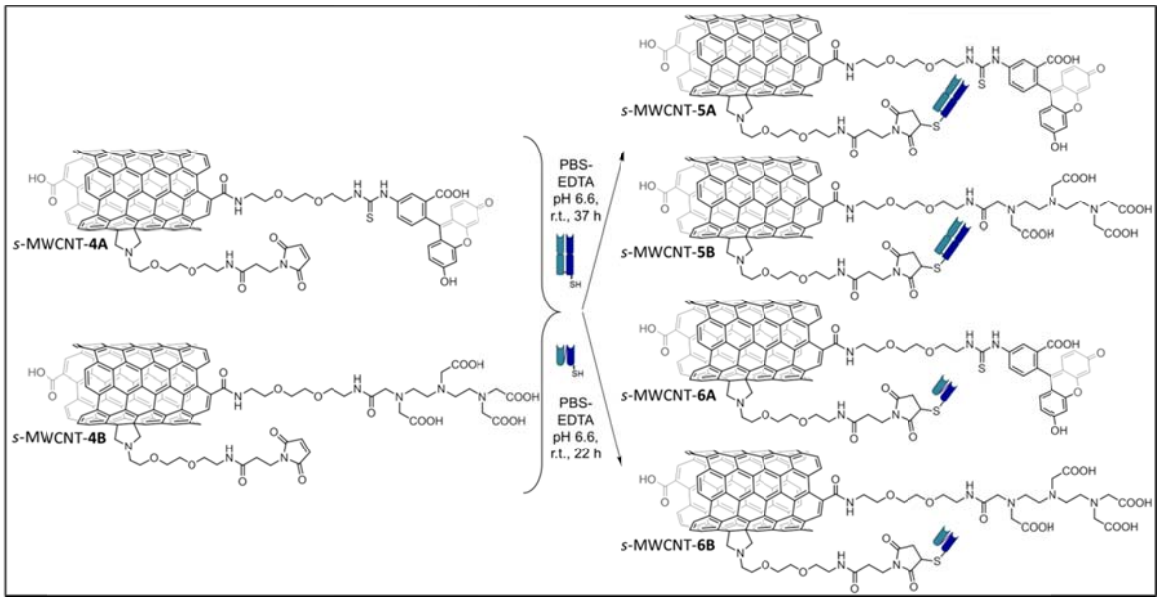

Scheme 9. (Fab'/scFv and CNT are not in size scale)

3.2.2 Characterization

For the characterization of the final conjugates we exploited the same techniques already used for the Ab-DWCNTs constructs. TEM was used to assess the quality of the final conjugates obtained, and images clearly showed that CNT structure was preserved throughout all the synthetic steps (Figure 14).

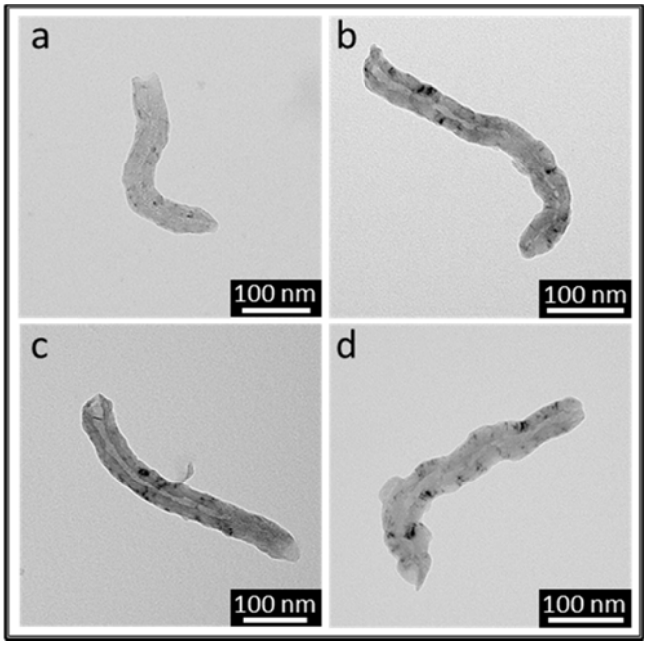

Figure 14. Representative TEM images of *s*-MWCNT-**5A** (**a**), **5B** (**b**), **6A** (**c**) and **6B** (**d**).

An electrophoretic analysis was performed both in reducing and non-reducing conditions (Figure 15). In the first case we assessed the lack of unbound proteic material, since,

when running the gel, the MWCNTs stayed in the loading well and only the unbound material could move. On the other hand, in reducing conditions, the disulphide bonds are broken, and we could observe the pattern of proteic fragments present in Fab', while of course for the scFv we did not see anything. The presence of two bands in the reducing gel of *s*-MWCNT- **5A** and **5B** is related to the light and heavy chains of the Fab'. Since the Fab' was bound through its thiol located in the heavy chain, we should expect to observe only the light chain band in the gel, and in fact the contribution from this band is stronger. However, it is possible that, during the reduction step of the Fab' dimer with cysteamine, also a part of the disulphide bonds between the two chains was reduced. Nevertheless, they remained coupled because of hydrophobic interactions and they could subsequently form dimers again but in a rearranged way, i.e. coupling different thiols. Therefore it is possible that part of the Fab' finally bound to CNTs through the thiol on the light chain, therefore leaving the heavy chain free to move in the reducing electrophoretic gel.

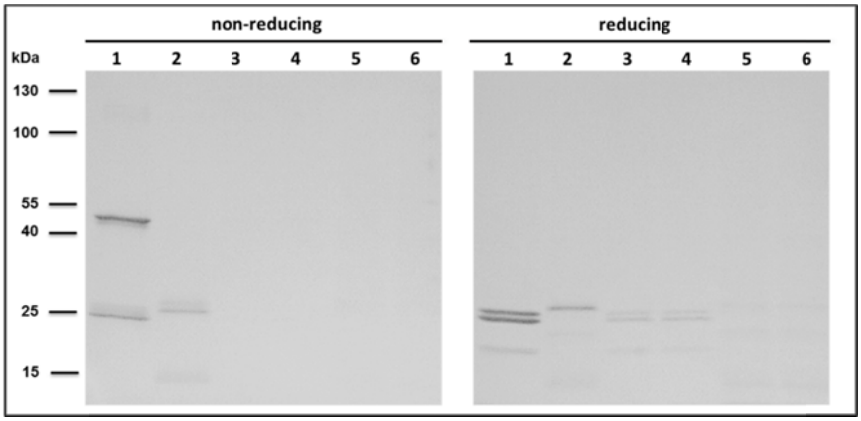

Figure 15. Electrophoretic gels under non-reducing or reducing conditions of Fab' (lane 1), scFv (lane 2), *s*-MWCNT-**5A** (lane 3), **5B** (lane 4), **6A** (lane 5) and **6B** (lane 6).

A very important piece of information was given by a negative control we prepared in this case, to confirm that the bond between the Ab fragments and the CNT was covalent and that the washing treatments were actually able to remove any adsorbed proteins. In fact, the lack of proteins in the non-reducing gels of the final conjugates prove that the Ab are strongly bound to CNTs, but not that the bond is covalent. Therefore we treated *s*-MWCNT-**1** with Fab' and scFv and then we washed them following exactly the same protocol used for the real coupling reactions. The products obtained with these control reactions were finally analysed with electrophoresis. As clearly shown in Figure 16, no proteic material was detected in the electrophoretic gel, for none of the two controls, both under non-reducing or reducing conditions.

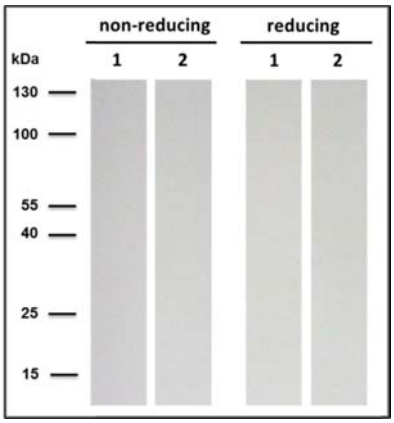

Figure 16. Electrophoretic gels under non-reducing or reducing conditions of the control reactions between *s*-MWCNT-**1** and Fab' (lane 1) or scFv (lane 2).

The detection limit of the electrophoretic gel was estimated to be 0.12 µg of protein per well by a calibration performed with a standard. Considering the concentration of CNTs dispersions used and the volume loaded for each well, this value implies that the non-specific binding of Fab' or scFv to *s*-MWCNT, if any, was at most of 0.8% (expressed as weight % of protein in the conjugate), one order of magnitude less than the loading obtained by covalent strategy as calculated from TGA values (Table 1). Thus, we indirectly proved the actual establishment of the desired covalent bond between CNTs and the Ab fragments.

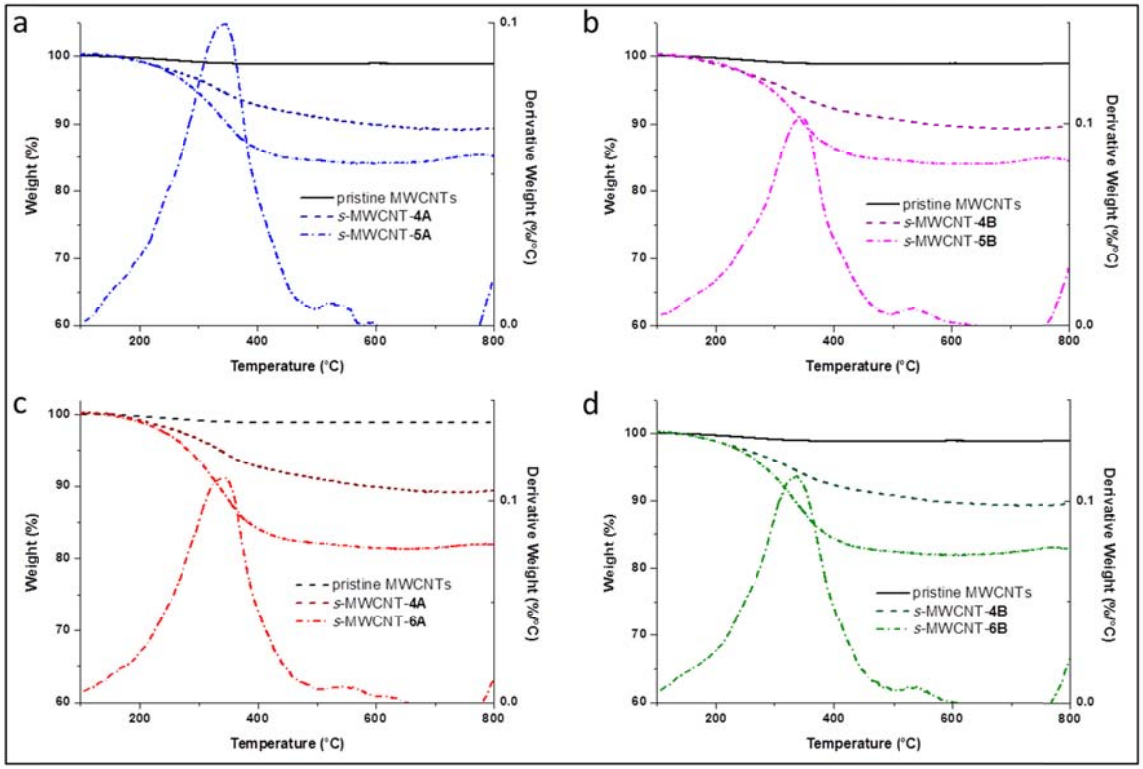

Figure 17. TGA (N_2) of MWCNTs derivatives.

The degree of loading related to Fab' and scFv was evaluated using TGA (Figure 17). The increase in the weight loss for the final conjugates relative to their precursors (at the temperature at which, according to the first derivative, the weight loss was complete) corresponds to the Fab' or the scFv bound to the MWCNTs.

Loading of Fab' or scFv	**s-MWCNT-5A**	**s-MWCNT-5B**	**s-MWCNT-6A**	**s-MWCNT-6B**
Weight % in the conjugate	6.8	6.3	9	8.4
µmol/g of CNT precursor	1.5	1.4	3.3	3.1

Table 1. Loading values relative to Fab' and scFv for *s*-MWCNT-**5A**, **5B**, **6A** and **6B**.

Thus, it was possible to calculate how much protein was attached on the nanotubes (Table 1). These values are in good agreement with the decrease of Fab' or scFv concentration in the supernatants of the coupling reactions, considering that part of the Ab fragments, especially scFv, was simply adsorbed on CNT and therefore it was washed off after the reaction. Moreover, they correlate well also with the relative intensities of electrophoretic spots, considering the amount of material loaded for each well (Figure 15).

As for the previous conjugates, the most important characterization of the material was SPR. All the compounds gave a positive response (Figure 18), even if with lower intensity than the response obtained with the Ab-DWCNTs constructs. This is probably due to the lower degree of functionalization obtained for these conjugates, and to the lower affinity for the antigen possessed by Fab' and scFv, with respect to the full IgG.

In conclusion, we prepared different kinds of covalent Ab-CNT conjugates, using DWCNTs and MWCNTs and either the whole IgG or smaller fragments, i.e. Fab' and scFv. In the case of MWCNTs we used a double functionalization strategy in order to introduce on the CNTs also a probe, necessary for biological studies. We proved the effectiveness of the covalent strategy by means of different complementary techniques, and, importantly, we assessed the capability of all the constructs to specifically recognize the antigen.

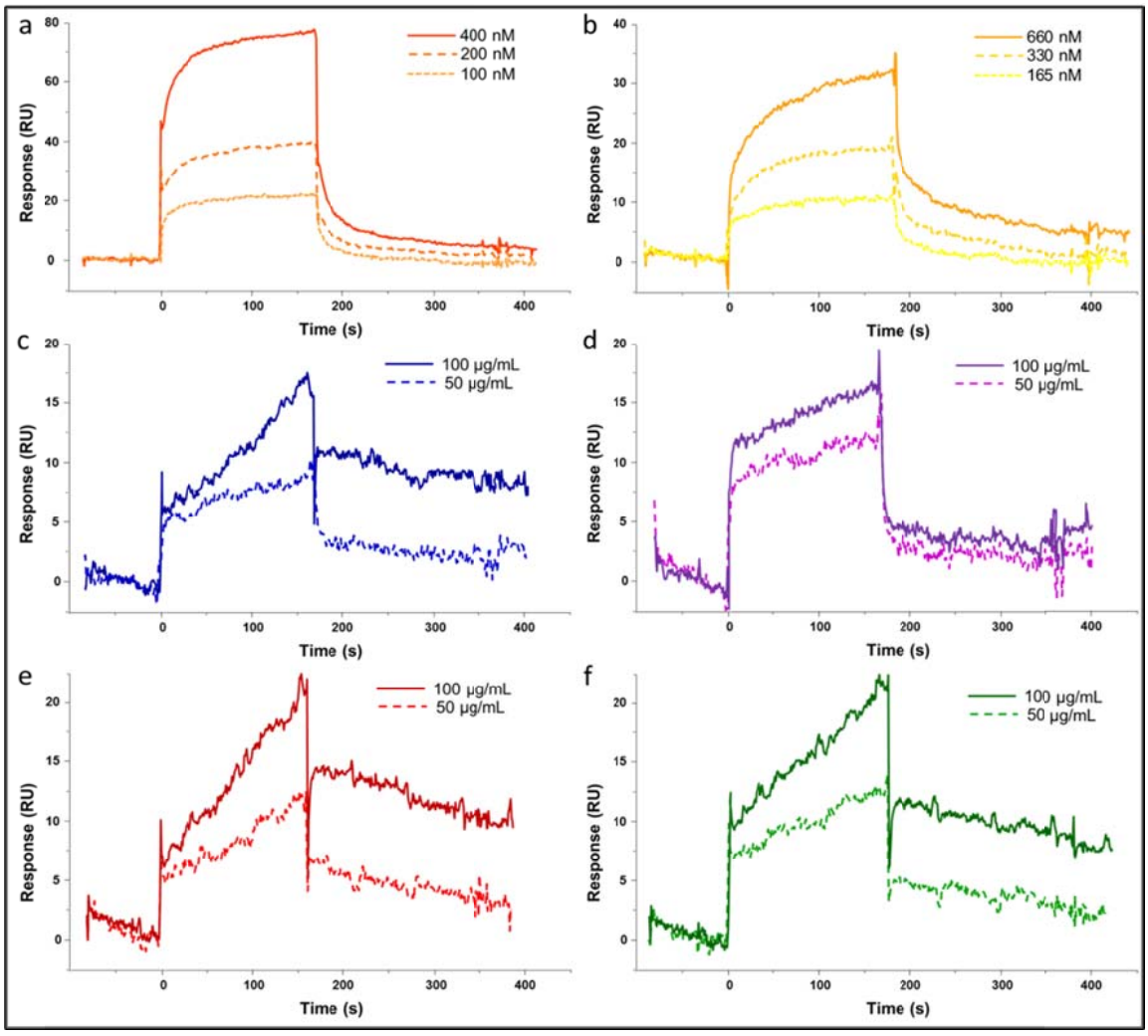

Figure 18. SPR analyses of hCTM01 Fab' (a), scFv (b), *s*-MWCNT-**5A** (c), **5B** (d), **6A** (e) and **6B** (d).

3.2.3 Preliminary biological results

We studied the *in vivo* behaviour of our conjugates exploiting the DTPA attached on the CNTs, that let us couple them with a radionuclide, ^{111}In. The coupling was made by simply mixing the DTPA-MWCNTs with $^{111}InCl_3$ for 30 min at r.t. and then washing unbound ^{111}In with EDTA-containing buffer. In this way, by injecting BALB/c mice via the tail vein with the different constructs, we could follow their *in vivo* fate through a SPECT/CT (single photon emission computed tomography/computed tomography) scanner (Figures 19, 20 and 21). Only for CNTs **3B**, we could also assess quantitatively the organ biodistribution (Figure 22). The mice were injected, as in the previous experiments, via the tail vein with the [^{111}In]DTPA-MWCNTs. After 24 h the animals were killed, and blood was collected. The different organs and tissues of interest were sampled, each sample being weighted and counted on a Gamma Counter together with a dilution of the injected dose, in order to calculate the percentage of injected dose per organ or

per gram of tissue. Quantitative organ biodistribution will be evaluated for CNTs **5B** and **6B** as well.

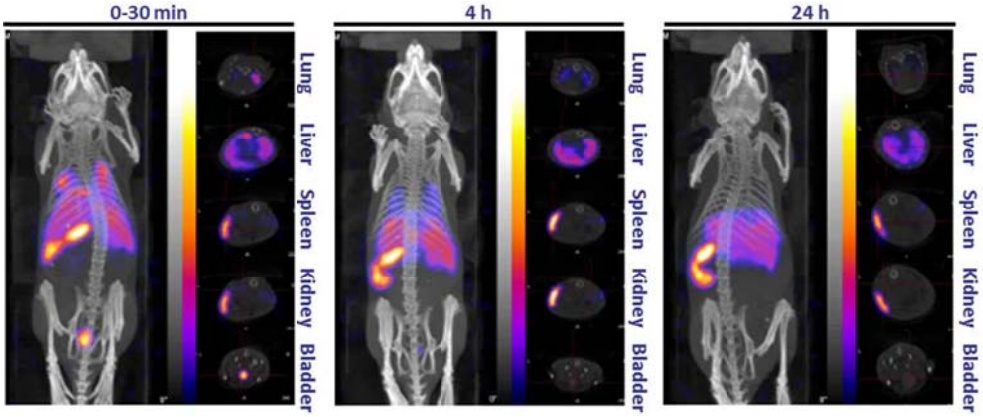

Figure 19. Whole Body 3D Imaging (SPECT/CT) showing distribution of [^{111}In]DTPA-MWNCTs **3B** in rats after 30 min, 4 h, and 24 h post-injection.

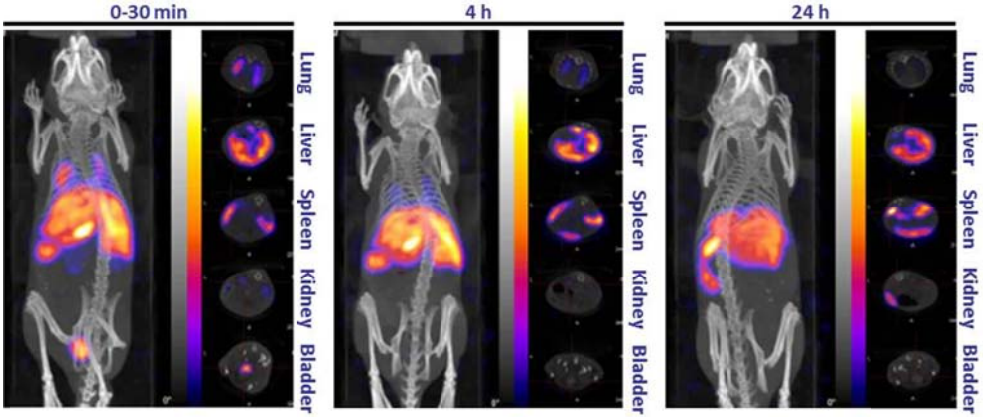

Figure 20. Whole Body 3D Imaging (SPECT/CT) showing distribution of [^{111}In]DTPA-MWNCTs **5B** in rats after 30 min, 4 h, and 24 h post-injection.

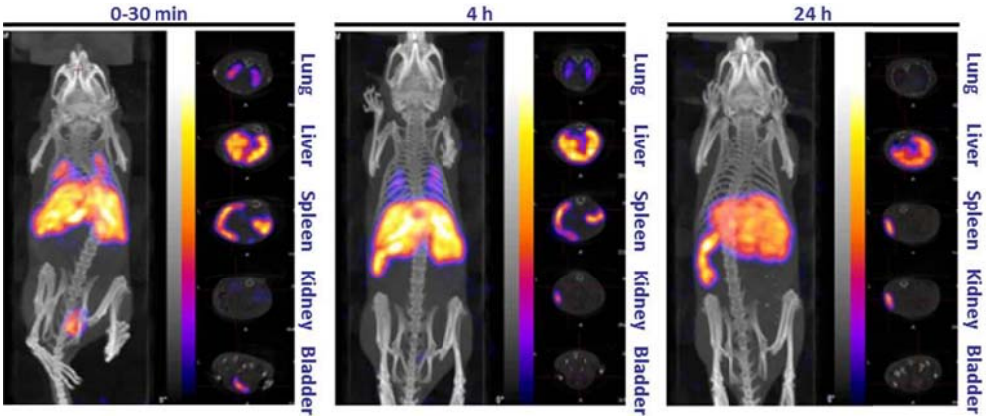

Figure 21. Whole Body 3D Imaging (SPECT/CT) showing distribution of [^{111}In]DTPA-MWNCTs **6B** in rats after 30 min, 4 h, and 24 h post-injection.

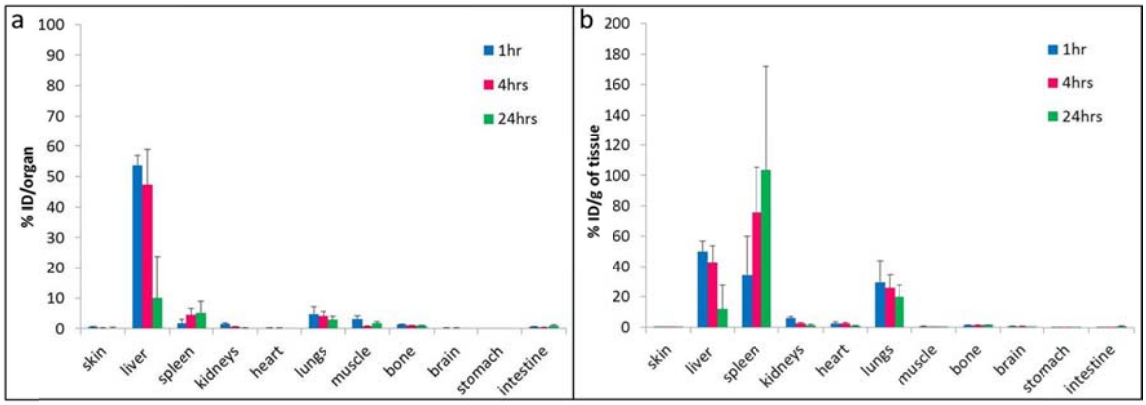

Figure 22. Organ biodistribution expressed as % of injected dose (ID) radioactivity per organ (**a**) or per gram of tissue (**b**) at 1 h, 4 h and 24 h after intravenous administration of [^{111}In]DTPA-MWCNTs **3B**, quantified by gamma counting (*n* = 3, error bars for standard deviation).

The organ biodistribution for *s*-MWCNT-**3B** (i.e. not bearing any Ab fragment) showed early accumulation in liver, spleen and lung, with gradual clearance from the liver in 24 h (Figure 22). Comparing the three constructs through the whole body SPECT/CT imaging, even though these observations need to be confirmed by quantitative organ biodistribution for *s*-MWCNT-**5B** and **6B**, we could state that Fab' and scFv conjugation to CNTs increased their liver and spleen accumulation and reduced kidney elimination.

A further important step will be the study of our conjugates in a PEM-positive tumour-bearing mouse model, to assess whether the Fab' and the scFv would be able to act as targeting agents for the whole conjugate, leading to accumulation in the tumour and therefore allowing a selective cancer treatment.

Also the internalization and the cellular trafficking of the compounds (using the fluorescein-tagged ones) was assessed, in both a PEM-positive (human breast carcinoma, MCF-7) and a PEM-negative (human lung carcinoma, Calu-6) cell line. Cells were treated, alternatively, with Fab' alone, *s*-MWCNT-**3A**, **5A** or **6A**. The localization of CNTs was detected with the green fluorescence given by the fluorescein, while the Fab' (both alone, and in the Fab'-CNT conjugate **5A**) was localized using a secondary anti-human antibody labelled with the red fluorescent dye Cy3 (hCy3). The scFv is not recognized by hCy3, since it is too small. As the confocal microscopy images show (Figures 23a and 24a), we observed cellular uptake for Fab' only in PEM-positive cells, and for the three CNTs constructs in both cell lines. Fab' was internalized through receptor-mediated endocytosis, due to the recognition of PEM on cell surface. In the case of CNT derivatives, instead, also an energy-independent pathway was probably involved, since internalization was observed as well after incubation at 4°C, i.e. under endocytosis-inhibiting conditions (data not shown).

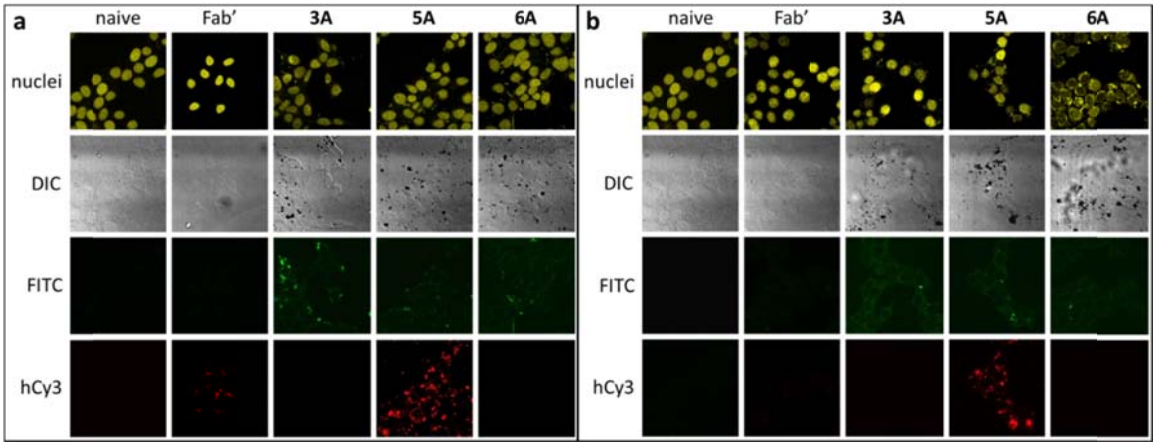

Figure 23. Confocal microscopy images of MCF-7 cells untreated or treated with Fab' (0.7 μg/mL), *s*-MWCNT-**3A**, **5A** or **6A** (10 μg/mL). First line: nuclei, second line: differential interference contrast (DIC) channel, third line: FITC (green fluorescence) channel, fourth line: Cy3 (red fluorescence) channel. Panel **a** shows treatment for 3 h at 37°C. Panel **b** shows the same treatment followed by incubation with full media for 24 h.

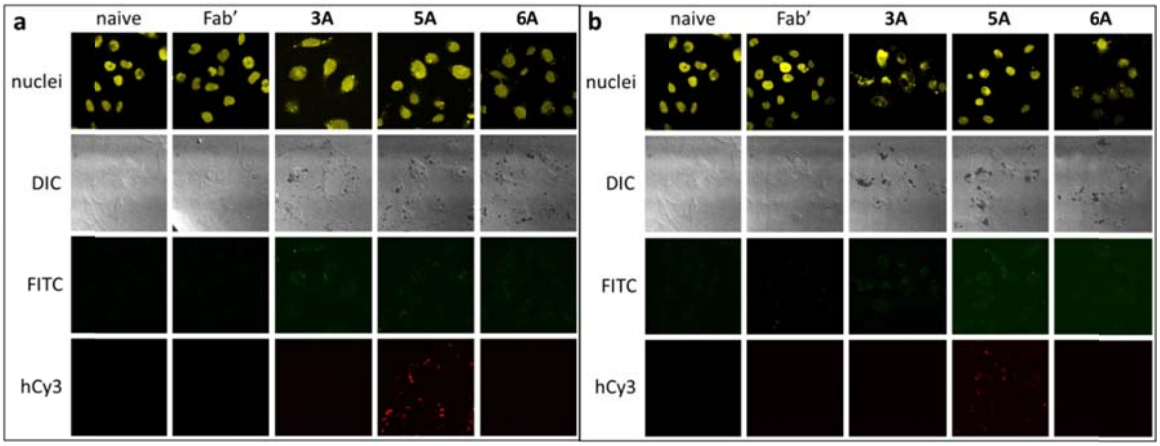

Figure 24. Confocal microscopy images of Calu-6 cells untreated or treated with Fab' (0.7 μg/mL), *s*-MWCNT-**3A**, **5A** or **6A** (10 μg/mL). First line: nuclei, second line: differential interference contrast (DIC) channel, third line: FITC (green fluorescence) channel, fourth line: Cy3 (red fluorescence) channel. Panel **a** shows treatment for 3 h at 37°C. Panel **b** shows the same treatment followed by incubation with full media for 24 h.

Furthermore, it is worth noting that when cells were treated and then incubated in full media for 24 h before the confocal analysis, the scenario was different (Figures 23b and 24b). In fact the Fab', according to the fluorescence given by the hCy3, was not present anymore inside the cells, probably because, after the endocytotic internalization, its intracellular fate was lysosomal degradation. Differently, the CNT derivatives could still be found inside the cells

according to the fluorescein green signal and, for *s*-MWCNT-**5A**, to the red fluorescence of hCy3 bound to the Fab'.

It is possible to conclude that the uptake and the intracellular trafficking of the Fab'-CNT and of the scFv-CNT conjugates were driven, at least in part, by CNTs. In fact, all the constructs were internalized even by PEM negative cells (while Fab' alone was not) and the fate of Fab' after 24 h was different if it was alone or bound to the CNTs. Considering these preliminary *in vitro* results we could not state if these conjugates would be specifically targeted *in vivo* towards PEM-positive cells, but we can conclude that CNTs were able to deliver their Ab cargo inside cells, following also an energy-independent pathway, and therefore dramatically changing the intracellular fate of the material. This important observation paves the way to the use of CNTs to deliver antibodies inside cells, thus leading to a variety of unexplored therapeutic possibilities.

3.3 Acknowledgments

The work described in this Chapter was part of the FP7 European Project ANTICARB, which involves different collaborations. I wish to thank the group of Dr. Alberto Bianco (CNRS, Institut de Biologie Moléculaire et Cellulaire, Laboratoire d'Immunologie et Chimie Thérapeutiques in Strasbourg, France) and in particular Enrica Venturelli for the syntheses of the antigen and the "scrambled" antigen peptides, and for some of the electrophoretic gels, and Dr. Olivier Chaloin for the SPR analyses.

For what concerns the biological data, I wish to thank the group of Prof. Kostas Kostarelos (Nanomedicine Laboratory, Centre for Drug Delivery, The School of Pharmacy in London, UK), and in particular Antonio Nunes and Dr. Khuloud Al-Jamal for the *in vivo* studies, and Dr. Chang Guo for the *in vitro* ones.

3.4 References

1. J. R. Adair, P. R. Hamann, R. J. Owens, T. S. Baker, A. H. Lyons, L. M. Hinman, and A. T. Menendez. WO/1993/006231.
2. E. Kaiser, R. L. Colescott, C. D. Bossinger, and P. I. Cook, *Anal. Biochem*. **1970**, *34*, 595-598
3. R. R. Traut, A. Bollen, T. T. Sun, J. W. B. Hershey, J. Sundberg, and L. R. Pierce, *Biochemistry* **1973**, *12*, 3266-3273.
4. G. L. Ellman, *Arch. Biochem. Biophys*. **1959**, *82*, 70-77.
5. R. Singh, L. Kats, W. A. Blattler, and J. M. Lambert, *Anal. Biochem.*, 1996, 114-125.

6. a) R. Karlsson, *J. Mol. Recognit.*, 2004, 17, 151-161; b) M. A. Cooper, *Nat. Rev.*, 2002, 1, 515-528.

7. A. P. Spicer, G. Parry, S. Patton, and S. J. Gendler, *J. Biol. Chem.*, 1991, 266, 15099-15109.

Conjugation of doxorubicin to CNSs

Doxorubicin is an antineoplastic drug that exerts its activity mainly at the level of DNA, by inhibition of topoisomerase II, an essential enzyme for DNA replication. Though being widely used, its clinical utility is hindered by the onset of a severe cardiomyopathy, due to its lack of selectivity, and by multi-drug resistance (MDR). Both these limitations, and the way nanocarriers could help in overcoming them, have been already analysed in the Introduction (see Chapter 1.5). Many studies have been published so far in which CNT-based systems were used for the delivery of doxorubicin, making it a promising tool (see Chapter 1.5.2 and in particular Table 1).[1]

Nevertheless, none of these works used a covalent approach for the conjugation of the drug to CNTs. The major limitation of a non-covalent construct is its lack of stability *in vivo*, as already explained (see Chapter 1.2.1). In fact, most of the above papers that addressed this question reported the undesired partial release of non-covalently bound doxorubicin from the carrier.[1c,g,h] For this reason we decided to prepare covalent doxorubicin-CNT conjugates, exploiting the primary amine present on the sugar of the drug. However, it is known from the literature that substituents in that position strongly affect its activity.[2] Therefore, also another construct was prepared, introducing a cleavable linker between the carrier and doxorubicin, to trigger its release once the system is internalized. To this end we choose a tetrapeptide, glycine-phenylalanine-leucine-glycine (GFLG), known to be cleaved by lysosomal cathepsins and already used as a linker to release polymer-bound doxorubicin.[3]

In order to better study the chemistry of the conjugates we first prepared fullerene derivatives and then we translated the same chemistry to CNTs. Additionally, this strategy led to an expansion in the kinds of constructs to be tested, thus allowing a comparison between the biological behaviour of the different carbon nanostructures (CNSs).

4.1 Fullerene derivatives

4.1.1 Synthesis

The first step for the preparation of the fullerene derivatives was the synthesis of the fullero-pyrrolidine **1** by 1,3-dipolar cycloaddition of azomethine ylides to the [6,6] double bonds of fullerene C_{60}, as depicted in Scheme 1. The reaction actually affords a mixture of the monoadduct and different poly-adducts. Nevertheless, by use of 1 equivalent of the reagents and by subsequent chromatographic purification of the mixture, the desired mono-adduct is obtained in 29% yield. The terminal amine of the triethylene glycol chain on the pyrrolidinic nitrogen was then Boc-deprotected by treatment with trifluoroacetic acid to yield the fulleropyrrolidine **2**.

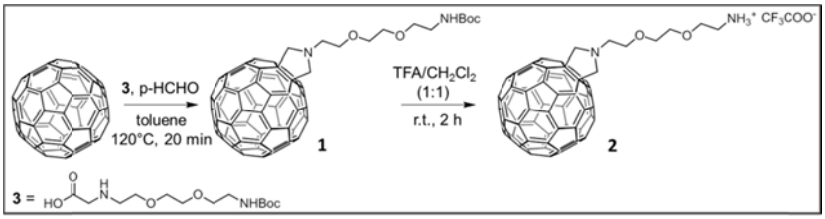

Scheme 1

Once obtained the fullerene monoadduct, it was derivatized with fluorescein. Also doxorubicin is fluorescent, with the consequent advantage of behaving simultaneously as a probe for *in vitro* localization, but a different fluorophore was used, to first study the behaviour of the vector with a non-toxic molecule. The fluorescein-derivatized fullerene **3** was prepared, as illustrated in Scheme 2, by coupling fluorescein isothiocyanate (FITC) with the free amine of fullerene **2**, followed by precipitation of reaction crude (in DMF) by addition of MeOH (63% yield).

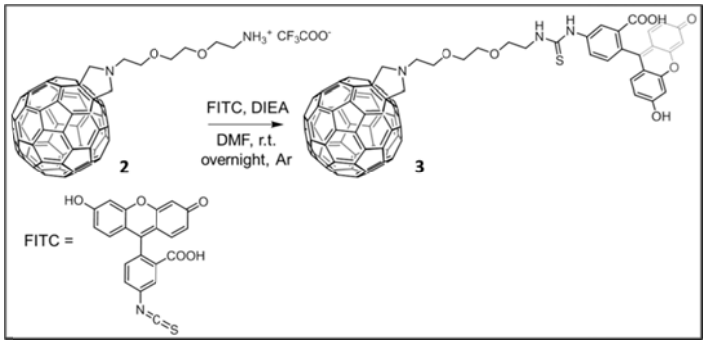

Scheme 2

On the other hand, to prepare doxorubicin-bearing derivatives, a further step was required, to introduce a carboxyl group. Fullerene **2** was treated with succinic anhydride, which

reacted with its terminal amine, with consequent opening of the ring, and exposure of the carboxylic acid. The reaction crude (in DMF) was purified by precipitation with MeOH, to afford fullerene **4** in 75% yield (Scheme 3).

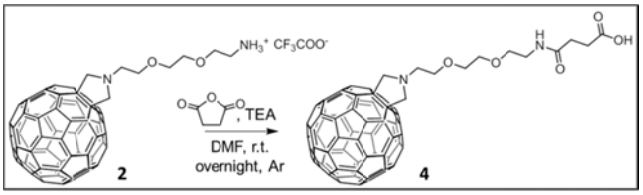

Scheme 3

The amino Boc-protected tetrapeptide Boc-GFLG was then coupled to doxorubicin by activation of the carboxylic acid via EDC·HCl/HOBt, and product **8** was obtained after column chromatography purification (79% yield, Scheme 4). Subsequently, the deprotection of the Boc group was attempted using different conditions, as depicted in Table 1, which resulted to be unsuccessful, probably due to degradation of the product triggered by the acidic conditions.

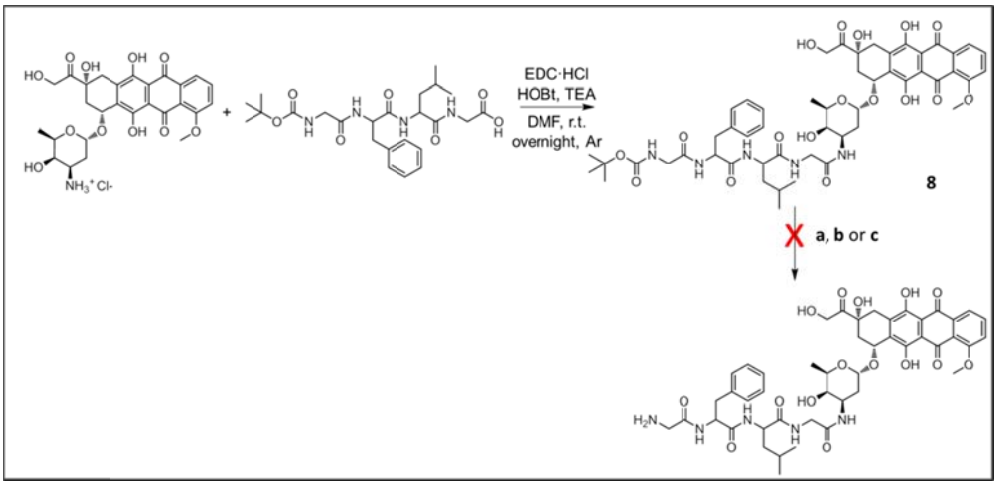

Scheme 4

a	HCl(g)/CH_2Cl_2, r.t.
b	TFA/CH_2Cl_2 (1:1), r.t.
c	Me_3SiCl, phenol, CH_2Cl_2, r.t.[4]

Table 1. Conditions tested for the deprotection reaction of Boc-GFLG-doxorubicin **8**.

Therefore a different protecting group for the peptide's terminal amine was chosen, namely allyloxycarbonyl (Alloc). The coupling between Alloc-GFLG and doxorubicin was performed in the same conditions used for **8**, affording **9** with 74% yield, after chromatographic purification. The deprotection of the terminal amine from the Alloc group was successful, even though in low yield. Treating Alloc-GFLG-doxorubicin **9** with tetrakis (triphenyl phosphine)

palladium(0) in the presence of dimedone,[5] we obtained **10**, which was purified by column chromatography, with 38% yield (Scheme 5). An attempt to increase reaction yield, using *N*,*N'*-dimethylbarbituric acid (see inset in Scheme 5) instead of dimedone was done.[6] The use of this allyl group scavenger, in fact, should avoid the undesired formation of the ketoenamine by-product, by reaction of the deprotected amine with one of dimedone's carbonyl groups. However, results did not improve.

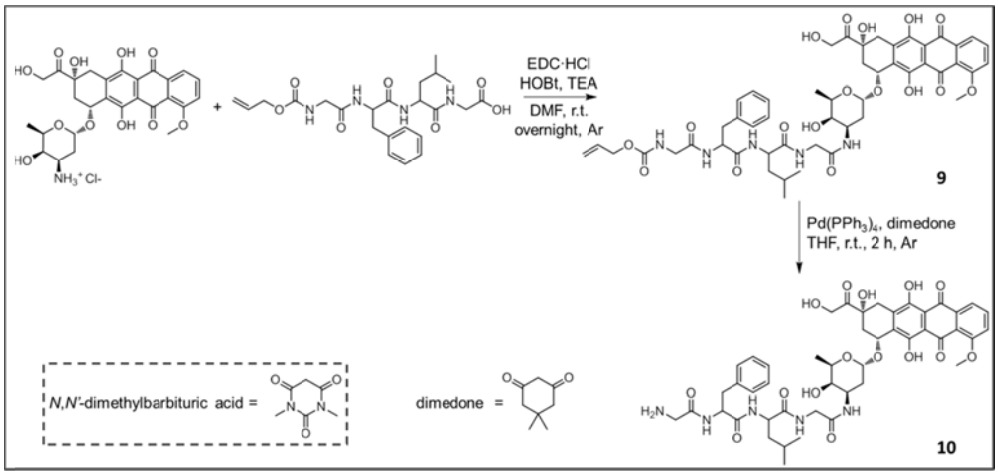

Scheme 5

Finally, in order to obtain the target doxorubicin-bearing derivatives, fullerene **4** was conjugated with both free doxorubicin and GFLG-doxorubicin **10**, using PyAOP as coupling agent. The final products **5** and **6** were obtained, after purification by preparative thin layer chromatography, with 42% and 48% yield, respectively (Schemes 6 and 7).

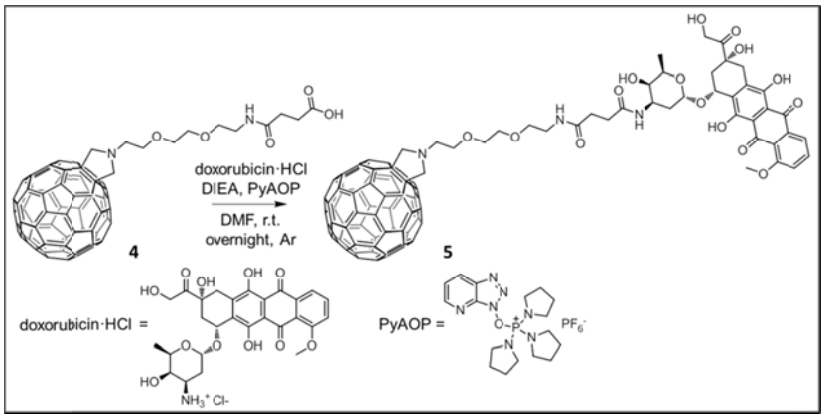

Scheme 6

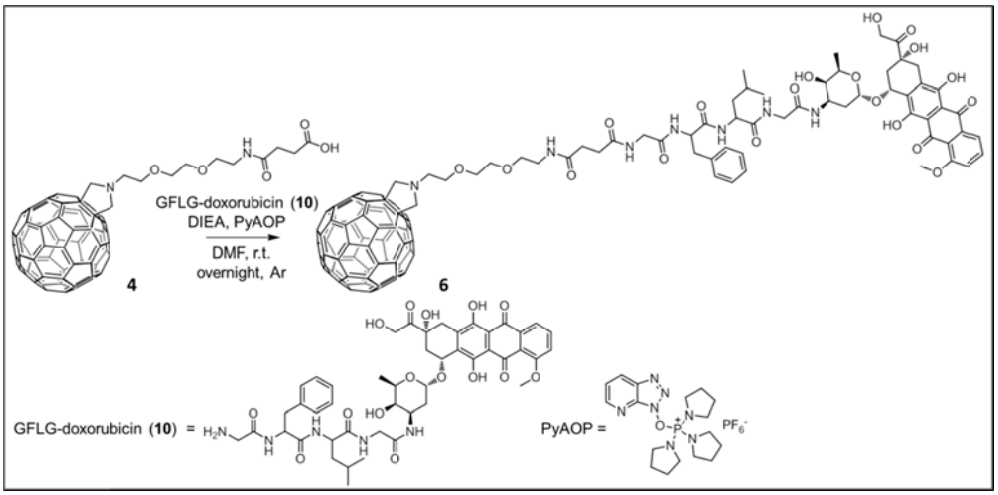

Scheme 7

4.1.2 Spectroscopic characterization

Absorption spectrum of fullerene **2**, as Figures 1a and 2a show, presented the typical shape of fullerene monoadducts, with a maximum at 433 nm.[7] Fullerene derivatives **3**, **5** and **6** gave absorption profiles similar to the ones of FITC and doxorubicin, respectively, plus the contribution of fullerene **2**.

Fluorescence spectroscopy of the final fluorophore-bearing fullerene **3**, **5** and **6** revealed in all cases a strong quenching of the fluorescence with respect to the fluorophores alone, as can be appreciated in Figures 1b and 2b. On the other hand, the presence in the fluorophores' solution of an equimolar amount of fullerene **2** did not cause strong decreases in the emission intensity.

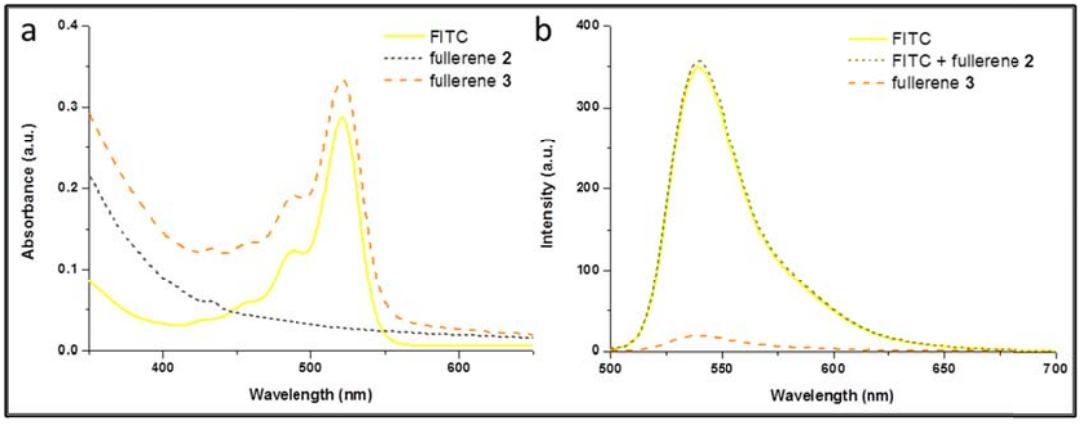

Figure 1. a) Absorption spectra of FITC, fullerene **2** and fullerene **3** ($2 \cdot 10^{-5}$ M in DMSO/TEA 0.1 M); **b**) fluorescence spectra of FITC, FITC + fullerene **2** and fullerene **3** (10^{-6} M in DMSO/TEA 0.1 M). Spectra were recorded upon excitation at 488 nm.

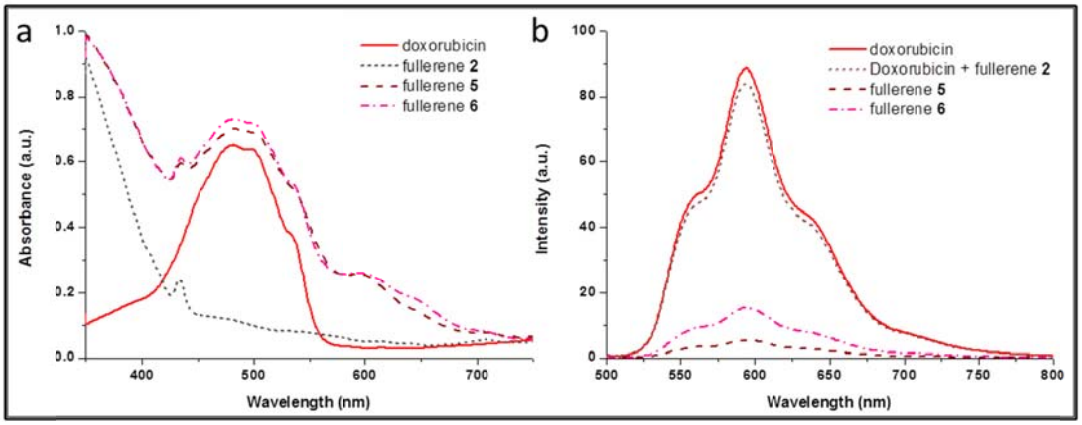

Figure 2. a) Absorption spectra of doxorubicin, fullerene **2**, fullerene **5** and fullerene **6** (10^{-4} M in DMSO); **b**) fluorescence spectra of doxorubicin, doxorubicin + fullerene **2**, fullerene **5** and fullerene **6** ($5 \cdot 10^{-6}$ M in DMSO). Spectra were recorded upon excitation at 482 nm.

Quite interestingly, comparing fullerene **5** and fullerene **6**, the quenching was higher in the case of the first compound, where the chain between the fluorophore and fullerene was shorter.

The reason for the quenching of the fluorescence could lie in energy transfer between the fluorescent molecule, once excited, and the fullerene, as already observed by others.[8] Transient spectroscopy would help in better understanding the mechanism, since the present data are not sufficient to fully elucidate it.

However, considering the intended biological application of the constructs, the main concern was related to the decrease in the fluorescent signal during *in vitro* experiments.

4.2 CNT derivatives: preparation and characterization

Once prepared the fullerene derivatives, we moved to CNTs, using the same chemistry, and we choose pristine MWCNTs. However, the first attempt to perform 1,3-dipolar cycloaddition on these CNTs was unsuccessful. We performed the reaction by thermal treatment (120°C) of a DMF dispersion of CNTs, aldehyde and α-aminoacid, i.e. in the same conditions normally working for oxidized CNTs (see Chapters 3.1.1 and 3.2.1). However, we obtained, after treatment in hydrochloric acid, a very low kaiser test (15 μmol/g), meaning that very little functionalization occurred, probably due to the lower dispersibility in DMF of pristine MWCNTs with respect to the oxidized tubes.

Microwave (MW)-assisted organic synthesis is known to provide enhanced reaction rates and improved product yields. Moreover, the use of MW irradiation for CNT functionalization was recently reported by our group.[9] It seems that CNTs, in the absence of

solvent, are strongly heated by microwave irradiation due to resonance phenomena.[10] It was proposed also that the heating of the sample is the result of magnetic resonance of the residual metal in the microwave field.[11]

Therefore we decided to perform cycloaddition under MW irradiation, testing different conditions. In all cases the reactants were mixed in a quartz microwave tube by little sonication in CH_2Cl_2, and subsequently the solvent was evaporated. The tube was then placed within the microwave reactor where the reaction mixture was irradiated. Table 2 shows the different conditions tested, in terms of aminoacid (a.a.) and aldehyde used, presence or absence of solvent, temperature and reaction time.

	a.a.	aldehyde	solvent	T (°C)	Time (h)	kaiser test after deprotection (μmol/g)
a	**3**	p-HCHO	-	120	1	35
b	**3**	**y**	-	120	1	20
c	**3**	p-HCHO	-	140	1	50
d	**3**	p-HCHO	DMF	140	1	15
e	**3**	p-HCHO	-	160	1	70
f	**7**	p-HCHO	-	160	1	100
g	**7**	p-HCHO	-	160	2	100
h	**7**	**z**	-	160	1	90

Table 2. Different MW experimental conditions tested for 1,3-dipolar cycloaddition of azomethine ylides on pristine MWCNTs.

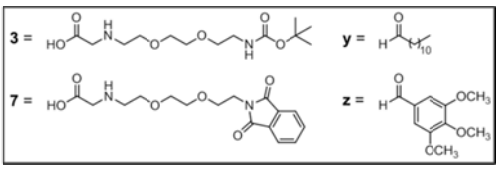

Figure 3. Structures of aminoacids **3** and **7**, and aldehydes **y** and **z**.

As can clearly be seen by comparison of the results obtained (Table 2), an increase of temperature (conditions **a**, **c** and **e**) resulted in increased yields, as expected. The presence of solvent with respect to neat conditions (conditions **d** vs. **c**) led to a decrease in the yield, probably because MW irradiation was absorbed by solvent, and not by CNTs, with a consequent lower local heating of the sample. Moreover, the use of different aldehydes than paraformaldehyde (conditions **b** vs. **a**, and conditions **h** vs. **f**) did not improve the results, fact that could be explained considering steric hindrance effect.

Importantly, a big improvement was obtained when using aminoacid **7** instead of **3** and this behaviour was not unexpected. In fact, the Boc protecting group of aminoacid **3** is thermally unstable, and could therefore undergo deprotection during reactions performed at temperatures equal to or above 140°C, especially considering the formation of “hot spots” in the

neat reaction mixture during CNT microwave irradiation. As can be seen by TGA in air of aminoacid **3** (Figure 4), the thermal decomposition of the molecule starts early above 140°C, and it is probably due to loss of Boc and decarboxylation. Kaiser test performed before Boc-deprotection for reactions **c** and **e**, indeed, was positive, confirming this hypothesis. In this way, part of the primary amine could become available to the aldehyde during the reaction, with a consequent lower efficiency in the formation of the azomethine ylide.

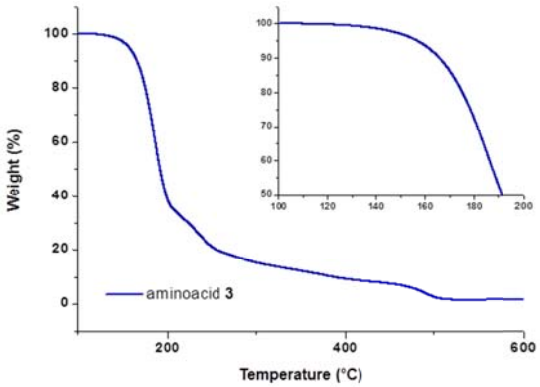

Figure 4. TGA (air) of aminoacid **3**. In the inset the enlargement of temperature range 100-200°C is shown.

On the other hand, using aminoacid **7**, whose terminal amine is protected with the thermally stable phthalimide, this problem was avoided. Therefore, considering also that no improvement was observed prolonging reaction time to 2 h (conditions **g** vs. **f** in Table 1), conditions **f** were selected to prepare MWCNT-**7**, which after deprotection of the phthalimide by a treatment with hydrazine, afforded MWCNT-**8** (Scheme 8). TGA-MS analysis (Figure 5) confirmed the presence of the desired chain on the CNTs, by comparison with the profile of fulleropyrrolidine **1**.

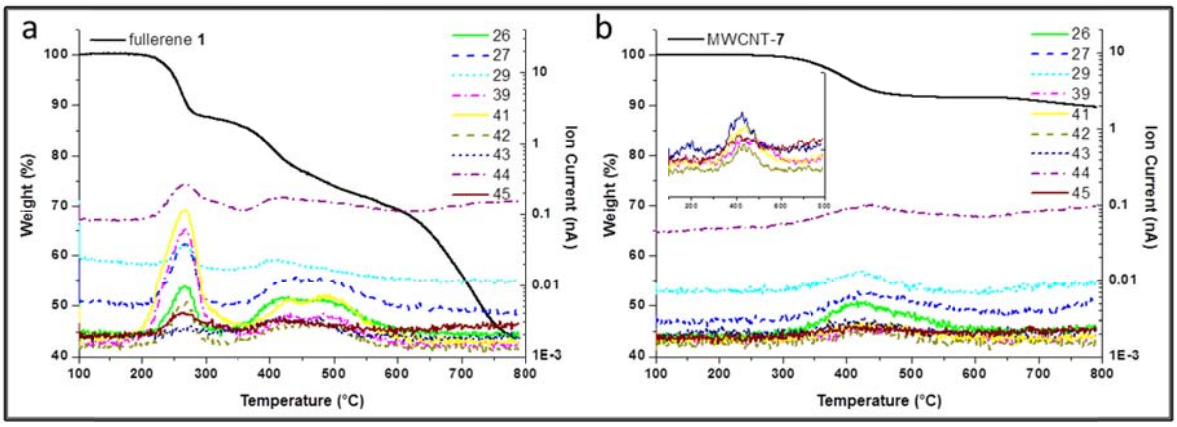

Figure 5. TGA-MS analyses (He) of fullerene **1** (**a**) and MWCNT-**7** (**b**).

In fact, the same pattern of peaks, given by fragmentation and ionization of the appended molecules during the thermogravimetric experiment, appeared, even if with lower intensity in the case of CNTs, consistently with their lower degree of functionalization. The only exceptions were given by the protecting groups, being Boc for fullerene **1**, and phthalimide for MWCNT-**7**. The peaks ascribable to the protecting groups were extrapolated by comparison with TGA-MS analyses of fullerene **2** and MWCNT-**8**, respectively (data not shown).

The following steps were performed as for fullerene derivatives: MWCNT-**9** were prepared by reaction of MWCNT-**8** with succinic anhydride, and then MWCNT-**10** and **11** were obtained by amidic coupling with doxorubicin and GFLG-doxorubicin **10**, respectively (Scheme 8). To monitor the formation of MWCNT-**9** we used kaiser test, which gave a degree of functionalization of 55 µmol/g. Some concern may arise from the incompleteness of the coupling (amine loading was 100 µmol/g) , since the free amines that did not react with succinic anhydride could possible cross react during the following step. However, the attempt to improve reaction yield (increasing molar equivalents of succinic anhydride, prolonging reaction time, and raising temperatures up to 50°C) did not succeed. Therefore it was concluded that part of the amines were probably hindered to react in that conditions, due to aggregation phenomena, but gave positive response at Kaiser test, being it performed at 120°C.

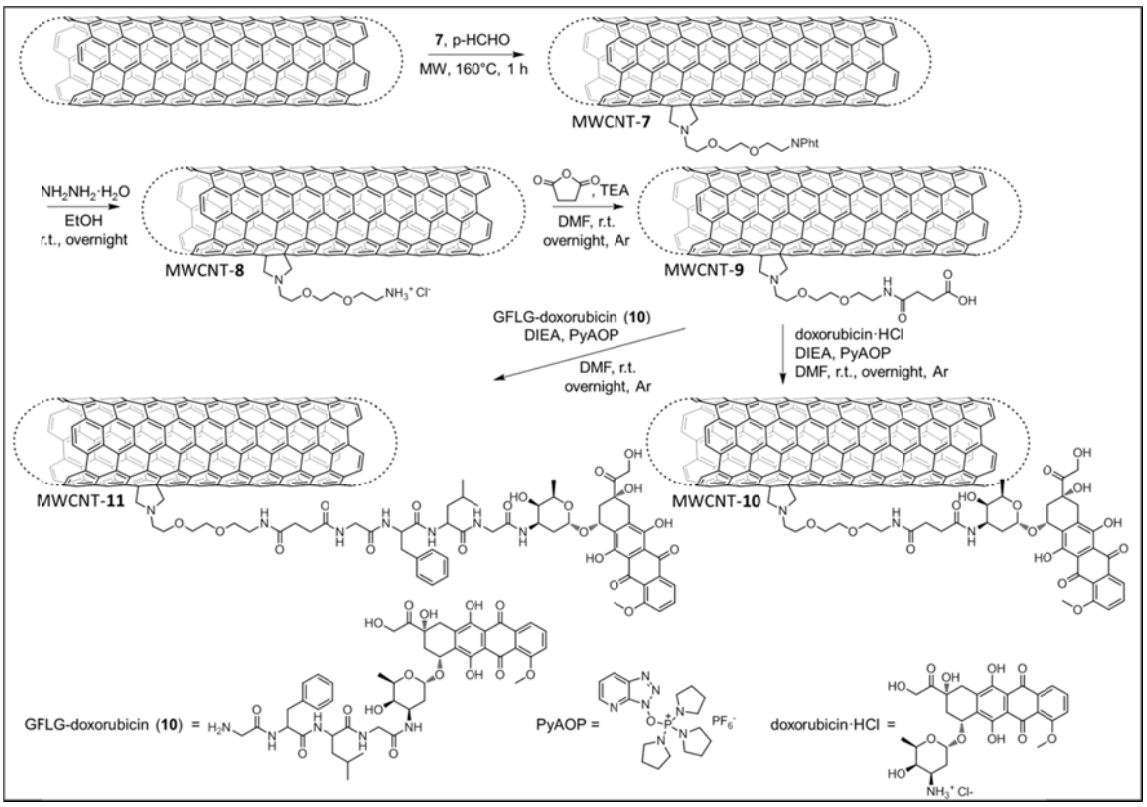

Scheme 8

The loading of doxorubicin and GFLG-doxorubicin was evaluated by TGA, as shown in Figure 6a. The difference in the weight loss with respect to MWCNT-**9** was of 4.1% for MWCNT-**10** and 2.4% for MWCNT-**11**, and these values correspond to 75 µmol/g and 45 µmol/g of doxorubicin for the two conjugates, respectively. The discrepancy between the amount of doxorubicin in MWCNT-**10** and the amount of carboxylic groups calculated for MWCNT-**9** could be explained considering that the two values were gathered from different methods, namely kaiser test and TGA, which are not always in perfect agreement.

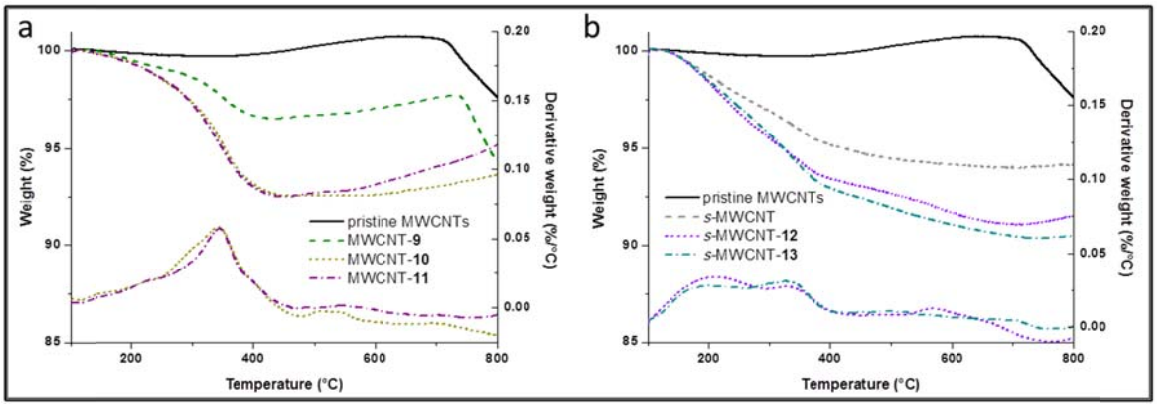

Figure 6. TGA (N_2) of MWCNTs derivatives.

In addition to these conjugates we prepared also other doxorubicin-bearing MWCNT derivatives, performing an oxidation step to introduce carboxyl groups and then coupling them directly with the amine of doxorubicin and GFLG-doxorubicin **10**. The same oxidation protocol described in Chapter 3.2.1 was used, namely sonicating the nanotubes in a sonic bath with a mixture of aqueous sulphuric and nitric acids.

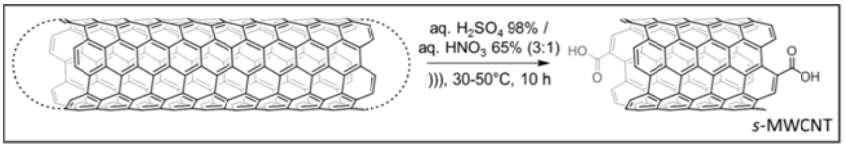

Scheme 9

However, since the length distribution of this batch of pristine MWCNTs was shifted toward smaller values (average length: 311 nm ± 236 nm) with respect to the batch used before (see Chapter 3.2.1), we performed a shorter treatment, i.e. 10 h long (instead of 24 h), yielding *s*-MWCNT with an average length of 215 ± 148 nm (Scheme 9 and Figure 7).

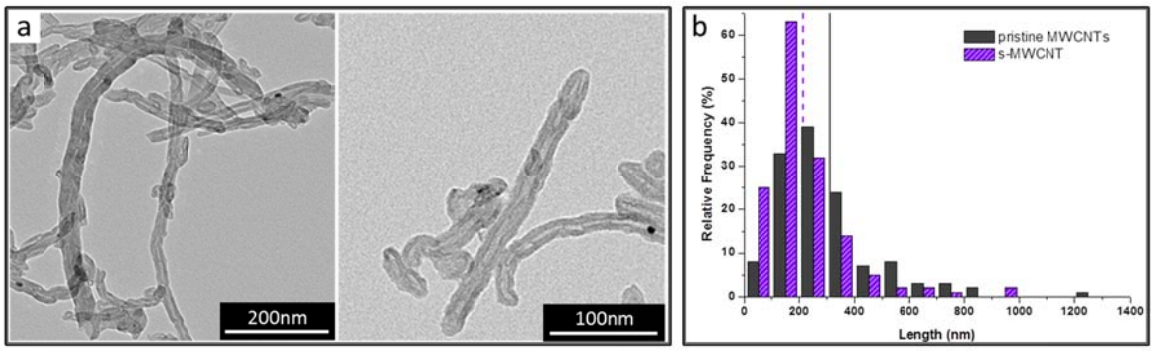

Figure 7. a) Representative TEM images of pristine MWCNTs (left) and *s*-MWCNTs (right); **b**) length distributions of pristine MWCNTs (count = 129) and *s*-MWCNT (count = 146). Vertical lines indicate the average length values.

Afterwards, an amidic coupling was performed, as described in Scheme 10, following the same protocol used for fullerene **4** and MWCNT-**9**, affording *s*-MWCNT-**12** and **13**. Also in this case, TGA was used to assess the degree of functionalization, considering the weight loss increase with respect to *s*-MWCNT (Figure 6b). For *s*-MWCNT-**12** the loading of doxorubicin was found to be 3.0%, corresponding to 55 µmol/g, while for *s*-MWCNT-**13** the loading of GFLG-doxorubicin was 2.2%, i.e. 40 µmol/g.

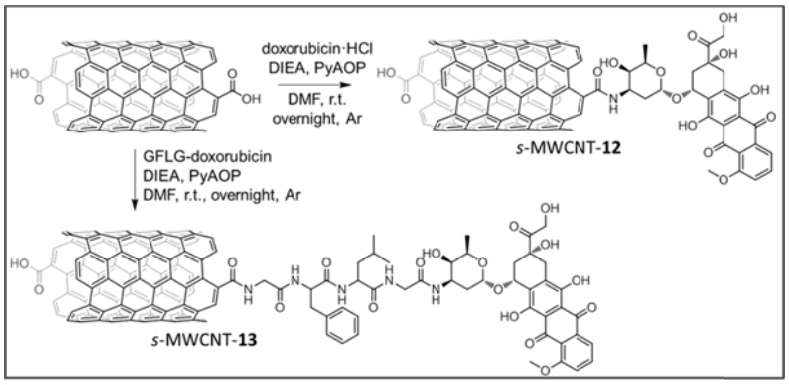

Scheme 10

TEM analyses confirmed the quality of the four final conjugates, showing clean nanotubes, with a preserved morphological structure (Figure 8).

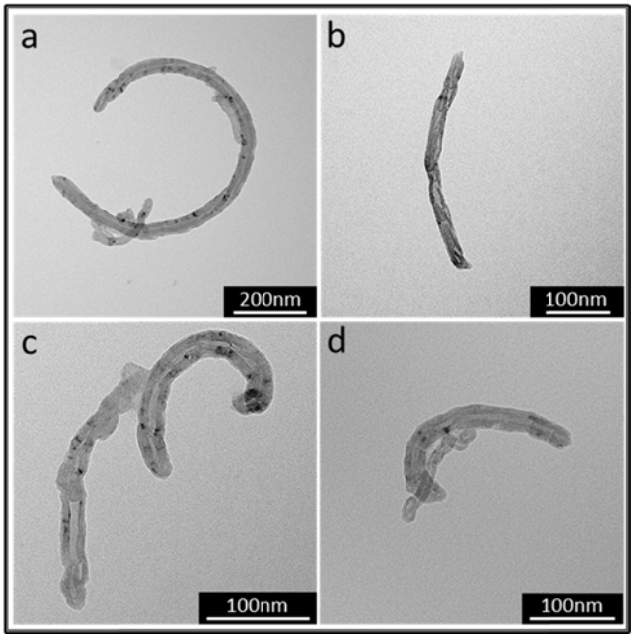

Figure 8. Representative TEM images of MWCNT-**10** (**a**) and **11** (**b**), and *s*-MWCNT-**12** (**c**) and **13** (**d**).

The fluorescence of DMSO dispersions of the four final conjugates was studied. As for the fullerene derivatives, a strong quenching of emission was observed. Moreover, in this case, the presence itself of CNTs in the dispersion gave a greater contribution in reducing doxorubicin fluorescence with respect to fullerene derivatives, because of the lower degree of functionalization.

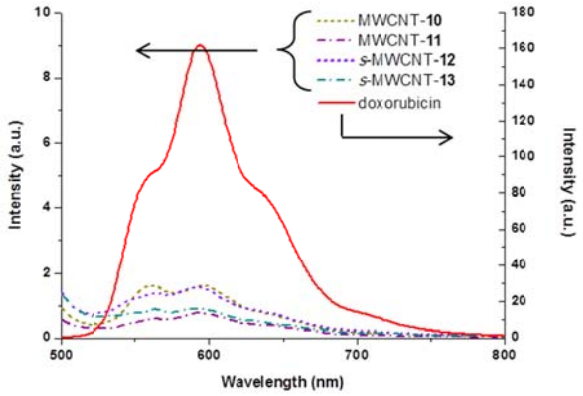

Figure 9. Fluorescence spectra of DMSO dispersions of MWCNT-**10** and MWCNT-**11** (10^{-5} M in DMSO, relative to doxorubicin) and of *s*-MWCNT-**12** and *s*-MWCNT-**13** (10^{-6} M in DMSO, relative to doxorubicin), compared to the one of doxorubicin (10^{-5} M in DMSO). Spectra were recorded upon excitation at 482 nm. Note that CNT samples intensity refers to left axes, while doxorubicin intensity refers to right axes.

In fact doxorubicin loading of fullerene derivatives, if expressed in the same unit used for CNTs, would be 658 µmol/g for fullerene **5** and 528 µmol/g for fullerene **6**, meaning that the CNT constructs are about ten times less functionalized than the corresponding fullerene derivatives.

Therefore CNT content in the dispersion is most likely responsible for the very low fluorescence of these conjugates. It should also be pointed out that, for *s*-MWCNT-**12** and **13**, the dispersions were diluted ten times, in order to detect an emission signal. Being these CNTs oxidized, their dispersibility in DMSO was higher, resulting in dispersions with deeper black colour, and CNTs were probably completely absorbing doxorubicin emission.

In conclusion, different carbon nanostructures-based conjugates were prepared for studying doxorubicin delivery. Both fullerene and CNTs, pristine or oxidized, were used and the drug was attached either directly or introducing a cleavable peptidic sequence to trigger its release inside cells. Furthermore, fullerene was functionalized with a non-toxic fluorophore as well.

4.3 Preliminary biological results with fullerene derivatives

First of all, we wanted to assess the lack of cytotoxicity of the fullerene carrier toward human breast carcinoma cells, i.e. the model to study the anticancer activity of doxorubicin-fullerene conjugates **5** and **6**. The cell lines studied were two, one sensitive to doxorubicin (MCF-7) and one resistant to the drug (MCF-7/ADR), due to overexpression of P-glycoprotein (P-gp), an efflux pump able to recognize the drug and transport it out of the cell once it has been internalized, thus preventing it from exerting its cytotoxic action.

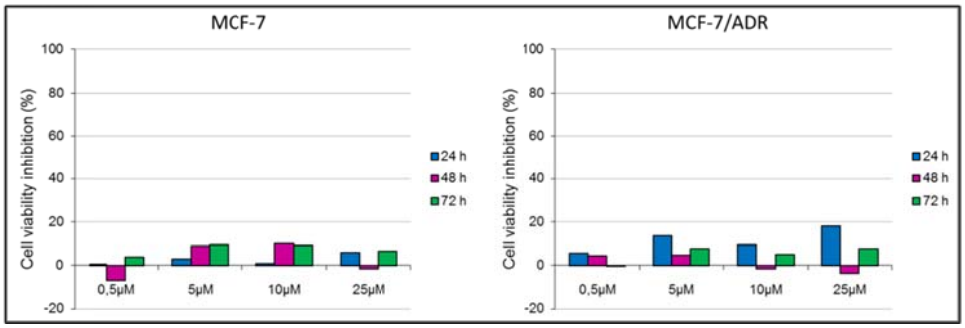

Figure 10. Cell viability (assessed by MTT assay) of MCF7 and MCF7/ADR cells after exposure to fullerene **2** at various concentrations for different time (data are shown as mean values ± SD of a sextuplicate experiment).

The results showed a lack of cytotoxicity in both cell lines for fullerene **2**, at concentrations up to 25 µM, thus confirming the feasibility of using fullerene as a drug carrier (Figure 10).

Another important information was obtained by a propidium iodide (PI)/3,3'-dihexyloxacarbocyanine iodide (DiOC6) test. These two fluorescent dyes are used to investigate cell health status. In fact PI is a DNA intercalating probe, which is excluded by viable cells but can penetrate cell membranes of dying or dead cells. On the other hand, DiOC6 gives indications on the metabolic activity of mitochondria. A decrease in the level of DiOC6 fluorescence with respect to a healthy cell corresponds to an apoptotic phase. Combining the information given by the two probes, a cellular population could be divided into four groups: dead cells, late apoptotic cells, apoptotic cells and viable cells (Figure 11). By comparison of MCF-7 cell population after treatment with fullerene **2** with the untreated one, it is possible to appreciate that no substantial changes occurred, with the majority of the cells in the "viable" zone, indicating that the compound did not alter cell viability. MCF-7/ADR cells gave the same results (data not shown).

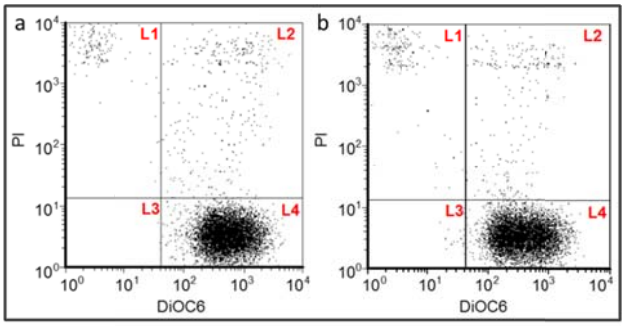

Figure 11. Cell population distribution for MCF-7 cells untreated (**a**), or treated with fullerene **2** (25 µM, 48 h) (**b**). L1: dead cells (PI+/DiOC6-); L2: late apoptotic cells (PI+/DiOC6+); L3: apoptotic cells (PI-/DiOC6-); L4: viable cells (PI-/DiOC6+).

Once assessed the lack of toxicity of the carrier fullerene **2** toward MCF-7 and MCF-7/ADR cells, the following step was studying the internalization of the system. To do so we exploited the fluorescence of fullerene derivative **3**, even though it was lower with respect to the free fluorophore due to quenching phenomena, as already mentioned. Uptake by MCF-7 and MCF-7/ADR cells was studied by flow cytofluorimetry. Cells were incubated with fullerene **3** for 1 h, at a concentration of 25 µM and then analysed, showing an increase in the fluorescence intensity (yellow lines in Figure 12). This value did not decrease after treatment with Trypan Blue (TB), which is a dye used to quench extracellular fluorescence. In fact, TB is not internalized by cells, thus quenching only fluorescence given by extracellular dyes, and it is used to exclude the non-internalized component during cytofluorimetric analysis. Nevertheless, washing the cells, the fluorescence intensity decreases to the values of the control (grey lines in Figure 12). This behaviour means that probably fullerene **3**, 1 h after treatment, was interacting with cellular

membrane to such an extent that it was hindered from TB action, but it was not fully internalized and therefore it was then washed off.

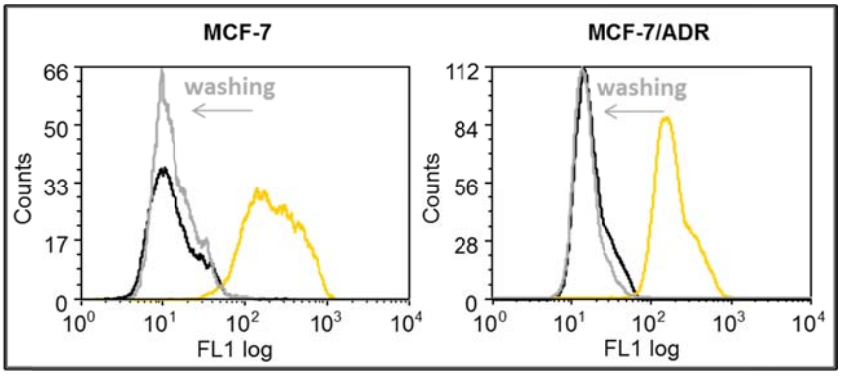

Figure 12. Count of fluorescent cells (one representative experiment is shown) by flow cytofluorimetry analysis of MCF-7 and MCF-7/ADR cells treated with fullerene **3** (25 µM, 1 h), before (yellow line) and after (grey line) washing. Black line represents untreated cells.

We therefore prolonged exposure time, to let cells the time to fully internalize the fullerene derivative. As expected, for 12 h or longer treatments, cells actually internalized fullerene **3**, reaching soon a plateaux (Figure 13). It should be pointed out that, for these longer treatments, cells were always washed before the flow cytofluorimetry analysis, being this a requirement of the experimental procedure.

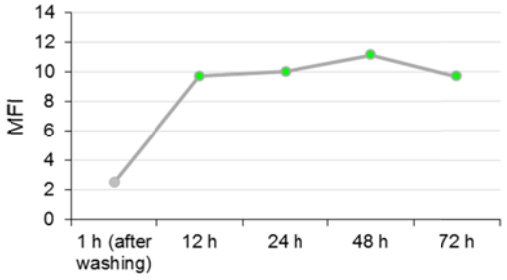

Figure 13. Uptake of fullerene **3** (25 µM) by MCF-7 cells, plotted as mean fluorescence intensity (with addition of Trypan Blue) vs. time.

Moreover, we observed a concentration-dependence of the uptake, as shown in Figure 14 for the 48 h treatment, with values of mean fluorescence intensity (MFI) almost doubled for the 25 µM treatment with respect to the 10 µM one.

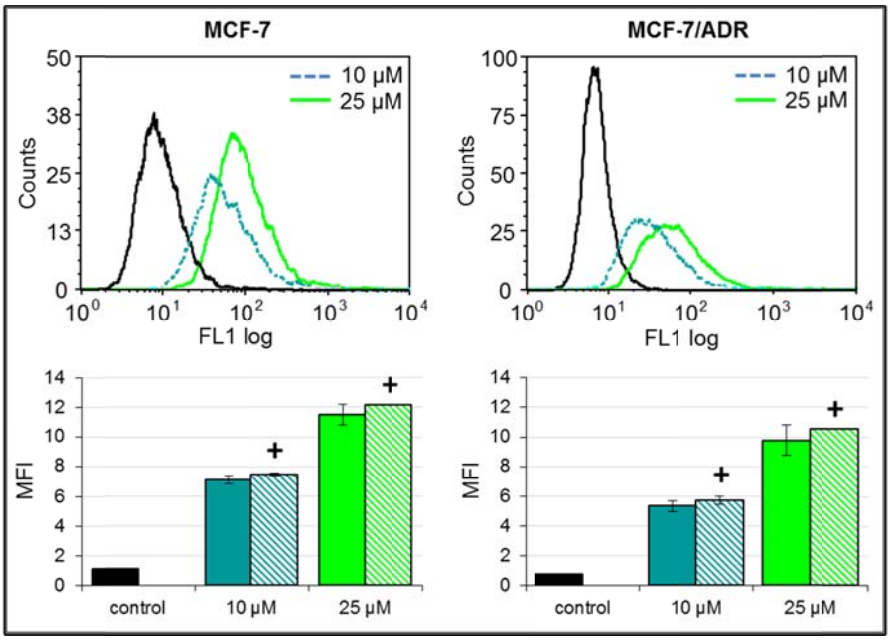

Figure 14. Flow cytofluorimetry analyses of MCF-7 and MCF-7/ADR cells treated with fullerene **3** (10 or 25 μM, 48 h). Upper panels show the count of fluorescent cells, with black line relative to untreated cells (one representative experiment is shown). Lower panels show the mean fluorescence intensity (MFI) with (striped histograms) or without (full histograms) the addition of Trypan Blue (mean MFI ± SD of a duplicate experiment is shown).

According to these preliminary data, uptake in the time frame 1-12 h will be studied, to assess the kinetics of the internalization.

Furthermore, the cytotoxicity of doxorubicin-bearing fullerene **5** and **6** will be studied. Also the CNT series of compounds will be evaluated. In particular, the effect of the cleavable peptidic sequence will be assessed, to verify the importance of drug release from the covalent conjugates prepared.

4.4 Acknowledgments

I wish to thank Dr. Alberto Bianco (CNRS, Institut de Biologie Moléculaire et Cellulaire, Laboratoire d'Immunologie et Chimie Thérapeutiques in Strasbourg, France) for the syntheses of the Boc-protected and Alloc-protected GFLG tetrapeptides.

I would also like to thank Dr. Luigi Feruglio for the 500 MHz NMR analyses, and Prof. M. Antonia Herrero (Departamento de Química Orgánica, Facultad de Químicas-IRICA, Universidad de Castilla-La Mancha in Ciudad Real, Spain) for the MALDI-TOF-MS analyses.

For the biological studies, I wish to thank Marianna Lucafò, Dr. Sabrina Pacor, Dr. Sonia Zorzet and Prof. Gianni Sava (Dipartimento di Scienze della vita, Università di Trieste).

4.5 References

1. a) H. Ali-Boucetta, K. T. Al-Jamal, D. McCarthy, M. Prato, A. Bianco, and K. Kostarelos, *Chem. Commun.*, 2008, 459-461; b) Liu, X. Sun, N. Nakayama-Ratchford, and H. Dai, *ACS Nano*, 2007, 1, 50-56; c) Z. Liu, A. C. Fan, K. Rakhra, S. Sherlock, A. Goodwin, X. Chen, Q. Yang, D. W. Felsher, and H. Dai, *Angew. Chem. Int. Ed.*, 2009, 48, 7668-7672; d) Z. Liu, W. Cai, L. He, N. Nakayama, K. Chen, X. Sun, X. Chen, and H. Dai, *Nat. Nanotechnol.*, 2007, 2, 47-52; e) X. Zhang, L. Meng, Q. Lu, Z. Fei, and P. J. Dyson, *Biomaterials*, 2009, 30, 6041-6047; f) E. Heister, V. Neves, C. Tîlmaciu, K. Lipert, V. S. Beltran, H. M. Coley, S. R. P. Silva, and J. McFadden, *Carbon*, 2009, 47, 2152-2160; g) P. Chaudhuri, S. Soni, and S. Sengupta, *Nanotechnology*, 2010, 21, 025102 (11pp); h) R. Li, R. Wu, L. Zhao, M. Wu, L. Yang, and H. Zou, *ACS Nano*, 2010, 4, 1399-1408.
2. M. Binaschi, R. Farinosi, M. E. Borgnetto, and G. Capranico, *Cancer Res.*, 2000, 60, 3770-3776.
3. S. R. Wedge, R. Duncan, and P. Kopeckova, *Br. J. Cancer*, 1991, 63, 546-549.
4. E. Kaiser, J. P. Tam, T. M. Kubiak, and R. B. Merrifield, *Tetrahedron Lett.*, 1988, 29, 303-306.
5. H. Kunz and C. Unverzagt, *Angew. Chem. Int. Ed.*, 1984, 23, 436-437.
6. H. Kunz and J. März, *Angew. Chem. Int. Ed.*, 1988, 27, 1375-1377.
7. K. Kordatos, T. Da Ros, M. Prato, R. V. Bensasson, and S. Leach, *Chem. Phys.*, 2003, 293, 263-280.
8. a) S. A. Vail, P. J. Krawczuk, D. M. Guldi, A. Palkar, L. Echegoyen, J. P. C. Tomé, M. A. Fazio, and D. I. Schuster, *Chem. Eur. J.*, 2005, 11, 3375-3388; b) D. M. Guldi, M. Maggini, G. Scorrano, and M. Prato, *J. Am. Chem. Soc.*, 1997, 119, 974-980.
9. F. G. Brunetti, M. A. Herrero, J. D. M. Munoz, S. Giordani, A. Diaz-Ortiz, S. Filippone, G. Ruaro, M. Meneghetti, M. Prato, and E. Vazquez, *J. Am. Chem. Soc.*, 2007, 129, 14580-14581.
10. Z. Ye, W. Deering, A. Krokhin, and J. Roberts, *Phys. Rev. B*, 2006, 74, 075425 (1-5).
11. A. Wadhawan, D. Garrett, and J. M. Perez, *Appl. Phys. Lett.*, 2003, 83, 2683-2685.

Experimental part

5.1 Materials and Methods

Chemicals were purchased from *Sigma-Aldrich* or *Acros Organics* and used as received, when not differently specified. **Solvents** were purchased from Sigma-*Aldrich*, and deuterated solvents from *Cambridge Isotope Laboratories*.

Single-Walled carbon nanotubes (HiPCO), were purchased from *Carbon Nanotechnologies* (lot #R0510C).

Double-walled carbon nanotubes (CCVD), were provided both as pristine and as shortened and oxidized by *Nanocyl*.

Multi-walled carbon nanotubes (CCVD), were purchased from *Nanostructured & Amorphous Materials* (stock# 1240XH and 1237YJS).

Antibody hCTM01 IgG, Fab' and scFv were obtained from *UCB*.

Column chromatography was carried out with *Merck* silica gel 60 (particle size 40-63 μm).

Preparative thin layer chromatography was carried out with *Analtech* pre-coated glass plates with 1.5 mm thick silica gel.

Thin layer chromatography was carried out on *Merck* pre-coated aluminium plates with silica gel 60 F_{254}.

When **anhydrous reaction conditions** were required, reaction flasks were dried with a heating gun (300-500 °C), placed under high vacuum using a Schlenk line and purged with Ar. To keep the atmosphere dry and inert balloons filled with Ar where used.

CNTs washing procedure by filtration consisted in dispersing the nanotubes in the specified solvent (at a concentration of about 1mg/mL), followed by sonication for 15-20 min and vacuum filtration on polytetrafluoroethylene (PTFE) *Millipore* filters of the specified pore size. The procedure was normally repeated twice or three times for each solvent. Et_2O was subsequently poured on the filtered CNTs, and vacuum was applied for 30 min after emptying the filtration flask. Finally, CNTs were scratched from the filter and dries under high vacuum.

Kaiser test was performed using *Fluka* Kaiser test kit. In a typical test, 0.3-0.5 mg of CNTs were weighted. 75 μL of the kit solution of phenol (80% in EtOH) and 100 μL of the kit solution of

KCN (in H_2O/pyridine) were added and the dispersion was sonicated for 2 minutes in a sonic bath. Subsequently, 75 µL of the kit solution of ninhydrin (6% in ethanol) were added, and the mixture was heated at 120 °C for 10 minutes. Then, it was cooled and diluted with EtOH/H_2O (60%) to a final volume of 3mL. After centrifugation, the absorption spectrum of the supernatant was measured, using as a blank a solution obtained in the same way as above but without CNTs. The value of the absorption maximum at 570 nm was used to calculate amine loading in the CNT sample (Ɛ = 15000 $M^{-1}cm^{-1}$). Reported values are average of at least two separate measurements.

Dialysis of Ab or Ab-CNTs samples was carried out with *Spectrum Laboratories* membranes (regenerated cellulose membrane with a 12-14 KDa molecular weight cutoff and cellulose ester membranes with a 300 KDa molecular weight cutoff).

Size-exclusion chromatography of Fab' and scFv samples was performed using PD-10 Desalting Columns pre-packed with Sephadex G-25 Medium, equipped with a LabMate PD-10 Buffer Reservoir (*GE Healthcare*).

Gel electrophoresis was performed with a mini-vertical electrophoresis system (*Invitrogen* XCell SureLock), using a Novex®8-16% Tris-Glycine gel (*Invitrogen*) and run under either non-reducing or reducing conditions (by addition of 5% β-mercaptoethanol). The gels were stained with Coomassie blue.

Ellman's assay was performed as follows: a stock 0.01 M solution of 5,5'-Dithio-*bis*-(2-nitrobenzoic acid) (DTNB) in PBS-EDTA-$NaHCO_3$ (pH 7.8) was prepared; 10 µL of DTNB stock solution were diluted with 500 µL of buffer, and 50 µL of analyte solution was added. After incubation at r.t. for 15 min, the absorption spectrum of the solution was measured, using as a blank a solution obtained in the same way, adding 50 µL of buffer in place of the analyte solution. The value of the absorption maximum at 412 nm was used to quantify free sulfhydryl groups in the analyte solution (Ɛ = 14150 $M^{-1}cm^{-1}$).

5.2 Instrumentation

Ball milling treatments were carried out in a PM100 Planetary Mill (*Retsch*).

Microwave-assisted reactions were carried out in a *CEM* Discover reactor.

Nuclear magnetic resonance (NMR) 200 MHz 1H-NMR and 50 MHz 13C-NMR spectra were obtained on a *Varian Gemini* 200 spectrometer. 500 MHz 1H-NMR spectra were obtained on a *Varian* Inova. Chemical shifts are reported in ppm using the solvent residual signal as an internal reference ($CDCl_3$: δ H = 7.26 ppm, CD_3OD: δ H = 3.31 ppm, DMSO-d6: δ H = 2.50 ppm).

The resonance multiplicity is described as *s* (singlet), *d* (doublet), *t* (triplet), *q* (quartet), *dd* (doublet of doublets), *ddd* (doublet of doublets of doublets) *m* (multiplet), *br* (broad signal).

Mass spectrometry: Electrospray Ionization (ESI) mass analysis was performed on a *Perkin-Elmer* API1. Matrix-assisted laser desorption-time of flight (MALDI-TOF) mass analysis was performed on a *Bruker Daltonics* instrument, using a matrix of 1,8-dihydroxy-9(10H)-anthracenone (dithranol)/silver trifluoroacetate. Mass isotopic distribution simulation were performed with *IsoPro* 3.1 software.

UV–vis–NIR spectra were recorded on a Cary 5000 Spectrophotometer (*Varian*), using 1 cm path quartz or optical glass cuvettes.

Fluorescence spectra were recorded on a Cary Eclipse Fluorescence Spectrophotometer (*Agilent Technologies*), using 1 cm path quartz cuvettes.

Thermogravimetric analyses were performed using a TGA Q500 (*TA Instruments*), with the following procedure: isotherm at 100°C for 20 min (to remove residual solvent), ramp from 100 to 1000°C at 10°C/min, under N_2 or air with a flow rate on the sample of 60 mL/min. Reported graphs are average of at least two separate measurements. Ab-CNT samples (in PBS) were extensively washed with milliQ water by several cycles of centrifugation and removal of the supernatant, followed by a dialysis (12-14 kDa cutoff membrane), and subsequently lyophilized, prior to TGA analysis, in order to remove the salts present in the buffer.

TGA-MS experiments were performed on the same TGA instrument coupled with a ThermoStar Mass Spectrometer (*Pfeiffer Vacuum*) with the following procedure: isotherm at 100°C for 20 min, ramp from 100 to 800°C at 20°C/min, under He with a flow rate on the sample of 60 mL/min.

AFM analyses were carried out in Tapping-Mode (TM-AFM), in air at r.t., using a Nanoscope IIIa, MMAFMLN (*Veeco*). Surfaces were imaged with phosphorus-doped silicon tips (cantilever: thickness = 3.5–4.5 µm, length = 115–135 µm, frequency f_0 = 245–279 kHz, force constant k = 20–80 N/m; *Veeco*). Statistical analysis of the AFM images was carried out using *Gwyddion* 2.14 software. The surfaces for AFM analyses were prepared as follows: *s*-SWCNTs were dispersed in 1% SDBS aqueous solution at a concentration of 0.02 mg/mL, by 5 h sonication in a sonic bath. Nanotubes were then deposited on mica surfaces by spin-coating (3000 rpm, 3 min) 100–200 µL of these solutions. Finally, the surfaces were heated for 4 h in an oven at 180 °C, to remove the surfactant.

Raman spectroscopy analyses were performed on an inVia Raman microscope (*Renishaw*), equipped with lasers at 532 nm, 633 nm or 785 nm, on solid samples deposited onto

a glass coverslip. Reported spectra are average of at least 5 different analyses performed in different areas of the sample, and they are normalized to the G-band.

TEM analyses were performed with a *Philips* EM 208 microscope with an accelerating voltage of 100 kV (images were acquired using an *Olympus* Morada CCD camera). CNTs samples were typically suspended in DMF (apart from Ab-CNT sample, which were in PBS) with the help of sonication, and these suspensions were drop-casted on copper or nickel grids (diameter = 3.00 mm, 200 mesh, coated with carbon film), which were subsequently dried under high vacuum overnight, prior to the TEM analysis.

Surface plasmon resonance measurements were performed on a *Biacore* 3000 system. The sensor chip CM5, surfactant P20, amine coupling kit containing NHS and EDC·HCl were purchased from *Biacore* and streptavidin from *Sigma-Aldrich*. HEPES-buffered saline (10 mM HEPES, 150 mM sodium acetate, 3 mM magnesium acetate, 0.005% surfactant P20, pH 7.4) was used as running buffer. The sensor chip for the measurement was prepared as follows: the surface of a sensor CM5 chip was activated by EDC/NHS. Immobilization of streptavidin was performed by injection onto the activated surface with 35 µL of streptavidin (100 µg/mL in formate buffer, pH 4.3), which gave a signal of approximately 5000 RU, followed by 20 µL of ethanolamine hydrochloride (pH 8.5) to saturate the free activated sites of the matrix. Biotinylated antigen and scrambled antigen (1 µM in Hepes buffer) were allowed to interact with streptavidin until a response of 700 RU was obtained. The different analytes were dissolved/dispersed in the running buffer. Binding experiments were carried out at 25°C with a constant flow rate of 20 µL/min. Different concentrations of Ab or Ab-CNTs were injected for 3 min, followed by a dissociation phase of 3min. The sensor chip surface was regenerated after each experiment by injection of 10 µL of 10 mM HCl.

5.3 Experimental Procedures

5.3.1 Organic compounds

N-Boc-amino-diethoxy-ethyl amine (**1**)

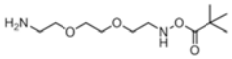

To a solution of amino-diethoxy-ethyl amine (20 g, 134.9 mmol) in CH_2Cl_2 (100 mL), a solution of Boc_2O (11.79 g, 54 mmol) in CH_2Cl_2 (100 mL) was added drop-wise over 3 h, stirring the mixture at 0°C. The reaction was then stirred at r.t. for 24 hours. The solvent was evaporated under vacuum, and the resulting white semi-solid was dissolved in H_2O (70 mL) and filtered over celite to remove the white precipitate corresponding to the doubly substituted by-product. The

aqueous filtrate was extracted with CH_2Cl_2 (50 mL x 3). The organic phase was backwashed with H_2O (50 mL) to remove the excess of diamine, and then dried with Na_2SO_4. Evaporation of the solvent under vacuum yielded compound **1** (7.9 g, 58%) as a colourless viscous oil. Characterizations were in accordance with literature.[1]

N-Boc-amino-diethoxy-ethylamino-acetic acid benzyl ester (**2**)

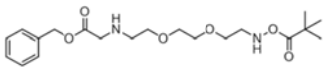

To a solution of **1** (7 g, 28.2 mol) in CH_2Cl_2 (30 mL) at 0 °C, TEA (4.69 mL, 33.8 mmol) was added. Then, a solution of benzyl bromoacetate (6.46 g, 28.2 mol) in CH_2Cl_2 (40 mL) was added drop-wise over 3 h at 0°C , and the reaction mixture was stirred at r.t. overnight. The solvent was evaporated under vacuum, and the residue was dissolved in CH_2Cl_2 (70 mL) and washed with H_2O (70 ml x 3). The combined organic phases were dried over Na_2SO_4, and the solvent was removed under vacuum. Purification by column chromatography (CH_2Cl_2/MeOH 97:3) afforded the desired compound **2** (5.52 g, 49%) as a colourless oil. Characterizations were in accordance with literature.[1]

N-Boc-amino-diethoxy-ethylamino-acetic acid (**3**)

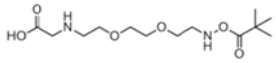

To a deoxygenated MeOH solution (90 mL) of **2** (5 g, 12.6 mmol), 10% Pd/C (90 mg) was added, and the reaction flask was purged with H_2 three times and then stirred at r.t. for 24 h. The catalyst was removed by filtration over celite, and the solvent was evaporated. The resulting product was triturated in diethyl ether to give a white solid in quantitative yield. Characterizations were in accordance with literature.[1]

N-Pht-*N*-Boc-amino-diethoxy-ethyl amine (**4**)

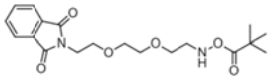

N-Boc-amino-diethoxy-ethyl amine **1** (4 g, 16.1 mmol) and phthalic anhydride (2.39 g, 16.1 mmol) were dissolved in toluene (80 mL), and the mixture was stirred at 120°C in a Dean-Stark apparatus for 20 h. The solvent was then evaporated under vacuum and chromatographic column purification (toluene/AcOEt 7:3) afforded the pure product (4.33 g, 71%) as a colourless oil. Characterizations were in accordance with literature.[1]

N-Pht-amino-diethoxy-ethyl amine (**5**)

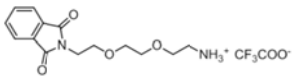

The *N*-phthalimido-*N*-Boc-amino-diethoxy-ethyl amine **4** (4 g, 10.6 mmol) was dissolved in CH_2Cl_2 (15 mL), and TFA (15 mL) was slowly added to the solution, while stirring at 0°C. The reaction mixture was then allowed to reach r.t. and it was stirred for 2 h. The solvent was removed under vacuum and the resulting product, as trifluoroacetic acid salt, was triturated in diethyl ether to give a white solid in quantitative yield. Characterizations were in accordance with literature.[1]

N-Pht-amino-diethoxy-ethylamino-acetic acid benzyl ester (**6**)

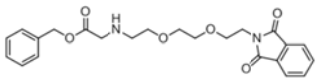

To a solution of **5** (3.41 g, 8.7 mmol) in THF (40 mL) at 0 °C, TEA (3.64 mL, 26.1 mmol) was added. Then, a solution of benzyl bromoacetate (1.99 g, 8.7 mmol) in THF (60 mL) was added drop-wise over 3 h at 0°C , and the reaction mixture was stirred at r.t. for 6 h. The solvent was evaporated under vacuum, and the residue was dissolved in CH_2Cl_2 (50 mL) and washed with H_2O (50 ml x 3). The combined organic phases were dried over Na_2SO_4, and the solvent was removed under vacuum. Purification by column chromatography (AcOEt/MeOH 95:5) afforded the desired product **6** (1.48 g, 40%) as a colourless oil. Characterizations were in accordance with literature.[1]

N-Pht-amino-diethoxy-ethylamino-acetic acid (**7**)

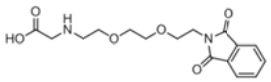

To a deoxygenated MeOH solution (40 mL) of **6** (1.48 g, 3.5 mmol), 10% Pd/C (40 mg) was added, and the reaction flask was purged with H_2 three times and then stirred at r.t. for 24 h. The catalyst was removed by filtration over celite, and the solvent was evaporated. The resulting product was triturated in diethyl ether to give a white solid in quantitative yield. Characterizations were in accordance with literature.[1]

Boc-GFLG-doxorubicin (**8**)

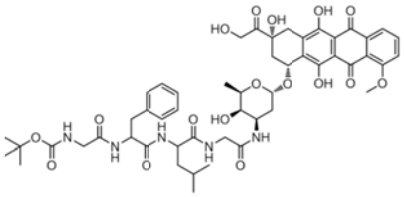

To a solution of Boc-GFLG peptide (84.7 mg, 172 µmol) in dry DMF (1.5 mL), HOBt (containing 12% H_2O, 31.7 mg, 207 µmol) and EDC·HCl (39.7 mg, 207 µmol) were added, stirring the solution at 0°C. Then TEA (29 µL, 207 µmol) was added, and the mixture was allowed to

reach r.t., and it was stirred under Ar for 15 min. A solution of doxorubicin·HCl (100 mg, 172 µmol) and TEA (29 µL, 207 µmol) in dry DMF (2 mL) was added, and the reaction was stirred at r.t. under Ar, in the dark, overnight. The crude reaction mixture was precipitated and then washed twice with Et_2O, to remove DMF, TEA and HOBt, and it was finally purified by column chromatography (CH_2Cl_2/MeOH, 9:1), affording the pure product (138 mg, 79%) as a red solid. ^{1}H-NMR (500 MHz, $CDCl_3$): δ 13.96 (s, 1H), 13.29 (s, 1H), 8.05 (d, *J* = 7.6 Hz, 1H), 7.78 (t, *J* = 8.1 Hz, 1H), 7.39 (d, *J* = 8.4 Hz, 1H), 7.36-7.28 (m, 3H), 7.18 (d, *J* = 7.5 Hz, 2H), 7.13 (br, 1H), 6.88 (br, 1H), 6.67 (d, *J* = 8.8 Hz, 1H), 6.63 (d, *J* = 6.0 Hz, 1H), 5.53 (d, *J* = 3.6 Hz, 1H), 5.32 (br, 1H), 5.20 (br, 1H), 4.78 (dd, *J* = 4.8, 2.8 Hz, 2H), 4.71 (s, 1H), 4.57 (dd, *J* = 11.3, 5.7 Hz, 1H), 4.25 (br, 1H), 4.08 (s, 3H), 4.06-4.04 (m, 1H), 4.04-3.99 (m, 1H), 3.92 (d, *J* = 3.3 Hz, 1H), 3.77-3.58 (m, 4H), 3.30 (d, *J* = 18.8 Hz, 2H), 3.25 (br, 1H), 3.10 (br, 1H), 2.99 (t, *J* = 5.0 Hz, 1H), 2.38 (d, *J* = 14.7 Hz, 1H), 2.14 (dd, *J* = 14.6, 3.7 Hz, 1H), 2.07-1.95 (m, 1H), 1.83 (d, *J* = 8.0 Hz, 1H), 1.70 (s, 1H), 1.45-1.39 (m, 2H), 1.35 (s, 9H), 1.33 (d, *J* = 6.6 Hz, 3H), 0.92-0.85 (m, 6H); ESI-MS: 1040.5 $(M+Na)^+$ [calculated = 1040.41], 1056.5 $(M+K)^+$[calculated = 1056.52], 1016.3 $(M-1)^-$ [calculated = 1016.41].

Alloc-GFLG-doxorubicin (**9**)

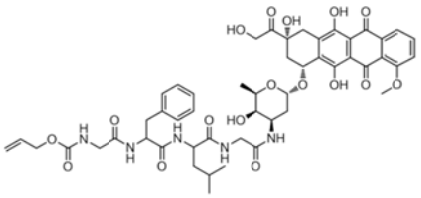

To a solution of Alloc-GFLG peptide (82.2 mg, 172 µmol) in dry DMF (3 mL), HOBt (containing 12% H_2O, 31.7 mg, 207 µmol) and EDC·HCl (39.7 mg, 207 µmol) were added, stirring the solution at 0°C. Then TEA (29 µL, 207 µmol) was added, and the mixture was allowed to reach r.t., and it was stirred under Ar for 15 min. A solution of doxorubicin·HCl (100 mg, 172 µmol) and TEA (29 µL, 207 µmol) in dry DMF (4 mL) was added, and the reaction was stirred at r.t. under Ar, in the dark, overnight. The crude reaction mixture was precipitated and then washed twice with Et_2O, to remove DMF, TEA and HOBt, and it was finally purified by column chromatography (CH_2Cl_2/MeOH, 9:1), affording, after precipitation with Et_2O, the pure product (127.5 mg, 74%) as a red solid. ^{1}H-NMR (500 MHz, $CDCl_3$): δ 13.96 (s, 1H), 13.28 (s, 1H), 8.05 (d, *J* = 7.7 Hz, 1H), 7.78 (t, 1H), 7.38 (d, *J* = 8.6 Hz, 1H), 7.37-7.28 (m, 3H), 7.17 (d, *J* = 6.8 Hz, 2H), 7.05 (br, 1H), 6.88 (d, *J* = 4.9 Hz, 1H), 6.69 (d, *J* = 7.7 Hz, 1H), 6.64 (d, *J* = 5.3 Hz, 1H), 5.83 (ddd, *J* = 22.7, 10.9, 5.7 Hz, 1H), 5.57 (br, 1H), 5.53 (d, *J* = 3.7 Hz, 1H), 5.31 (br, 1H), 5.29-5.26 (m, 1H), 5.24 (s, 1H), 4.78 (dd, *J* = 4.9, 2.1 Hz, 2H), 4.71 (s, 1H), 4.56 (dd, *J* = 10.9, 5.5 Hz, 1H), 4.44 (dd, *J* = 13.0, 5.8 Hz, 1H), 4.38-4.31 (m, 1H), 4.24-4.15 (m, 1H), 4.08 (br, 1H), 4.07 (s, 3H), 4.01 (dd, *J* = 16.3, 6.4 Hz, 1H), 3.93 (d, *J* = 4.3 Hz, 1H), 3.76-3.61 (m, 4H), 3.32 (s, 1H), 3.30-3.23 (m, 1H), 3.10-3.02 (m,

2H), 3.00 (t, *J* = 4.9 Hz, 1H), 2.38 (d, *J* = 15.0 Hz, 1H), 2.14 (dd, *J* = 14.7, 4.0 Hz, 1H), 2.02-1.93 (m, 1H), 1.81 (dd, *J* = 13.2, 4.6 Hz, 1H), 1.63 (dd, *J* = 16.9, 7.1 Hz, 1H), 1.32 (d, *J* = 6.5 Hz, 3H), 1.31-1.27 (m, 2H), 0.87 (dd, *J* = 12.4, 6.5 Hz, 6H).

GFLG-doxorubicin (**10**)

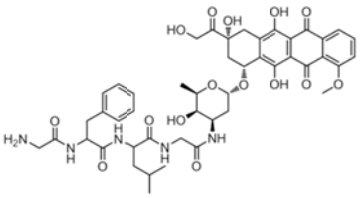

Alloc-GFLG-doxorubicin **9** (20 mg, 20 µmol) was dissolved in dry, deoxygenated THF (4 mL). Dimedone (28 mg, 200 µmol) and $Pd(PPh_3)_4$ (2.3 mg, 2 µmol) were added. The reaction was stirred at r.t., under Ar and in the dark, for 2 h. Then, the crude was precipitated with cold cyclohexane, and then washed twice by precipitation from CH_2Cl_2 with cyclohexane, to remove excess dimedone, and once with Et_2O. Purification by column chromatography (CH_2Cl_2/MeOH, 95:5, then 9:1), followed by re-precipitation from CH2Cl2/MeOH with Et2O, yielded the desired product (10 mg, 54%) as a dark red solid. ^{1}H-NMR (500 MHz, CD_3OD): δ 8.01 (d, *J* = 7.7 Hz, 1H), 7.89-7.81 (m, 1H), 7.59 (d, *J* = 8.4 Hz, 1H), 7.20 (d, *J* = 4.0 Hz, 3H), 7.16-7.10 (m, 2H), 5.42 (d, *J* = 2.8 Hz, 1H), 5.19 (br, 1H), 4.74 (d, *J* = 3.6 Hz, 2H), 4.62 (dd, *J* = 8.1, 5.9 Hz, 1H), 4.28 (dd, *J* = 12.3, 5.6 Hz, 1H), 4.26-4.20 (m, 1H), 4.13 (d, *J* = 12.6 Hz, 1H), 4.04 (s, 3H), 3.90 (d, *J* = 16.8 Hz, 2H), 3.68 (d, *J* = 16.9 Hz, 2H), 3.62 (br, 1H), 3.25 (d, *J* = 17.1 Hz, 1H), 3.15-3.08 (m, 2H), 2.92 (dd, *J* = 14.0, 8.3 Hz, 1H), 2.38 (d, *J* = 14.0 Hz, 1H), 2.19 (dd, *J* = 14.7, 4.8 Hz, 1H), 2.05-1.96 (m, 1H), 1.67-1.52 (m, 4H), 1.27 (d, *J* = 6.5 Hz, 3H), 0.90 (dd, *J* = 20.2, 5.3 Hz, 6H).

5.3.2 Fullerene derivatives

Fullerene **1**

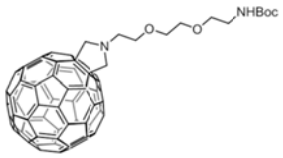

A toluene solution (300 mL) of C_{60} (400 mg, 560 µmol), *N*-Boc-amino-diethoxy-ethylamino-acetic acid **3** (170 mg, 560 µmol) and *p*-HCHO (167 mg, 5.56 mmol) was heated at 120 °C for 20 min. Then, the reaction mixture was allowed to reach r.t., and it was purified by column chromatography (toluene, followed by toluene/AcOEt 8:2). Finally, the product was dissolved in CH_2Cl_2 and precipitated by addition of MeOH, to yield fullerene **1** (160 mg, 29%) as a brown solid. Characterizations were in accordance with literature.[2]

Fullerene **2**

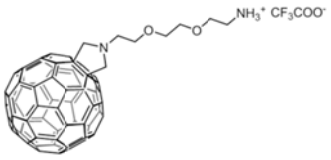

Fullerene **1** (140 mg, 141 µmol) was dissolved in CH_2Cl_2 (25 mL), and TFA (25 mL) was slowly added to the solution, while stirring at 0°C. The reaction mixture was then allowed to reach r.t. and it was stirred for 4 h. The solvent was removed under vacuum and the solid residue was washed by re-precipitation with CH_2Cl_2 in order to remove any trace of the starting product, affording fullerene **2** in quantitative yield. Characterizations were in accordance with literature.[2]

Fullerene **3**

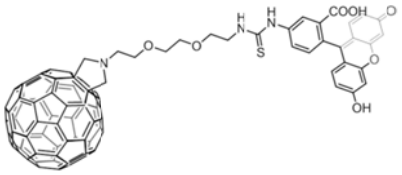

To a solution of fullerene **2** (25 mg, 25 µmol) in dry DMF (4 mL), DIEA (9 µL, 50 µmol) and FITC (9.7 mg, 25 µmol) were added, and the reaction mixture was stirred at r.t., under Ar, in the dark, overnight. Finally, the crude mixture was precipitated with MeOH and then thoroughly washed by re-precipitation from toluene, with MeOH and from CH_2Cl_2 with MeOH, to afford the desired product (20 mg, 63%) as an ochre-brown solid. ^{1}H-NMR (500 MHz, DMSO-d6): δ 10.09 (s, 1H), 10.04 (br, 1H), 8.35 (s, 1H), 7.98 (br, 1H), 7.71 (br, 1H), 7.13 (d, *J* = 8.3 Hz, 1H), 6.65 (s, 2H), 6.53 (s, 4H), 4.55 (s, 4H), 4.01 – 3.94 (m, 2H), 3.80 (d, *J* = 4.5 Hz, 2H), 3.75 (d, *J* = 4.2 Hz, 2H), 3.69 (br, 4H), 2 H of the ethylene glycol chain are probably covered by the H_2O signal; ESI-MS: 1284.2 $(M+1)^+$ [calculated = 1284.18], 1306.2 $(M+Na)^+$ [calculated = 1306.16], 1282.1 $(M-1)^-$ [calculated = 1282.16].

Fullerene **4**

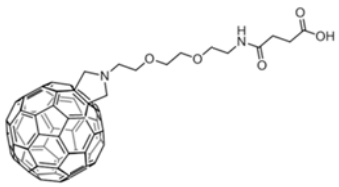

Fullerene **2** (100 mg, 99 µmol) was suspended in dry CH_2Cl_2 (30 mL) by sonication in a sonic bath. To this suspension, a solution of succinic anhydride (19.9 mg, 198 µmol) in CH_2Cl_2 (10 mL) and TEA (41 µL, 298 µmol) were added. The reaction mixture was stirred at r.t. under Ar overnight. Purification of reaction crude by precipitation and washing in MeOH, to remove TEA

and succinic anhydride, yielded the desired product (73.8 mg, 75%) as a brown solid. ^{1}H-NMR (500 MHz, $CDCl_3$) δ 4.64 (s, 4H), 4.10 (t, *J* = 5.5 Hz, 2H), 3.88-3.83 (m, 2H), 3.77-3.72 (m, 2H), 3.62-3.57 (m, 2H), 3.55-3.45 (m, 4H), 2.69 (m, 2H), 2.58 (m, 2H); ESI-MS: 995.2 $(M+1)^+$ [calculated = 995.16], 1017.1 $(M+Na)^+$ [calculated = 1017.14], 993.1 $(M-1)^-$ [calculated = 993.14].

Fullerene **5**

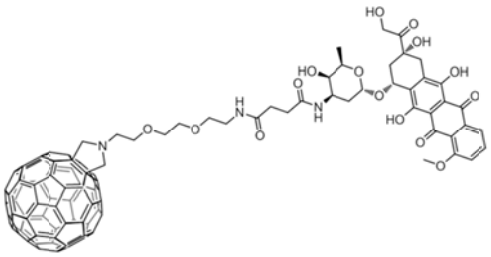

To a solution of fullerene **4** (15 mg, 15 µmol) in dry DMF (3 mL), a solution of PyAOP (11.8 mg, 23 µmol) in dry DMF (1 mL) and DIEA (4 µL, 23 µmol) were added and the mixture was stirred at r.t. under Ar for 20 min. Then, a solution of doxorubicin·HCl (10.5 mg, 18 µmol) and DIEA (4 µL, 23 µmol) in dry DMF (2 mL) was added, and the reaction was stirred at r.t. under Ar in the dark overnight. The crude was precipitated upon addition of MeOH, and then washed with MeOH and Et2O. Preparative thin layer chromatography purification (CH_2Cl_2/MeOH, 92:8) afforded the desired product (9.7 mg, 42%) as a reddish/brown solid. ^{1}H-NMR (500 MHz, DMSO-d6): δ 14.05 (s, 1H), 13.30 (s, 1H), 7.98-7.92 (m, 2H), 7.82 (t, 1H), 7.69 (dd, *J* = 7.6, 2.1 Hz, 1H), 7.49 (d, *J* = 7.6 Hz, 1H), 5.39 (s, 1H), 5.23 (br, 1H), 4.98-4.92 (m, 1H), 4.83 (t, *J* = 6.0 Hz, 1H), 4.67 (d, *J* = 5.8 Hz, 1H), 4.55 (d, *J* = 6.0 Hz, 2H), 4.49 (s, 4H), 4.10-4.03 (m, 1H), 4.00 (s, 3H), 3.97-3.90 (m, 2H), 3.82 (br, 1H), 3.75-3.68 (m, 2H), 3.66-3.58 (m, 2H), 3.45 (t, *J* = 5.8 Hz, 2H), 3.43 (br, 1H), 3.26-3.20 (m, 2H), 3.16-3.06 (m, 2H), 3.02 (d, *J* = 18.0 Hz, 1H), 2.93 (d, *J* = 18.2 Hz, 1H), 2.27-2.18 (m, Hz, 4H), 2.15 (d, *J* = 4.0 Hz, 2H), 1.86-1.73 (m, 1H), 1.38 (dd, *J* = 12.5, 4.0 Hz, 1H), 1.11 (d, *J* = 6.1 Hz, 3H); MALDI-TOF-MS: 1519.29, M-1 [calculated = 1519.32], 1106.23, (M-413.09) [calculated = 1106.23], 800.32 $(M-C_{60}+1)$ [calculated = 800.33].

Found and calculated mass isotopic distribution for fullerene **5**:

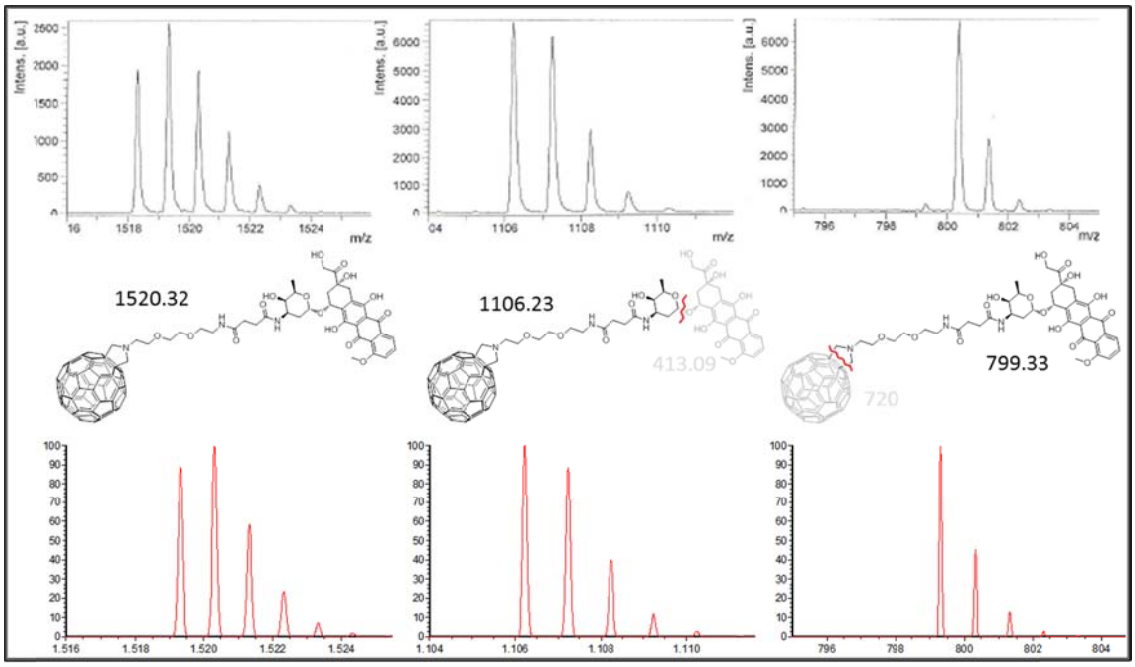

Fullerene **6**

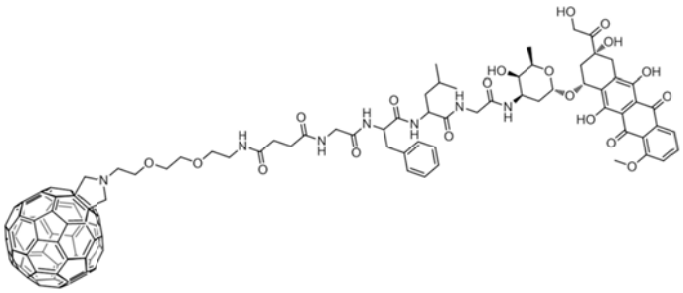

To a solution of fullerene **4** (10 mg, 10 µmol) in dry DMF (2 mL), a solution of PyAOP (7.9 mg, 15 µmol) in dry DMF (0.5 mL) and DIEA (3 µL, 15 µmol) were added and the mixture was stirred at r.t. under Ar for 20 min. Then, a solution of GFLG-doxorubicin **10** (11.1 mg, 12 µmol) and DIEA (3 µL, 15 µmol) in dry DMF (1.5 mL) was added, and the reaction was stirred at r.t. under Ar in the dark overnight. The crude was precipitated upon addition of MeOH, and then washed with MeOH and Et_2O. Preparative thin layer chromatography purification (CH_2Cl_2/MeOH, 92:8) afforded the desired product (9.2 mg, 48%) as a reddish/brown solid. ^{1}H-NMR (500 MHz, DMSO-d6): δ 14.05 (s, 1H), 13.27 (s, 1H), 8.29 (dd, *J* = 5.8, 5.4 Hz, 1H), 8.04 (d, *J* = 3.3 Hz, 1H), 8.03 (s, 1H), 7.94-7.91 (m, 2H), 7.84 (d, *J* = 8.1 Hz, 1H), 7.76 (q, *J* = 5.3 Hz, 1H), 7.70-7.63 (m, 1H), 7.45 (d, *J* = 7.8 Hz, 1H), 7.26-7.19 (m, 3H), 7.18-7.12 (m, 2H), 5.44 (s, 1H), 5.23 (d, *J* = 3.0 Hz, 1H), 4.95 (t, 1H), 4.82 (t, *J* = 6.1 Hz, 1H), 4.74 (d, *J* = 5.9 Hz, 1H), 4.56 (d, *J* = 6.0 Hz, 2H), 4.49 (s, 4H), 4.46-4.39 (m, 1H), 4.20 (dd, *J* = 14.4, 8.3 Hz, 1H), 4.14 (dd, *J* = 12.7, 6.5 Hz, 1H), 3.99 (s, 3H), 3.95 (br, 1H), 3.93 (t, *J* = 5.6 Hz, 2H), 3.72 (dd, *J* = 5.7, 3.7 Hz, 2H), 3.65-3.60 (m, 4H), 3.59 (t, 2H), 3.46 (t, *J* = 6.0 Hz, 2H), 3.41 (br, 1H), 3.28 (t, 2H), 3.21 (dd, *J* = 11.5, 5.6 Hz, 2H), 3.04 (dd, *J* = 14.2, 3.9

Hz, 1H), 2.97 (s, 2H), 2.84 (dd, *J* = 14.0, 10.3 Hz, 1H), 2.45-2.23 (m, 4H), 2.19 (dd, *J* = 14.3, 2.7 Hz, 1H), 2.12 (dd, *J* = 14.2, 5.5 Hz, 1H), 1.89-1.79 (m, 1H), 1.58-1.48 (m, 2H), 1.48-1.39 (m, 2H), 1.12 (d, *J* = 6.5 Hz, 3H), 0.83 (dd, *J* = 30.3, 6.4 Hz, 6H); MALDI-TOF-MS: 1893.61, M-1 [calculated = 1893.51], 1480.44, (M-413.09) [calculated = 1480.42], 1174.53 (M-C_{60}+1) [calculated = 1174.52].

Found and calculated mass isotopic distribution for fullerene **6**:

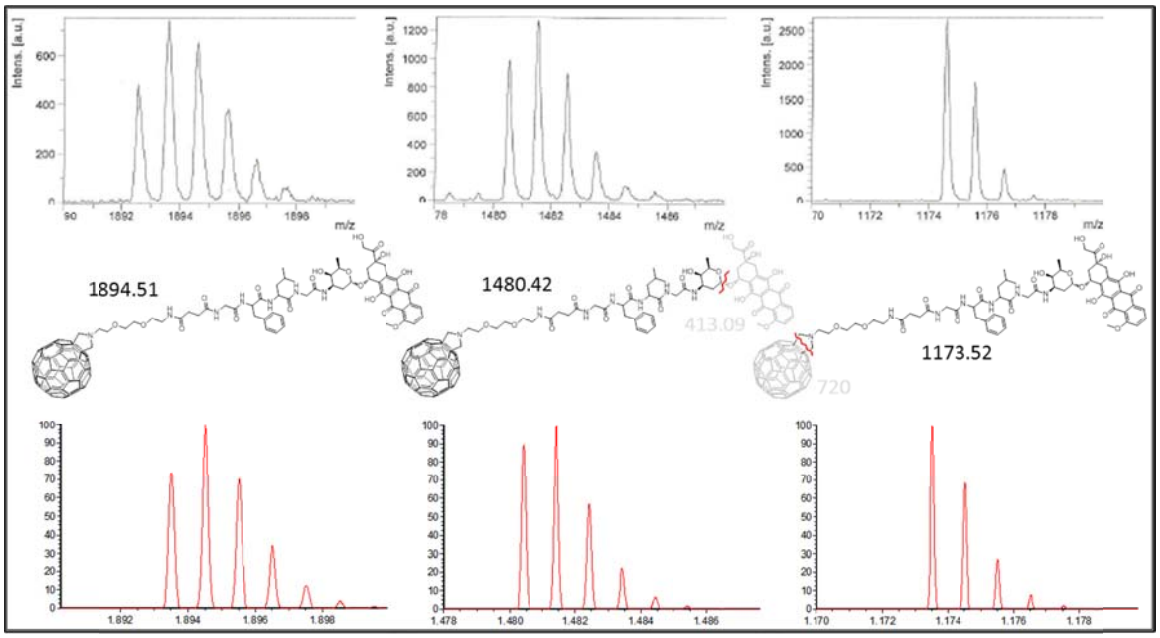

5.3.3 Antibodies

IgG-SH

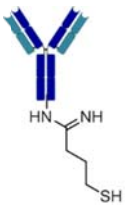

To an Ab solution (1 mL, 67 µM) in PBS (5 mM EDTA, 50 mM $NaHCO_3$, pH 7.8), a freshly prepared solution of 2-iminothiolane·HCl (2-IT, Traut's reagent) (90 µL, 14.5 mM) in the same buffer was added, to reach a final 2-IT concentration of 1.3 mM, corresponding to approximately 20 equivalents with respect to the Ab. The mixture was shaken for 1 h at r.t. and subsequently the excess of 2-IT was removed by dialysis (MWCO = 12-14 kDa) against PBS (5 mM EDTA, pH 6.5) at 4°C. The number of free sulfhydryl groups introduced was assessed by Ellman's assay to be approximately 5 per Ab.

Fab'-SH

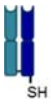

To a Fab' solution (1.8 mL, 123 μM) in 50 mM sodium acetate (2 mM EDTA, pH 5.6), a freshly prepared cysteamine solution (36 μL, 200 mM) in the same buffer was added, to reach a final cysteamine concentration of 4 mM, corresponding to approximately 32 equivalents with respect to Fab'. The mixture was shaken for 2 h at r.t. and then the pure Fab'-SH was obtained by size exclusion chromatography purification.

scFv-SH

To a scFv solution (7.5 mL, 20 μM) in 50 mM sodium acetate (2 mM EDTA, pH 5.6), a freshly prepared cysteamine solution (150 μL, 200 mM) in the same buffer was added, to reach a final cysteamine concentration of 4 mM, corresponding to approximately 200 equivalents with respect to Fab'. The mixture was shaken for 2 h at r.t. and subsequently the pure scFv-SH was obtained by size exclusion chromatography purification.

5.3.4 CNT derivatives

s-SWCNT-**1**

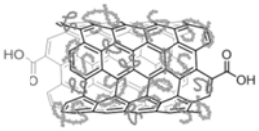

HiPCO SWCNTs (1000 g) were dispersed in oleum (500 mL), and the mixture was stirred for 12 h under Ar atmosphere. Then, of mixture of oleum and aqueous nitric acid (65%) (500 mL) was added, allowing air in, and stirring the mixture at 65°C for 2h. The reaction mixture was diluted in water and filtered (pore size = 5 μm). Afterwards, the material was washed several times with H_2O, up to a neutral pH in the filtrate, MeOH and Et_2O and finally dried under high vacuum, yielding 770 mg of *s*-SWCNT-**1**.

s-SWCNT-**2**

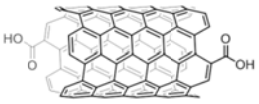

s-SWCNTs-**1** (100 mg) were dispersed in aqueous NaOH 8M (100 mL) by sonication and stirred at 100°C for 48h under Ar atmosphere (in a PTFE flask). Afterwards, CNTs were separated

from the dissolved amorphous material by filtration (pore size = 0.45 µm), and thoroughly washed with H_2O, MeOH and Et_2O to afford, after high vacuum drying, 40 mg of *s*-SWCNT-**2**.
In order to perform Raman analysis, the aqueous filtrate was neutralized by stirring the solution in 0.1 M HCl and subsequently filtering it (pore size = 0.45 µm), and washing it with H_2O, MeOH and Et_2O.

s-SWCNT-**3** (**A**, **B**, **C** and **D**)

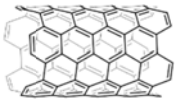

In a typical experiment, 30 mg of pristine SWCNTs were introduced in a 25 mL stainless steel grinding jar with eight stainless steel balls (1 cm diameter), which was then placed within the planetary mill. The different rotational speed and times used are detailed in Table 1 of Chapter 2.2. After the corresponding treatment, the *s*-SWCNTs were suspended in CH_2Cl_2, by sonication for 5 min, and filtered (pore size = 0.1 µm). The collected black solid was purified by cycles of sonication and centrifugation with HCl 37% (w/w) until the yellow color due to dissolved Fe^{3+} species disappeared. Afterwards, the *s*-SWCNTs were washed by filtration (pore size = 0.1 µm) with H_2O, MeOH and Et_2O and finally dried under high vacuum affording *s*-SWCNT-**3A**, **B**, **C** and **D**. The weight yields are reported in Table 1 of Chapter 2.2.

s-SWCNT-**4** (**B**, **C**, **E** and **F**)

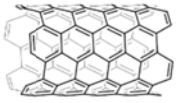

The preparation followed the same protocol as the one for *s*-SWCNT-**3**, with the only difference that the starting weighting operation was performed inside a glovebox workstation supplied with N_2, and that the grinding jar was sealed before placing it within the mill. Milling condition and final weight yields are reported in Table 1 of Chapter 2.2.

s-DWCNT-**1**

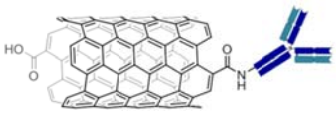

A suspension of *s*-DWCNT (10 mg) in DMF (5 mL) was sonicated in a water bath for 20 min. A solution of EDC·HCl (19.2 mg, 100 µmol), NHS (11.5 mg, 100 µmol) and DIEA (17 µL, 100 µmol) in DMF (5 mL) was added and the reaction mixture was stirred for 24 h at r.t. under Ar. The resulting NHS-activated *s*-DWCNT were then washed several times with isopropanol and

diethyl ether by successive sonication (water bath), centrifugation and removal of supernatant sequences, and they were finally dried under high vacuum.

NHS activated *s*-DWCNT (10 mg) were dispersed in 20 mL of IgG solution (0.45 mg/mL, 3 μM) in PBS (pH 7.4) and the mixture was shaken for 60 h at r.t., monitoring the reaction by the decrease of IgG concentration in the supernatant, after centrifugation of a small aliquot of the reaction. Finally, the suspension was centrifuged and the precipitate was collected and washed thoroughly with PBS (pH 7.4) until no Ab was detected in the supernatant (by UV-vis spectroscopy. The resulting Ab conjugate *s*-DWCNT-**2** was dialysed against PBS (pH 7.4) for 24 h and stored at 4 °C. The degree of functionalization, determined by TGA, was 2.1 μmol of Ab per gram of CNTs.

s-DWCNT-**2**

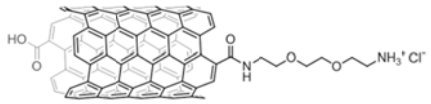

s-DWCNTs (100 mg) were suspended in thionyl chloride (20 mL), then DMF (0.4 mL) was added and the reaction was sonicated in a water bath for 30 min under Ar. Subsequently the reaction was stirred at 75°C under Ar for 24 h. After this period the solvent was dried under reduced pressure. The CNTs were suspended again in dry pyridine and *N*-Boc-amino-diethoxy-ethyl amine **1** (100 mg, 403 μmol) was added to the mixture, followed by sonication in a water bath for 30 min. Then the reaction mixture was heated at 90°C under Ar for 96 h. The nanotubes were washed several times by filtration (pore size = 0.45 μm) with DMF, MeOH and Et_2O, and dried under high vacuum.

Then, the Boc group was cleaved by dispersing CNTs (100 mg) in a 4 M HCl solution in dioxane (100 mL), by sonication for 30 min, and stirring it at r.t. overnight. The DWCNTs were washed by filtration (pore size = 0.45 μm) with DMF, MeOH and Et_2O and dried under high vacuum. The degree of functionalization, determined by Kaiser test, was 120 μmol/g.

s-DWCNT-**3**

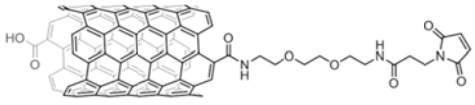

s-DWCNTs-**2** (20 mg, 2.4 μmol of amine groups) were suspended in dry DMF and neutralized with dry DIEA (21 μL, 120 μmol). A solution of *N*-succinimidyl-3-maleimidopropionate (12.8 mg, 48 μmol) in DMF (2 mL) was added. The reaction was sonicated for 20 min and then stirred at r.t. under Ar for 48 h. The obtained *s*-DWCNTs-**3** were extensively washed by filtration (pore size = 0.45 μm) with DMF, MeOH and Et_2O, and then dried under high

vacuum. The degree of functionalization, determined by comparison of the Kaiser test value with the one of *s*-DWCNT-**2**, was 60 µmol/g (Yield: 50%).

s-DWCNT-**4**

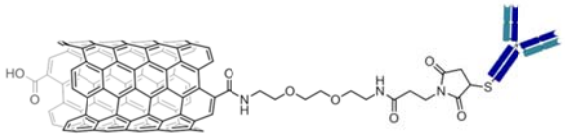

The maleimido-derivatized *s*-DWCNT-**3** (10 mg) were dispersed in 20 mL of IgG-SH solution (0.45 mg/mL, 3 µM) in PBS (5 mM EDTA, pH 6.5) and the mixture was shaken for 60 h at r.t., monitoring the reaction by the decrease of IgG concentration in the supernatant, after centrifugation of a small aliquot of the reaction. The CNTs were centrifuged and washed thoroughly with PBS (pH 7.4) until no Ab was detected in the supernatant (by UV-vis spectroscopy). The resulting Ab-conjugate *s*-DWCNT-**4** were stored at 4 °C as dispersions of 0.5 mg/mL in PBS (pH 7.4). The degree of functionalization, determined by TGA, was 2.2 µmol of Ab per gram of CNTs.

s-DWCNT-**5**

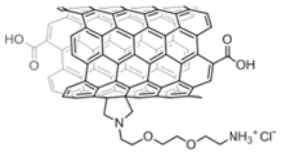

s-DWCNTs (100 mg) were suspended in 100 mL of DMF and sonicated in a water bath for 20 min. N-Boc-amino-diethoxy-ethylamino-acetic acid **3** (300 mg, 980 µmol) and paraformaldehyde (294 mg, 9.8 mmol) were added portion-wise over 2 days (1 addition per day) and the reaction mixture was heated at 120 °C for 2 days. CNTs were washed several times by filtration (pore size = 0.45 µm) with DMF, MeOH and Et_2O and dried under high vacuum.

Then, the Boc group was cleaved by dispersing CNTs (100 mg) in a 4 M HCl solution in dioxane (100 mL), by sonication for 30 min, and stirring it at r.t. overnight. The CNTs were washed by filtration (pore size = 0.45 µm) with DMF, MeOH and Et_2O and dried under high vacuum. The degree of functionalization, determined by the Kaiser test, was 80 µmol/g.

s-DWCNT-**6**

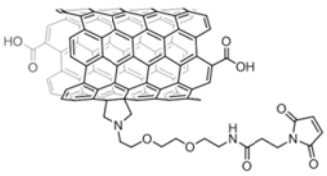

s-DWCNT-**5** (20 mg, 1.6 µmol of amine groups) were suspended in dry DMF and neutralized with dry DIEA (14 µL, 80 µmol). A solution of *N*-succinimidyl-3-maleimidopropionate (8.5 mg, 32 µmol) in DMF (2 mL) was added. The reaction was sonicated for 20 min and then stirred at r.t. under Ar for 48 h. The obtained *s*-DWCNTs-**6** were extensively washed by filtration (pore size = 0.45 µm) with DMF, MeOH and Et_2O, and then dried under high vacuum. The degree of functionalization, determined by comparison of the Kaiser test value with the one of *s*-DWCNT-**5**, was 30 µmol/g (Yield: 38%).

s-DWCNT-**7**

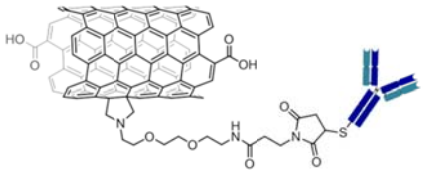

The maleimido-derivatized *s*-DWCNT-**6** (10 mg) were dispersed in 20 mL of IgG-SH solution (0.45 mg/mL, 3 µM) in PBS (5mM EDTA, pH 6.5) and the mixture was shaken for 60 h at r.t., monitoring the reaction by the decrease of IgG concentration in the supernatant, after centrifugation of a small aliquot of the reaction. Finally, the CNTs were centrifuged and washed thoroughly with PBS (pH 7.4) until no Ab was detected in the supernatant (by UV-vis spectroscopy). The resulting Ab-conjugate *s*-DWCNT-**7** were stored at 4 °C as dispersions of 0.5 mg/mL in PBS (pH 7.4). The degree of functionalization, determined by TGA, was 2.6 µmol of Ab per gram of CNTs.

s-MWCNT

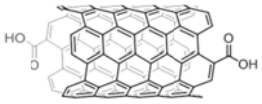

Pristine MWCNTs (100 mg) were dispersed in 50 mL of aq. sulfuric acid/nitric acid mixture (3:1 v/v, 98% and 65%, respectively), and the mixture was sonicated in a water bath for 24 h, keeping temperature below 50°C. Deionized water was then carefully added up to a final volume of 150 mL and the mixture was filtered (pore size = 0.1 µm), and washed by filtration in H_2O until filtrate reached a neutral pH, then in MeOH and Et_2O. Finally CNTs were dried under high vacuum (weight yield: 70%).

s-MWCNT-**1**

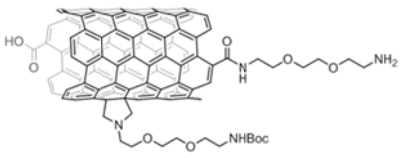

s-MWCNTs (100 mg) were suspended in oxalyl chloride (20 mL), then DMF (0.4 mL) was added and the reaction was sonicated in a water bath for 30 min under Ar. Subsequently, the reaction was stirred at 60°C under Ar for 24 h. After this period the solvent was dried under reduced pressure. The CNTs were suspended again in dry THF and *N*-Pht-amino-diethoxy-ethyl amine **5** (150 mg, 382 µmol) was added to the mixture, followed by sonication in a water bath for 30 min. Then the reaction mixture was heated at 70°C under Ar for 48 h. The nanotubes were washed several times by filtration (pore size = 0.1 µm) with DMF, MeOH and Et_2O, the and dried under high vacuum.

CNTs (100 mg) were then suspended in 100 mL of DMF and sonicated in a water bath for 20 min. N-Boc-amino-diethoxy-ethylamino-acetic acid **3** (300 mg, 980 µmol) and paraformaldehyde (294 mg, 9.8 mmol) were added portion-wise over 2 days (1 addition per day) and the reaction mixture was heated at 120 °C for 2 days. CNTs were washed several times by filtration (pore size = 0.1 µm) with DMF, MeOH and Et_2O and dried under high vacuum.

Finally, CNTs (100 mg) were dispersed in EtOH (100 mL) and hydrazine hydrate (600 µL) was added. After sonication for 20 min, the dispersion was stirred overnight at r.t.. The CNTs were washed by filtration (pore size = 0.1 µm) with EtOH, MeOH and Et_2O and dried under high vacuum, to afford *s*-MWCNT-**1**. The degree of functionalization, determined by the Kaiser test, was 170 µmol/g.

s-MWCNT-**2A**

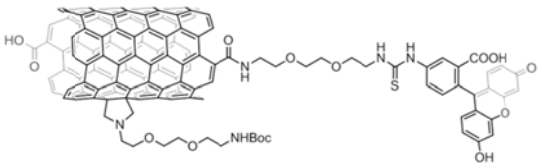

s-MWCNT-**1** (50 mg, 8.5 µmol of amine groups) were dispersed in dry DMF (10 mL). Dry DIEA (74 µL, 425 µmol) and FITC (99.3 mg, 255 µmol) were added and the reaction mixture was sonicated for 20 min under Ar and in the dark, and then stirred at r.t. overnight under Ar and in the dark. Reaction mixture was filtered (pore size = 0.1 µm) and then washed with DMF, MeOH and Et_2O and finally dried under high vacuum to afford *s*-MWCNT-**2A**. The degree of functionalization, determined by comparison of the Kaiser test value with the one of *s*-MWCNT-**1**, was 60 µmol/g (Yield: 35%).

s-MWCNT-**2B**

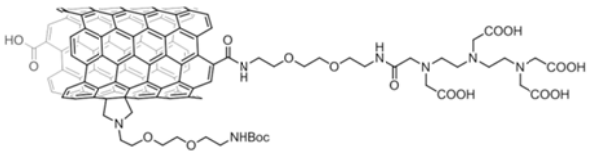

s-MWCNT-**1** (50 mg, 8.5 µmol of amine groups) were dispersed in dry DMF (10 mL). Dry DIEA (74 µL, 425 µmol) and DTPA (91.1 mg, 255 µmol) were added and the reaction mixture was sonicated for 20 min under Ar, and then stirred at r.t. overnight under Ar. Reaction mixture was filtered (pore size = 0.1 µm) and then washed with DMF, MeOH and Et_2O and finally dried under high vacuum to afford *s*-MWCNT-**2B**. The degree of functionalization, determined by comparison of the Kaiser test value with the one of *s*-MWCNT-**1**, was 50 µmol/g (Yield: 29%).

s-MWCNT-**3A** and **3B**

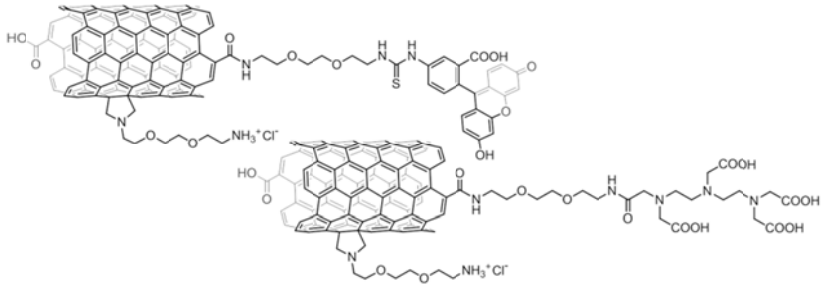

s-MWCNT-**2A** and **2B** (40 mg) were dispersed in a 4 M HCl solution in dioxane (40 mL), by sonication for 30 min, and stirring it at r.t. overnight. The CNTs were subsequently washed by filtration (pore size = 0.1 µm) with DMF, MeOH and Et_2O and dried under high vacuum. The degree of functionalization, determined by comparison of the Kaiser test value with the starting one, was 35 µmol/g in both cases.

s-MWCNT-**4A** and **4B**

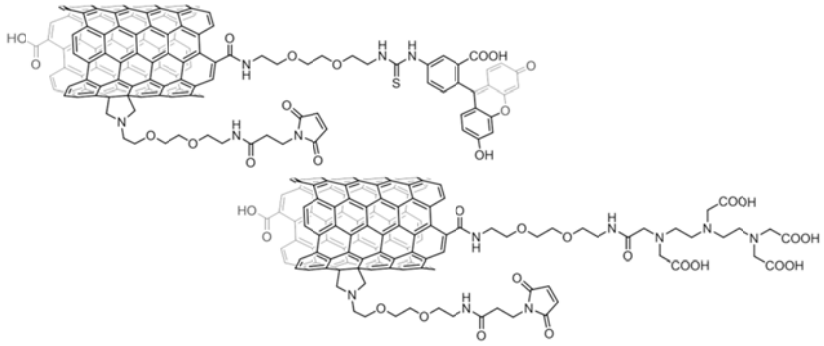

s-MWCNT-**3A** and **3B** (20 mg, 0.7 µmol of amine groups) were suspended in dry DMF and neutralized with dry DIEA (6 µL, 35 µmol). A solution of *N*-succinimidyl-3-maleimidopropionate (3.7 mg, 14 µmol) in DMF (2 mL) was added. The reaction was sonicated for 20 min and then stirred at r.t. under Ar for 48 h. The CNTs were washed by filtration (pore size = 0.1 µm) with DMF, MeOH and Et_2O, and then dried under high vacuum. The degree of functionalization, determined by comparison of the Kaiser test value with the starting one, was 35 µmol/g (Yield: 100%) in both cases.

s-MWCNT-**5A** and **5B**

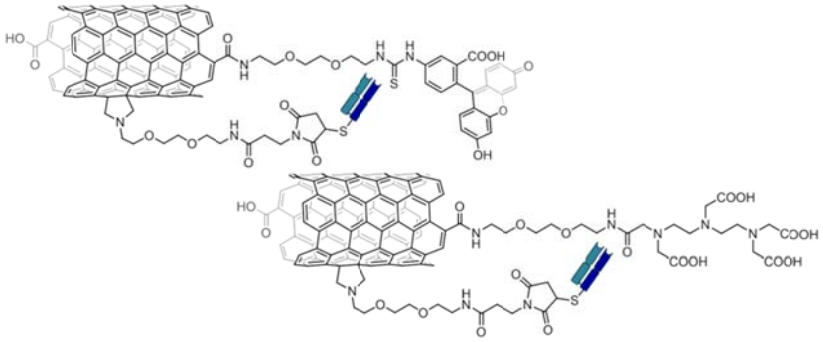

The maleimido-derivatized *s*-MWCNT-**4A** and **4B** (10 mg) were dispersed in 20 mL of Fab'-SH solution (0.4 mg/mL, 8.4 µM) in PBS (5 mM EDTA, pH 6.5) and the mixture was shaken for 37 h at r.t., monitoring the reaction by the decrease of Fab' concentration in the supernatant, after centrifugation of a small aliquot of the reaction. Finally, the CNTs were centrifuged and washed thoroughly with PBS (pH 7.4) until no Fab' was detected in the supernatant (by UV-vis spectroscopy). The resulting Fab'-MWCNT conjugates were stored at 4 °C as dispersions of 0.5 mg/mL in PBS (pH 7.4). The degree of functionalization, determined by TGA, was 1.5 and 1.4 µmol of Fab' per gram of CNTs, respectively.

s-MWCNT-**6A** and **6B**

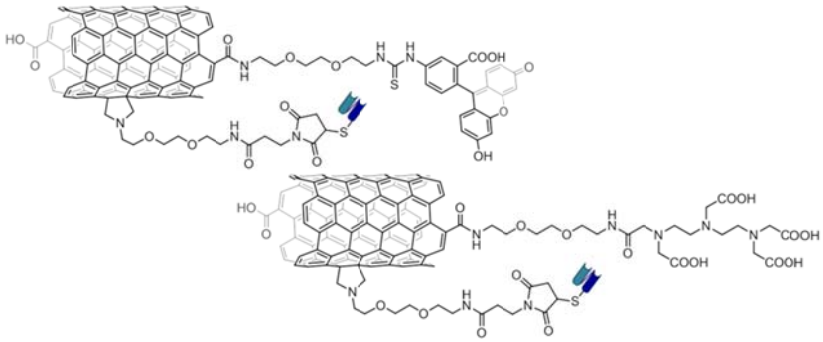

The maleimido-derivatized *s*-MWCNT-**4A** and **4B** (10 mg) were dispersed in 20 mL of scFv-SH solution (0.16 mg/mL, 5.2 µM) in PBS (5 mM EDTA, pH 6.5) and the mixture was shaken for 22 h at r.t., monitoring the reaction by the decrease of scFv concentration in the supernatant, after centrifugation of a small aliquot of the reaction. Finally, the CNTs were centrifuged and washed thoroughly with PBS (pH 7.4) until no scFv was detected in the supernatant (by UV-vis spectroscopy). The resulting scFv-MWCNT conjugates were stored at 4 °C as dispersions of 0.5 mg/mL in PBS (pH 7.4). The degree of functionalization, determined by TGA, was 3.3 and 3.1 µmol of scFv per gram of CNTs, respectively.

MWCNT-**7**

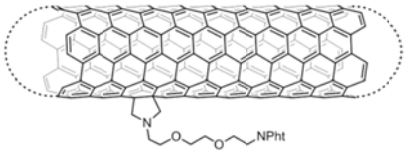

Pristine MWCNTs (100 mg), *N*-Boc-amino-diethoxy-ethylamino-acetic acid **7** (100 mg, 297 µmol), and *p*-HCHO (89.3 mg, 2.97 mmol) were suspended in CH_2Cl_2 (4 mL) by little sonication in a quartz microwave tube. Then, the solvent was evaporated by a N_2 flow, and the reaction was performed in the microwave reactor, with a 50 W power, using a step-wise heating procedure, in order to carefully control temperature increase:

- 1 min, 120°C
- 2 min, 140°C
- 60 min, 160°C

Then, CNTs were re-dispersed in DMF (200 mL) and washed by filtration (pore size = 0.45 µm) in DMF, MeOH and Et_2O, to afford, after high vacuum drying the final CNTs.

MWCNT-**8**

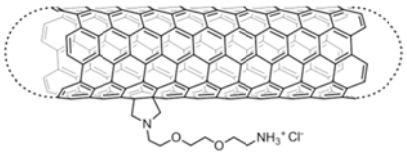

MWCNT-**7** (90 mg) were dispersed in EtOH (100 mL) and hydrazine hydrate (540 µL) was added. After sonication for 20 min, the dispersion was stirred overnight at r.t.. The CNTs were washed by filtration (pore size = 0.45 µm) with EtOH, aq. HCl 1N, H_2O, MeOH and Et_2O and dried under high vacuum, to afford MWCNT-**8**. The degree of functionalization, determined by the Kaiser test, was 100 µmol/g.

MWCNT-**9**

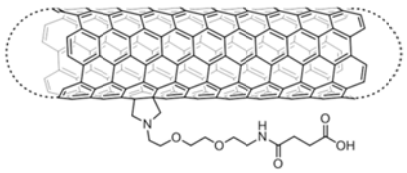

MWCNT-**8** (50 mg, 5 µmol of amine groups) were dispersed in dry DMF (20 mL) and succinic anhydride (5 mg, 50 µmol) and TEA (7 µL, 50 µmol) were added. The mixture was sonicated for 20 min under Ar, and then the reaction was stirred at r.t., under Ar for 24 h. Reaction mixture was filtered (pore size = 0.45 µm) and then washed with DMF, MeOH and Et_2O and finally dried under high vacuum to afford MWCNT-**9**. The degree of functionalization,

determined by comparison of the Kaiser test value with the one of MWCNT-**8**, was 55 μmol/g (Yield: 55%).

MWCNT-**10**

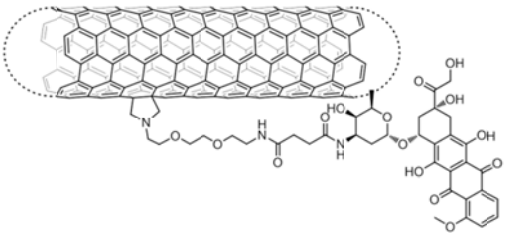

To a dispersion of MWCNT-**9** (15 mg, 0.83 μmol of carboxyl groups) in dry DMF (3 mL), a solution of PyAOP (2.6 mg, 5 μmol) in dry DMF (1 mL), a solution of doxorubicin·HCl (2.4 mg, 4 μmol) in dry DMF (2mL) and DIEA (6 μL, 33 μmol) were added. The mixture was sonicated for 20 min under Ar, and then it was stirred at r.t. under Ar in the dark overnight. CNTs were subsequently washed by filtration (pore size = 0.45 μm) with DMF until no doxorubicin was detected in the filtrate (by UV-vis spectroscopy), and then with MeOH and Et_2O and finally they were dried under high vacuum. The degree of functionalization, determined by TGA, was 75 μmol of doxorubicin per gram of CNTs.

MWCNT-**11**

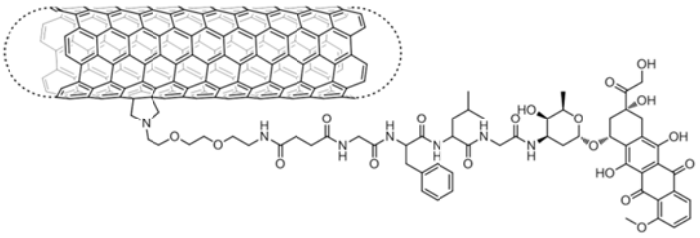

To a dispersion of MWCNT-**9** (15 mg, 0.83 μmol of carboxyl groups) in dry DMF (3 mL), a solution of PyAOP (2.6 mg, 5 μmol) in dry DMF (1 mL), a solution of GFLG-doxorubicin **10** (1.5 mg, 1.65 μmol) and DIEA (6 μL, 33 μmol) were added. The mixture was sonicated for 20 min under Ar, and then it was stirred at r.t. under Ar in the dark overnight. CNTs were subsequently washed by filtration (pore size = 0.45 μm) with DMF until no doxorubicin was detected in the filtrate (by UV-vis spectroscopy), and then with MeOH and Et_2O and finally they were dried under high vacuum. The degree of functionalization, determined by TGA, was 45 μmol of doxorubicin per gram of CNTs.

s-MWCNT

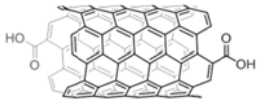

Pristine MWCNTs (100 mg) were dispersed in 50 mL of aq. sulfuric acid/nitric acid mixture (3:1 v/v, 98% and 65%, respectively), and the mixture was sonicated in a water bath for 10 h, keeping temperature below 50°C. Deionized water was then carefully added up to a final volume of 150 mL and the mixture was filtered (pore size = 0.1 µm), and washed by filtration in H_2O until filtrate reached a neutral pH, then in MeOH and Et_2O. Finally CNTs were dried under high vacuum (weight yield: 80%).

s-MWCNT-**12**

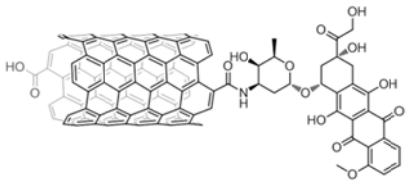

To a dispersion of *s*-MWCNT (15 mg) in dry DMF (3 mL), a solution of PyAOP (4.3 mg, 8.2 µmol) in dry DMF (1 mL) and DIEA (5 µL, 27 µmol) were added and the mixture was stirred at r.t. under Ar for 20 min. Then, a solution of doxorubicin·HCl (1.6 mg, 2.7 µmol) and DIEA (5 µL, 27 µmol) in dry DMF (2 mL) was added, and the reaction was stirred at r.t. under Ar in the dark overnight. CNTs were subsequently washed by filtration (pore size = 0.1 µm) with DMF until no doxorubicin was detected in the filtrate (by UV-vis spectroscopy), and then with MeOH and Et_2O and finally they were dried under high vacuum. The degree of functionalization, determined by TGA, was 55 µmol of doxorubicin per gram of CNTs.

s-MWCNT-**13**

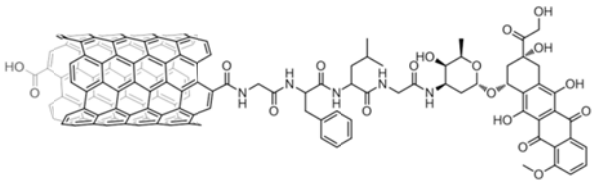

To a dispersion of *s*-MWCNT (15 mg) in dry DMF (3 mL), a solution of PyAOP (4.3 mg, 8.2 µmol) in dry DMF (1 mL) and DIEA (5 µL, 27 µmol) were added and the mixture was stirred at r.t. under Ar for 20 min. Then, a solution of GFLG-doxorubicin **10** (2.5 mg, 2.7 µmol) and DIEA (5 µL, 27 µmol) in dry DMF (2 mL) was added, and the reaction was stirred at r.t. under Ar in the dark overnight. CNTs were subsequently washed by filtration (pore size = 0.1 µm) with DMF until no doxorubicin was detected in the filtrate (by UV-vis spectroscopy), and then with MeOH and Et_2O and finally they were dried under high vacuum. The degree of functionalization, determined by TGA, was 40 µmol of doxorubicin per gram of CNTs.

5.4 References

1. G. Pastorin, W. Wu, S. Wieckowski, J.-Paul Briand, K. Kostarelos, M. Prato, and A. Bianco, *Chem. Commun.*, 2006, 1182-1184.
2. K. Kordatos, T. D. Ros, S. Bosi, E. Vazquez, M. Bergamin, C. Cusan, F. Pellarini, V. Tomberli, B. Baiti, D. Pantarotto, V. Georgakilas, G. Spalluto, and M. Prato, *J. Org. Chem.*, 2001, 66, 4915-4920.